ENTRAINMENT AND TRANSPORT OF COARSE STREAM BED MATERIAL IN A FLUVIOKARST WATERSHED, SOUTH-CENTRAL MISSOURI: A TRACER PARTICLE STUDY

A Thesis

presented to the Faculty of the Graduate School

at the University of Missouri

In Partial Fulfillment

of the Requirements for the Degree

Master of Science

---

by

NATHAN R ROSSMAN

Dr. Francisco Gomez, Thesis Advisor

MAY 2010

The undersigned, appointed by the Dean of the Graduate School, have examined the thesis entitled

ENTRAINMENT AND TRANSPORT OF COARSE STREAM BED MATERIAL IN A FLUVIOKARST WATERSHED, SOUTH-CENTRAL MISSOURI: A TRACER PARTICLE STUDY

presented by Nathan R. Rossman

a candidate for the degree of Master of Science

and hereby certify that in their opinion it is worthy of acceptance.

_____

Dr. Francisco Gomez, advisor

_____

Dr. Cheryl A. Kelley

_____

Dr. Michael A. Urban

ACKNOWLEDGEMENTS

First of all, I would like to give a big thank you to all of the professors, students, friends, and family who have helped me get to where I am today. I would especially like to thank my advisors Dr. Carol Wicks and Dr. Francisco 'Paco' Gomez for their encouragement, guidance, and support throughout my studies over the past two years. Thank you both as well, for transitioning me successfully from one advisor to the next, and for considering my desire to carry out my project at MU.

My thesis committee, which includes Dr. Cheryl Kelley and Dr. Michael Urban, both of whom provided a critical review of my thesis, are much appreciated. Much thanks goes to Tom and Cathy Aley for their willingness to grant access to and housing, as well as assisting me with field work, at the Ozark Underground Laboratory. The extent of the conservation, research, and education efforts carried out by Tom and Cathy over the years is also greatly admired and appreciated. I am sure that their efforts will continue to serve as inspiration for me in the future. Also, I would like to thank the staff of the Ozark Underground Laboratory for assisting me with correspondence, field trip planning, and field work. A big thank you goes to Dr. Richard Meyers for his meticulous work in collecting rain data within the recharge area of Tumbling Creek Cave.

Thanks to everybody who assisted me in the field, including Dr. Carol Wicks, Dr. Paco Gomez, Tom and Cathy Aley and other OUL staff, MU geology students Audrey Sima, Nathan Hopkins and Bjorn Held, as well as my girlfriend Brandi Gabrick, Julia Held and students from Dr. Gomez's surficial processes class, among others.

Lastly, I would like to thank the Department of Geological Sciences for the two years of financial support for living expenses and field work related expenses, without their support I may not have been able to complete my graduate degree.

TABLE OF CONTENTS

LIST OF TABLES

LIST OF FIGURES

ABSTRACT

The midcontinent of the U.S. is heavily karstified containing well developed subsurface drainage systems that are covered by beds of coarse-grained, poorly sorted fluvial sediments, resembling those found in upland surface streams. The movement of coarse sediment as bed load within karst streams has been considered negligible in the past as it was assumed that all karst is developed through dissolution rather than mechanical abrasion. The frequency and magnitude of sediment transporting events in karst streams has implications for models of fluviokarst landscape development and the stability of aquatic ecosystems.

Within Tumbling Creek Cave (TCC) in the Ozark Plateau of south-central Missouri, and Bear Cave Hollow (BCH), one of TCC's surface drainage streams, bed load entrainment and transport dynamics of coarse-grained (16-180 mm), mainly siliciclastic material, was evaluated using hydrological measurements and 670 painted tracer particles. Tracers are used in this research for the first time in a karst stream. Tracers are well suited for studying the stochastic and spatially variable nature of bed load transport because they reflect the movement of individual particles of known characteristics, and they are also inexpensive and simple to employ.

Median surficial sediment grain size in the study reaches ranged from 39 to 71 mm in TCC, and from 24 to 37 mm in BCH with bed and/or water slopes ranging from 0.006 to 0.077 in TCC and from 0.002 to 0.009 in BCH. TCC is classified as a pool-riffle channel morphology type and BCH is classified as a plane-bed channel. Preliminary data from surveys of the longitudinal (downstream) movement of tracers over a 10-month period indicate that minor amounts (0-13.2%) of coarse bed material in TCC are mobilized by relatively low flows (5-28% of bankfull) that recur somewhat frequently (less than 3.1 years). BCH transports a higher percentage of material (0-59.1%) during similar flows (2-29% of bankfull) and frequencies (less than 3.59 years). Bed load transport was observed to be in a state of partial transport for any one grain size class in TCC during the study, while the complete mobilization of tracer size classes was

observed in BCH at the highest observed flow, indicating “phase 2” transport and the break-up of the armor layer. The differences are attributed to the wider observed range of grain sizes covering the bed in TCC compared to BCH.

The use of the Shields (1936) criteria tends to over predict the critical shear stress required for entrainment of the largest mobilized grain size of individual tracers, while the empirical equation of Bagnold (1980) performs much better. Thus, the Shields equation may be better suited as a gage for complete mobilization of a grain size class across a reach, while the Bagnold (1980) equation may be better suited for estimating entrainment of grains from patches of the bed.

Chapter 1

Introduction

The transport of coarse stream bed material during moderate to high flows can make up a large proportion of mass passing through fluviokarst watersheds (i.e., those having both subsurface and surface reach components) and can be a major process involved in the denudation of fluviokarst landscapes. For instance, Worthington (1984) found that up to 95 to 98% of the mass transported through a fluviokarst system in West Virginia was fluvial sediments. This has implications for models of landscape evolution and effects on the stability of aquatic ecosystems.

Sediment transport studies in karst systems have been rare, with little quantitative work carried out (Bottrell et al., 1999; Dogwiler, 2002). Comparatively, sediment transport has been studied extensively in non-karst fluvial systems over the past century (Gomez, 1991), as reflected by the numerous scientific publications written on the subject in many different disciplines, including aquatic ecology (e.g., Lorang and Hauer, 2003; Gordon et al., 2004; Schwendel et al., 2009), river engineering (e.g., Shields, 1936; Yalin, 1977; Aguirre-Pe et al., 2003), and fluvial geomorphology (e.g., Leopold et al., 1964; Buffington and Montgomery, 1997; Nelson et al., 2003; Church, 2006). Many karst streams and passages in temperate latitudes have beds covered by large quantities of coarse-grained, poorly sorted, sediment (White and White, 1968; Gillieson, 1996; Farrant, 2004), while the movement of which may occur more frequently than previously thought (Dogwiler and Wicks, 2004; Farrant, 2004). In addition, bed load transport is the most complex sediment transport process in regards to its measurement and quantification (Beylich and Warburton, 2007), making observation of transport frequency a high priority in the field of karst geomorphology. Furthermore, there is an urgent need

for detailed process-based research into the mechanisms of transport of cave sediments, especially during flood events (Gillieson, 1996).

Past research on weathering and erosion in karst system development has appropriately focused on dissolution processes (e.g., White, 1988). Yet, physical sediment transport may be an important component of the mechanical erosion process, and, in turn, to the development of cave passages (e.g., White and White, 1968; Newson, 1971a, b). However, it remains unclear whether or not clastic sediments "act to enhance (through mechanical abrasion, Newson, 1971a) or hinder (by shielding the bedrock from dissolution, White and White, 1968; Renault, 1970) karst stream development" (Dogwiler, 2002). Farrant (2004) argues that many caves are modified by the latter speleogenetic process, especially in low-gradient systems with an allochthonous sediment source. In spite of this, the former explanation for mechanical abrasion as a speleogenetic process is apparent where siliciclastic units have been eroded.

These hypotheses have a similar corollary with hypotheses about incision into bedrock channels. As stated in Sklar and Dietrich (2001), Gilbert (1877) was the first to propose that the quantity of sediment supplied to the river should influence bedrock-incision rates in two essential yet opposing ways: (1) by providing tools for abrasion of exposed bedrock, and (2) by limiting the extent of exposure of bedrock on the channel bed. Therefore, the sediment transport rate, relative to the sediment transport capacity (and thus channel slope) plays a large role in whether or not abrasion is the dominant erosional process. In addition, the size distribution of sediment grains supplied to the channel is likely to affect incision rates for two reasons: (1) the coarse fraction is capable of forming an alluvial cover in actively incising river channels, and (2) because the fine fraction is carried in suspension, and collisions with the bedrock are rare (Sklar and Dietrich, 2001).

Karst streams are believed to function similarly to their surface stream counterparts in their modes of clastic sedimentation and bed load transport (Gillieson, 1996), and have been shown to exhibit hydraulically controlled passage geometries, stream gradients and planforms, that are comparable with surface streams (White and Deike, 1989). Because of this, studies from non-karst fluvial systems can be utilized to provide guidance for methodologies when studying sediment transport dynamics in karst or fluviokarst systems.

The work carried out during this study extends past investigations of fluviokarst systems and their ability to transport coarse bed load material by Dogwiler (2002), and Dogwiler and Wicks (2004). They provided estimates of the ability of karst stream reaches to erode bed material using both the median grain size diameter (D_{50}), and the diameter of the grain size greater than 85% of the bed (D_{85}), within two central U.S. systems. Following Dingman (1984, p 156), they evaluated the possibility that erosion would occur based on a basal shear stress analysis, where the ratio of the bankfull shear stress to the critical shear stress is evaluated. This type of approach, defined as a 'sediment entrainment potential' analysis, has recently been utilized by others investigators as well (e.g., Peterson et al., 2008; Davis, 2009). The findings of Dogwiler and Wicks (2004) suggested that common flows recurring frequently (less than one year) are capable of mobilizing coarse stream bed material throughout much of the length of karst streams in the midcontinent of the U.S. and similar upland karst streams in the U.K. Furthermore, their work provided quantitative information about channel morphology, channel roughness, and dominant discharge, all of which are fundamental fluvial characteristics, and are crucial to the better understanding of bed load sediment transport dynamics in fluviokarst watersheds.

A magnitude-frequency approach to sediment transport provides information about the importance of the mechanical erosion process (compared to chemical erosion processes) in karst development, as it has been suggested that a greater frequency of sediment transporting events will result in higher erosion rates through abrasion (e.g., Whipple and Tucker, 2002). Dogwiler and Wicks (2004) based their findings on surficial stream bed material size distributions, channel surveys of cross-section dimensions and channel slope, as well as continuous stage series data from one station, which led them to their conclusion that sediments, within cave stream channels, can be mobilized by bankfull flow conditions, and that bankfull flows recur about every 1.7 years. While their research does not provide quantifiable sediment transport rates, their findings are in agreement with the widely accepted notion introduced by Wolman and Miller (1960) that the discharge most effective in the long-term transport of sediment (i.e., effective discharge) is a relatively frequent event occurring, on average, about once a year. However, it has been observed that the return period of the effective discharge is highly variable, ranging from one week to several decades (Nash, 1994). It must also be noted that effective discharge and dominant discharge have two different meanings but are closely related (Wolman and Miller, 1960). The effective discharge is the discharge that transports the most sediment, while the dominant discharge is considered a channel-forming discharge. Further, the bankfull discharge and recurrence interval is usually associated with the effective discharge, even though there is not a single recurrence interval for bankfull discharge because bankfull can be defined several different ways, including, for example, the lowest width-depth ratio at a cross-section, and the height of the lower limit of perennial vegetation (Williams, 1978). Thus, further studies involving the recurrence interval of the effective discharge of coarse stream bed material is warranted.

Typically the effects of large storm events are rarely observed directly when large clast sizes are transported (Bosch and White, 2004). However, direct observation of such flows would be extremely hazardous under those conditions (Van Gundy and White, 2009). Therefore, a study of the movement of cave sediments is well suited for the use of sediment tracing methods.

This research uses natural painted tracer particles paired with continuous stream stage measurements (and calculated discharge) to determine the most appropriate functional relationships for estimating sediment entrainment, making it possible to more reliably predict when and why coarse sediment transport is occurring. The field work is carried out within a small fluviokarst watershed in the Ozark Plateaus Physiographic Province (known locally as the Ozarks) of south-central Missouri. Secondly, using a long record of rainfall from publically accessible weather station data, and correlations with stream discharge, this research provides estimates of the frequency of flow events that are capable of rearranging coarse stream bed material. These two aspects of sediment transport are primarily important because of the influence that sediment transport mechanisms have on the structure of benthic communities (Schwendel et al., 2009), especially important in biologically diverse fluviokarst systems. Tracers are also used to estimate the short-term erosion rate for the fraction of eroded material traveling through the studied stream network as bed load. This will make it possible for future researchers to develop estimates of denudation rates (when coupled with dissolved load and suspended sediment load measurements).

Objectives

The primary objective of this study is to quantify the grain-size specific critical entrainment thresholds of stream bed material found in surface and subsurface (cave)

reaches of a fluviokarst watershed. Observed critical entrainment threshold values are assessed and compared against commonly employed predictive equations for entrainment thresholds developed in surface streams. The analysis involves several different empirical expressions of three different hydrodynamic forces (hydraulic variables), including: shear stress, discharge and stream power. This approach is consistent with the general acknowledgement that several approaches to bed load transport should be used so that the results can be compared (Petit et al., 2005). An evaluation of bed load transport rate is also made, based on observed thresholds for entrainment and discharge data from both study reaches, as well as daily rainfall records from a nearby weather station.

The results of this research provide a detailed analysis of sediment transport processes, specifically a flow competence analysis and a magnitude-frequency analysis from the use of painted tracer particles and hydrological measurements. The primary hypothesis tested is that theoretical estimates for entrainment using a basal shear stress and traditional Shields (1936) criterion approach will yield lower frequencies of coarse bed load transporting events than those observed (because of relative size effects on heterogeneous beds and higher than predicted instantaneous shear stress fluctuations). This hypothesis is similar to findings by Buffington et al. (1992), and has implications for Wolman and Miller's (1960) conclusion about the one year (average) recurrence interval of effective discharge. A second hypothesis tested is that the critical entrainment threshold for coarse stream bed material will be similar, based on observed values, for surface fluvial stream reaches and subsurface karst stream reaches evaluated by grain size fractions (half-phi size class intervals; –log base 2 of the grain size in mm).

Field Site Description

Study Locality

The field study was conducted in Taney County in south-central Missouri, approximately 40 km east of the city of Branson within a stream reach of Tumbling Creek found within Tumbling Creek Cave (TCC), and one reach of Bear Cave Hollow (BCH). TCC is a branchwork cave (after Palmer, 1991) composed of two interlocking passages, while BCH is a headwater ephemeral surface stream located in the southeast of, and entirely within, the TCC recharge area (Figures 1.1 and 1.2). TCC has 2,788 m of surveyed passage (Aley and Thomson, 1971), 879 m of which is the length of Tumbling Creek. BCH is a first-order stream with a length of 2,982 m (delineated using the Protem 1:24,000 scale quadrangle map).

BCH and other nearby surface drainage networks (Figure 1.1) are hydrologically connected with TCC. Under flowing conditions water is pirated directly from lengthy segments of surface stream channels (i.e., water seeps beneath the stream bed to feed groundwater; losing stream reaches). Water travels beneath surface drainage divides and ultimately passes through TCC. Subterranean flow resurges at the TCC Spring (the only natural entrance to TCC; Figure 1.1) or any number of other springs (up to 20), depending on the flow conditions (Aley et al., 2007). Peak flow within the cave stream is typically reached within a day of rainfall events, and responds only slightly slower than the nearby surface streams (Aley and Thomson, 1971). During a dye injection study by Aley and Thomson (1971) within the upper reaches of BCH, flow recharging groundwater at the injection site accounted for about 4% of the flow in TCC. The recharge area for TCC has been delineated based on 62 groundwater traces, conducted by the Ozark Underground Laboratory, Inc. (OUL) and encompasses an area of approximately 23.36 km^2 (Aley et al., 2007). The approximate drainage area of the BCH watershed is 1.94 km^2, delineated from topographic boundaries. Tumbling Creek has a

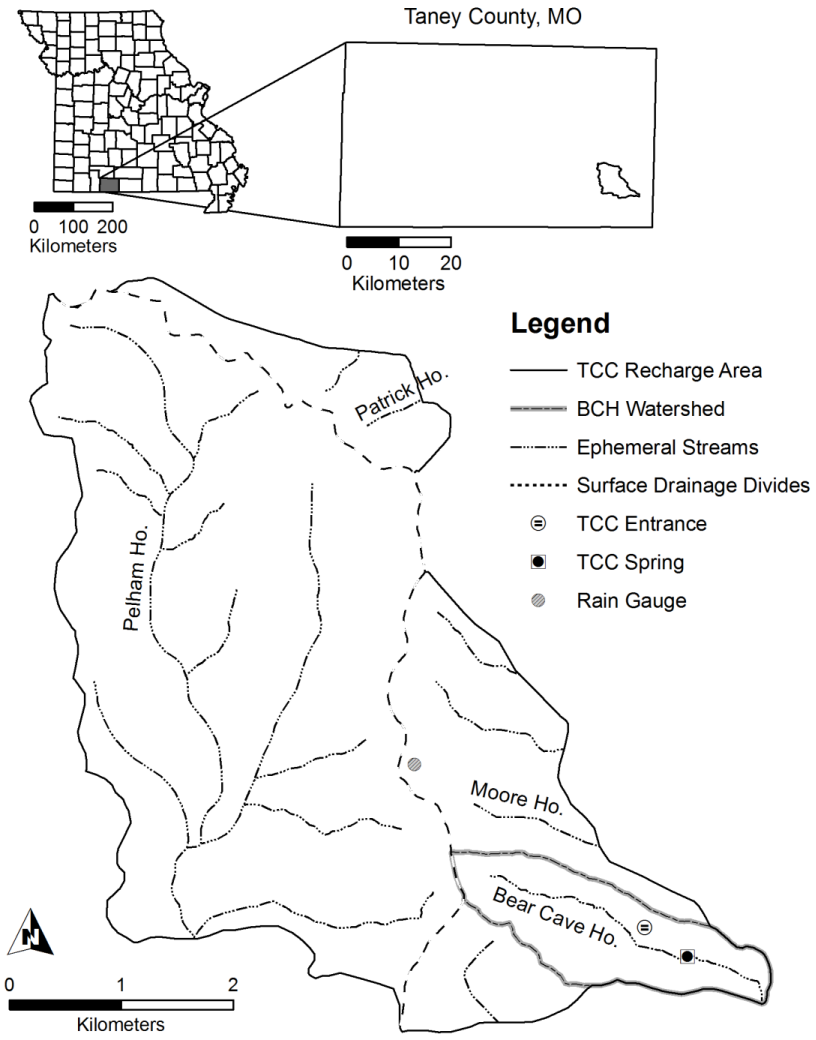

Figure 1.1. Location and hydrologic setting of the Tumbling Creek Cave (TCC) recharge area, including Bear Cave Hollow (BCH) and its watershed boundaries. The total recharge area for TCC is approximately 23.36 km^2 (Aley et al., 2007), and the total area of the BCH watershed is approximately 1.94 km^2. Groundwater recharging TCC is pirated via scattered sinkholes and losing stream reaches underneath major surface drainage divides (indicated as black dotted lines). Water emerges at the surface at Bear Cave spring (indicated as TCC Spring on the map). When TCC is under high-flow conditions, discharge from the cave to the surface may occur at 15-20 different locations (Aley et al., 2007). The TCC entrance is man-made. Surface water leaving TCC and the BCH watershed enters Big Creek which flows south into Bull Shoals Lake. [Modified from Elliott and Echols, 2007].

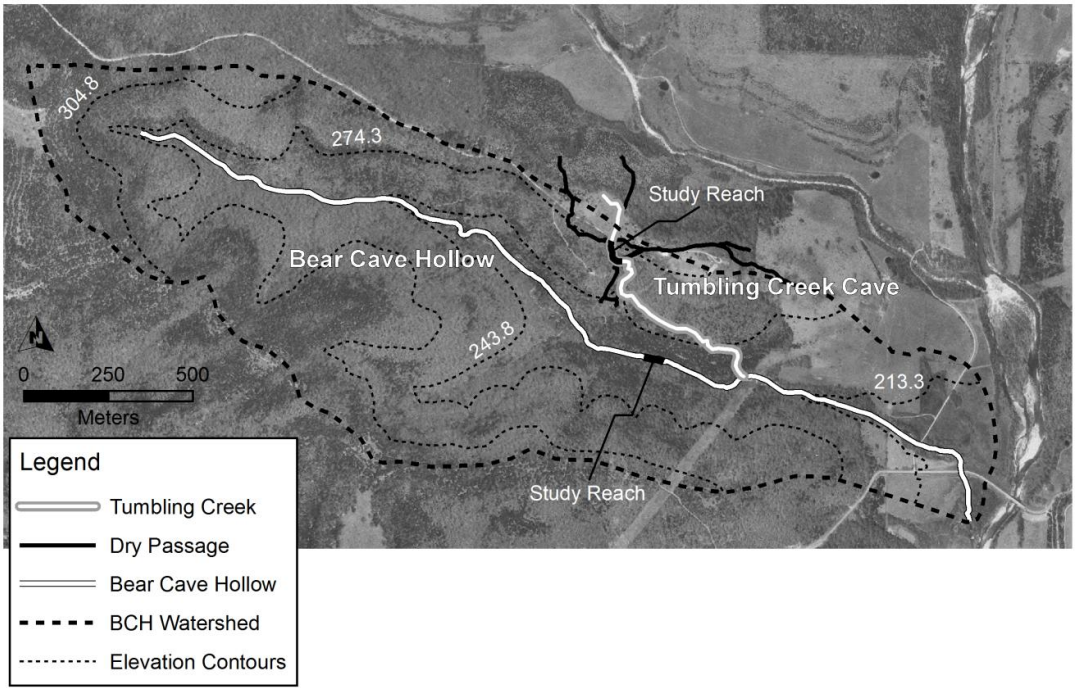

Figure 1.2. Location of study reaches within TCC and BCH, including BCH watershed boundaries. Tumbling Creek flows perennially with a typical low flow discharge of 0.01 to 0.06 m^3s^{-1}; peak discharge recorded during this study was 2.04 m^3s^{-1}. The gauging station at the weir receives water from an area draining approximately 22.55 km^2. Stream flow within BCH is ephemeral, occurring only after relatively intense rainfall events; peak hydraulic (mean) depth recorded during this study was 0.42 m, with an estimated discharge of 2.53 m^3s^{-1}. The gauging station receives surface runoff from an area draining approximately 1.41 km^2. [Imagery from MSDIS, http://msdis.missouri.edu; cave map modified from Elliott and Aley, 2005].

sinuosity (ratio of channel length to valley length) of 1.12 and BCH has a sinuosity of 1.06. The drainage density (ratio of total channel length to drainage area) for surface streams within the TCC recharge area is 1.31, while BCH has a drainage density of 1.54.

The TCC recharge area has undergone various human-related disturbances (i.e., land-use changes) that may have slightly increased rates of erosion and somewhat altered stream sediment and flow regimes. The introduction of pasture lands to the region are regarded as the primary reasons for increased sediment loading and turbidity within

Tumbling Creek (Neill et al., 2004). Between 1961 and 1996, forested areas within the recharge area had decreased from 80% to 57% with the addition of livestock grazing lands. However, a land management rehabilitation project (completed in 2004) has returned another 23.7% of riparian area within the recharge area back to forest (Neill et al., 2004). Within the BCH watershed, little change had taken place during that same time period, while most of the watershed remained forested. In 1973, the population of an endangered species of cavesnail living exclusively in Tumbling Creek (Tumbling Creek cavesnail, *Antrobia culveri*) was estimated at about 15,000 and had declined noticeably by 1991, probably a result of siltation which decreased the cavesnail's health and habitable area (Elliott and Aley, 2005). Yet, agriculture within the TCC recharge area is considered light.

Geologic Setting

Tumbling Creek Cave and its recharge area are located within the Salem Plateau, a karstified subprovince of the Ozark Plateaus Physiographic Province. The Salem Plateau is composed of Cambrian and Ordivician age (440 to 530 million years old) nearly flat-lying carbonaceous rocks exposed at the Earth's surface covering parts of south-central Missouri and north-central Arkansas (Noltie and Wicks, 2001). The TCC recharge area is entirely formed within the Cotter Formation (Aley et al., 2007), a lower Ordovician (Ibexian series) light brown to brown, medium to finely-crystalline, massive to thinly bedded dolomite interbedded with chert and minor local beds of thin sandstone, and quartz sand-rich dolomite beds (Thomson and Aley, 1971; Dodd and Dettman, 1996; Overstreet et al., 2003). Elevations within the TCC recharge area range from approximately 205 to 410 m above sea level.

Climatic Setting

Southern Missouri has a humid middle-latitude temperate climate. In the summer months, mean temperature is 23.9°C, in the winter months it is 1.8°C, and it is 13.1°C annually. During an average year, 59 days have a high temperature greater than 32°C and 114 days have lows of 0°C or less, but the record is highly variable (Figures 1.3 and 1.4). Rainfall is fairly heavy and well distributed throughout the year, and snow falls nearly every winter with cover lasting only a few days. The months of January and February have minimum precipitation, while June and November have maximum precipitation (Figure 1.4). Total annual precipitation is 1097 mm, 55% of which occurs in April through September[1].

Stream Reach Classification and Characteristics

Stream channel reaches were classified based on the Montgomery and Buffington (1997) system as a means for communication and comparison with other studies, because qualitatively defined channel types and features have been shown to exhibit quantitatively distinguishable channel characteristics (Montgomery and Buffington, 1997). The choice of the classification system was influenced by its use in one other study of the fluvial geomorphology of karst systems in the central U.S. by Dogwiler and Wicks (2004). While the use of classification systems in fluvial geomorphology is expanding, they must be used with caution as many (including the one used here for mountain channels) are not process-based, which diminishes their usefulness for assessing channel condition, response potential, and relations to ecological process (Montgomery and Buffington, 1997). Also, reach morphology can be controlled by

[1]Temperature and precipitation values based on 1971-2000, and average annual high and low temperature duration values based on 1949-2008 daily summary observations at the Ozark Beach, MO weather station, U.S. Cooperative Network Station 236460. All data are available from the National Climatic Data Center.

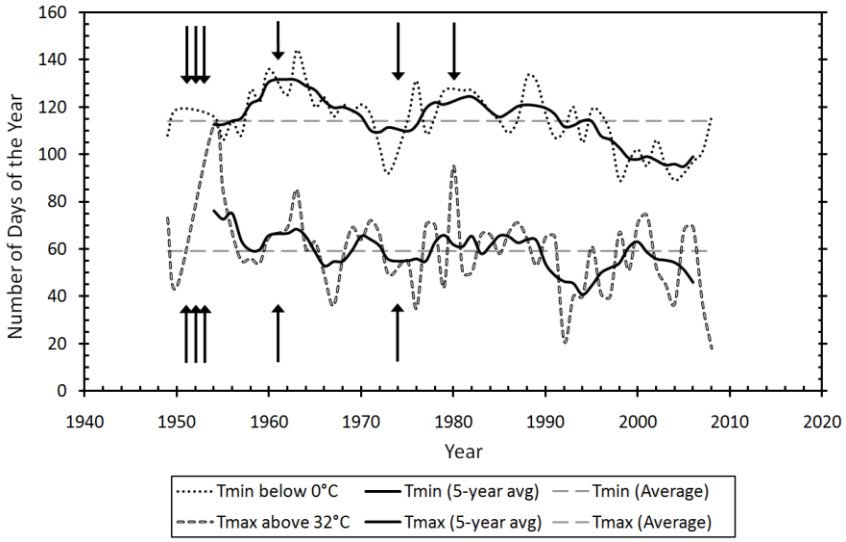

Figure 1.3. Temperature records in Taney Co showing the number of days per year in which minimum daily temperature values were below or equal to 0°C and maximum daily temperature values were above 32°C (including average and 5-year moving average values), during the period of 1949-2008. Arrows indicate years with insufficient or missing data. Data from the Ozark Beach weather station (U.S. Cooperative Network Station 236460).

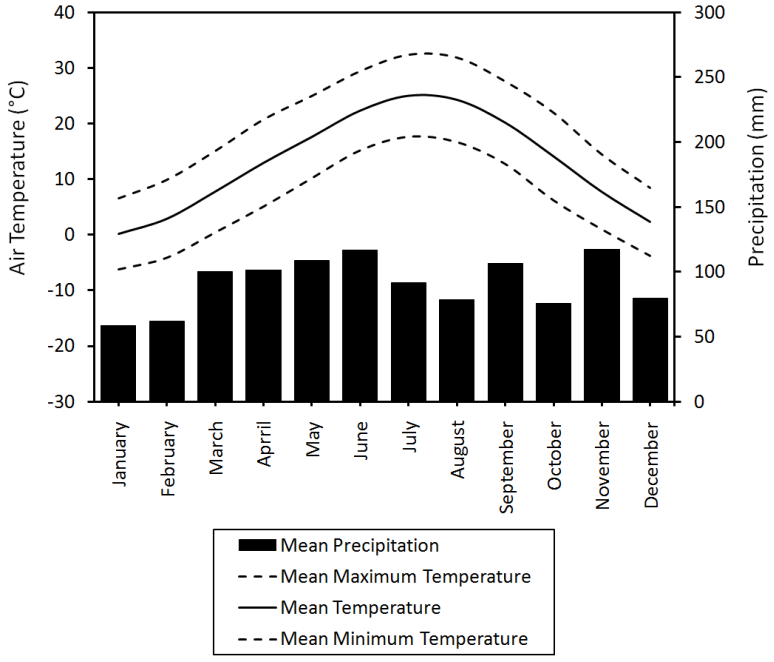

Figure 1.4. Summary of mean annual temperature and mean monthly precipitation in Taney Co from 1971-2000. Southern Missouri is characterized by mild winters, warm summers, and a relatively even distribution of precipitation throughout the year. Data are from the Ozark Beach weather station (U.S. Cooperative Network Station 236460).

lithology, which influences the amount, size and shape of material supplied to streams (Thompson and Croke, 2008). Within both the cave and surface streams of the TCC recharge area, the alluvial beds are covered primarily by siliciclastic rock-types (primarily chert), eroded from the Cotter Formation and left as residuum.

Classification type based on the Montgomery and Buffington (1997) system, along with channel reach characteristics from cross-section of this study are presented in Table 1.1 (see Appendix A for plots of cross-sections, and Appendix B for notation). Grain size distributions for sediment naturally occurring on the bed at seven cross-sections are plotted in Figure 1.5. The methodology for determining the grain size distributions and channel characteristics is described in Chapter 3. Study reaches exhibit both plane-bed and pool-riffle channel morphology (Figure 1.6) and represent a mixture of supply- and transport-limited characteristics. Although they were not selected for study as part of this research, BCH has frequent segments of the bed that lack continuous alluvium and only bedrock is visible. Therefore, BCH as a whole, may be classified as a mixed alluvial-bedrock channel. However, a forcing mechanism from fallen woody debris may be responsible for the exposed bedrock.

While fluvial process can be inferred using the classification system and observed channel characteristics, they may not be sufficient in describing all the processes acting and interacting to shape the landforms found within the TCC recharge area as well as similar low-order streams overlying highly soluble bedrock. The main controlling variable of channel morphology of headwater streams can typically be attributed to the influence of the drainage basin's hillslopes and how frequently debris flows occur and deposit their sediments within the stream channel (Whiting and Bradley, 1993). However, owing to the fact that debris flows are probably rare at BCH, and that little else besides chert is found covering its bed, it is thought that channel morphology is not

Table 1.1. Channel and sediment characteristics at cross-sections surveyed in the Tumbling Creek Cave recharge area.

Reach-Station*	MC	q_{bf} (N m^{-2})	$\tau_{0,bf}$ (N m^{-2})	ω_{bf} (W m^{-2})	w_{bf} (m)	d_{bf}/D_{84s} (m m^{-1})	D_{16s} (mm)	D_{50s} (mm)	D_{84s} (mm)	D_{16ss} (mm)	D_{50ss} (mm)	D_{84ss} (mm)	S_b (m m^{-1})	S_w (m m^{-1})
BCH-1 (TL 1)	PB	1.37	56.3	109	7.03	9.54	18	37	74				0.009	
BCH-2 (GS)	PB	1.56	58.7	121	5.57	11.2			68§				0.009	
BCH-3 (TL 2)	PB	1.49	51.9	103	5.73	12.3	14	29	61				0.008	
BCH-4	PB	0.59	11.4	10.8	5.79	12.1			52§				0.002	
BCH-5	PB	0.39	8.8	7.1	5.82	11.1	12	24	43	2‡	15‡	35‡	0.002	
TCC-6 (GS)														
TCC-7 (TL 3)	PR	1.43	172	423	6.54	3.43	28†	71†	155†					0.033
TCC-8	PR	1.48	172	420	6.65	3.88								
TCC-9	PR	7.58	527	3000	8.19	14.3	13	43	93				0.077	
TCC-10 (TL 4)	PR	0.72	28.5	34.8	10.2	7.13	21	39	82	6‡	15‡	32‡		0.006
TCC-11	PR	2.96	753	7411	5.52	9.38	15	44	112				0.022	

TL = tracer line; GS = gauging station; MC = morphological classification (Montgomery and Buffington, 1997); PB = plane-bed, PR = pool-riffle; q_{bf} = bankfull discharge per unit width; $\tau_{0,bf}$ = bankfull bed shear stress; ω_{bf} = bankfull stream power per unit area; w_{bf} = bankfull flow width; d_{bf} = bankfull mean depth; D_{16s} = 16th-percentile surface grain size; D_{50s} = 50th-percentile surface grain size; D_{84s} = 84th-percentile surface grain size; D_{16ss} = 16th-percentile subsurface grain size; D_{50ss} = 50th- percentile subsurface grain size; D_{84ss} = 84th-percentile subsurface grain size; S_b = bed slope; S_w = water slope.
*Locations for BCH stations are shown in Figure 1.7; locations for TCC stations are shown in Figure 1.8.
§ Value is computed average using D_{84s} from adjacent cross-section stations.
†Representative of both cross-section stations (TCC-7 and TCC-8) because of their close proximity.
‡Sampling locations most closely coincide with cross-section stations.

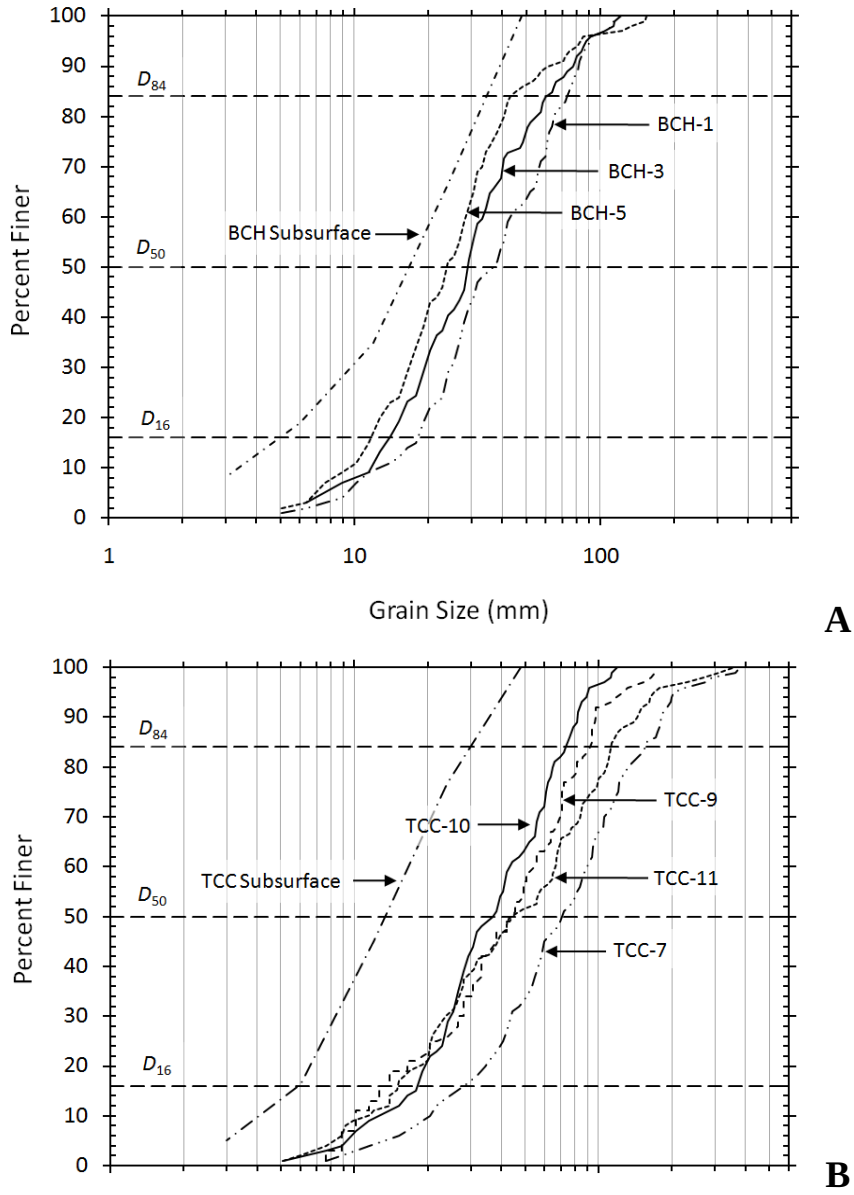

Figure 1.5. Cumulative grain size distribution curves for surface and subsurface sediment samples from (A) BCH and (B) TCC. Values for D_{16}, D_{50}, and D_{84} are given in Table 1.1.

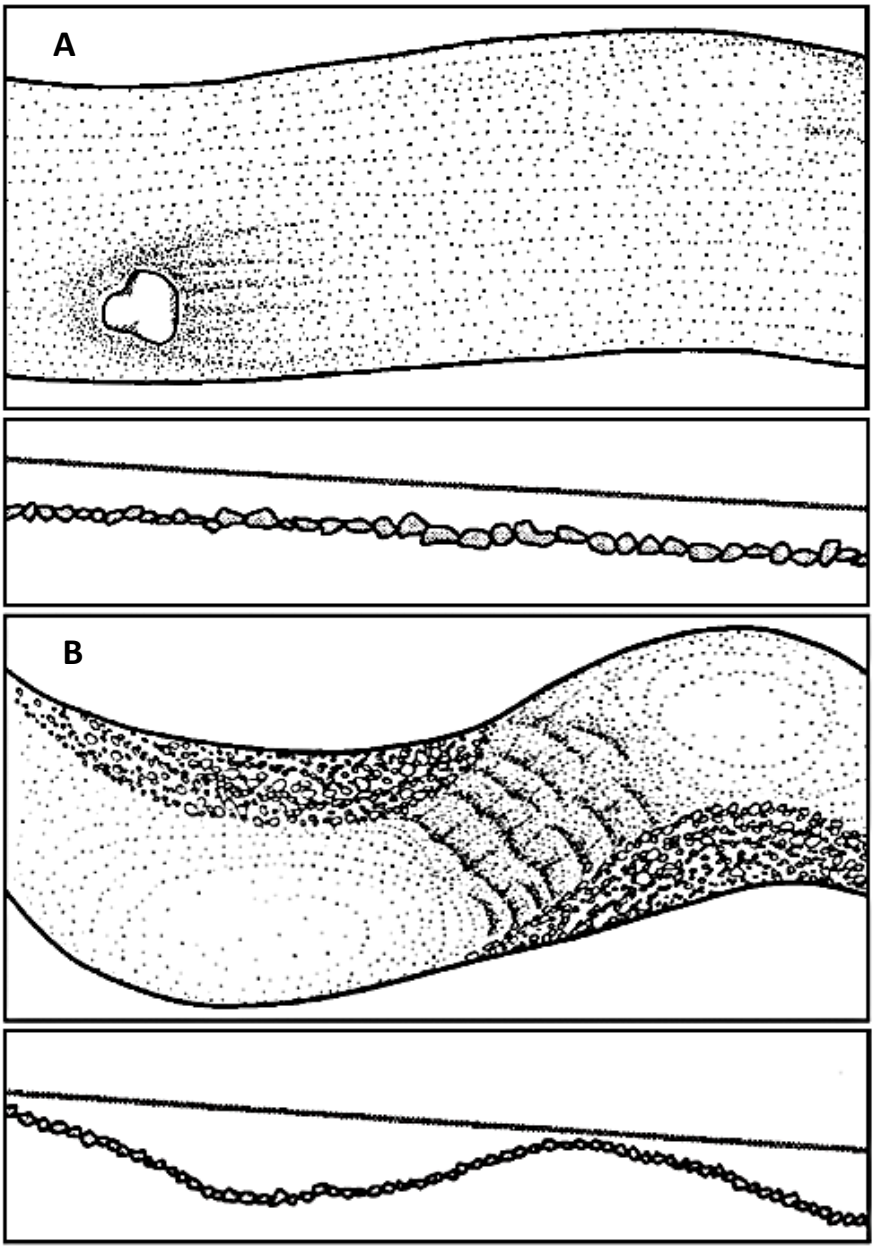

Figure 1.6. Schematic planview and longitudinal low flow profiles of channel classification types found within the TCC recharge area: (A) plane-bed channel showing single boulder protruding through otherwise uniform flow; (B) pool-riffle channel showing exposed bars, highly turbulent flow through riffles, and more tranquil flow through pools [after Montgomery and Buffington, 1997].

heavily influenced by hillslope processes. Rather, because of the soluble dolomitic bedrock, the surface of the TCC recharge area has valleys and channel morphology that are heavily influenced by the development of sinkholes which may be leading to the development of widened valleys. Moreover, widened valleys are minimally influenced by hillslope processes.

Within Tumbling Creek Cave itself (see Aley and Thomson, 1971), the most active process determining channel morphology is more related to the "hillslopes", which in the case of the studied cave reach are the cave walls. This is because the cave walls confine the stream almost everywhere throughout the mapped cave system. The difference between the cave and surface study reaches can be described using descriptions by Bunte and Abt (2001)–BCH being described as self-formed, and TCC being described as relict/non-fluvial.

Under the Montgomery and Buffington (1997) classification scheme, plane-bed reaches are distinguished by (1) long stretches of relatively featureless beds (i.e., no prominent bed forms), (2) lacking sufficient lateral flow convergence to develop pool-riffle morphology, (3) relatively low width to depth ratios and large relative roughness, and (4) dominantly gravel (2-64 mm) to cobble (64-256 mm) size bed materials. The dominant sources of sediment are fluvial, bank material, and debris flows, and the sediment storage element is overbank. Pool-riffle reaches, on the other hand, are distinguished by a rhythmic succession of bars, pools, and riffles. Pools are topographic depressions and bars are corresponding high points with pools typically spaced about every five to seven channel widths (may be more closely spaced if influenced by large woody debris as a forcing mechanism). They are composed of predominantly gravel sized bed materials. The dominant sources of sediments are fluvial, and bank material, while the sediment storage elements are overbank and bed forms. Slopes in pool-riffle

channels are generally lower than plane-bed channels, however, this does not seem to be the case in the reaches studied in the recharge area of TCC.

The BCH study reach (Figure 1.7) is primarily a plane-bed channel, but it does exhibit lateral bars marked by smaller grain sizes and higher elevations within the stream reach. This may warrant an intermediate classification as a riffle bar morphology type (see Montgomery and Buffington, 1997). Flow obstructions caused by woody debris and living plants also force reach morphology in a small percentage of the study reach, but do not exhibit a large effect on the tracers used for this study. Other reaches of BCH, however, have been observed to be nearly completely jammed with woody debris forcing local pool-riffle and bedrock channel reach morphology. Several fallen trees were removed from the upstream and downstream ends of the study reach and from adjacent reaches before the commencement of the current study. Removal of trees was thought to minimally impact stream reach morphology as many of those trees had only been within the stream for the winter season (with relatively low rainfall and snow amounts) following a heavy ice storm, and therefore, were not in the channel for a long enough period, or during intense enough storms, to have caused drastic changes in channel morphology.

Local bed packing arrangements such as pebble clusters may play a role in the entrainment process by acting like a large single grain and requiring relatively large hydrodynamic forces to initiate motion. Pebble clusters have been observed in both study reaches but only make up a small percentage of the bed, and along with the many interrelated variables influencing the entrainment process, the role that pebble clusters play was regarded as minimal and was not investigated further.

The TCC study reach (Figure 1.8) is a pool-riffle channel, but it is somewhat affected by local channel constrictions and expansions in the bedrock and from large

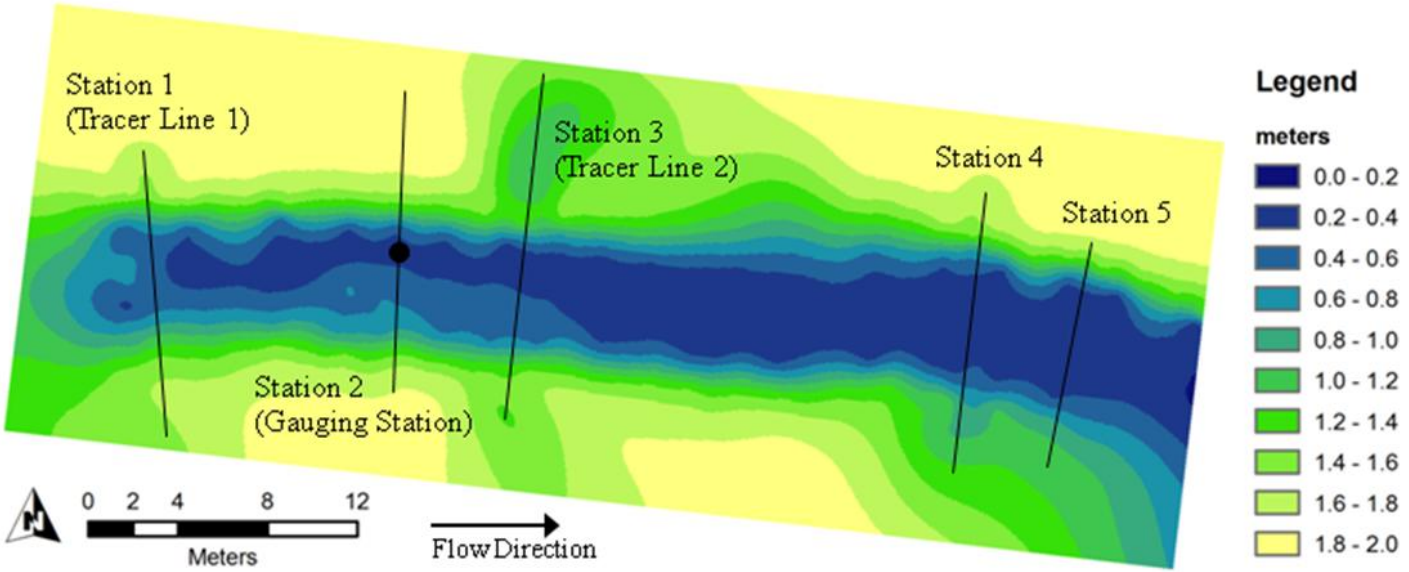

Figure 1.7. BCH study reach topographic map surveyed by total station on October 3, 2009 including 173 survey points created using the Topo to Raster interpolation function of the ArcGIS 3D Analyst tool. Contours are at 0.2 m intervals. The entire length of the reach is ~ 40 m. Cross-section stations and tracer line locations (black lines) and the location of the stilling well (black dot) are indicated. Flow is to the east.

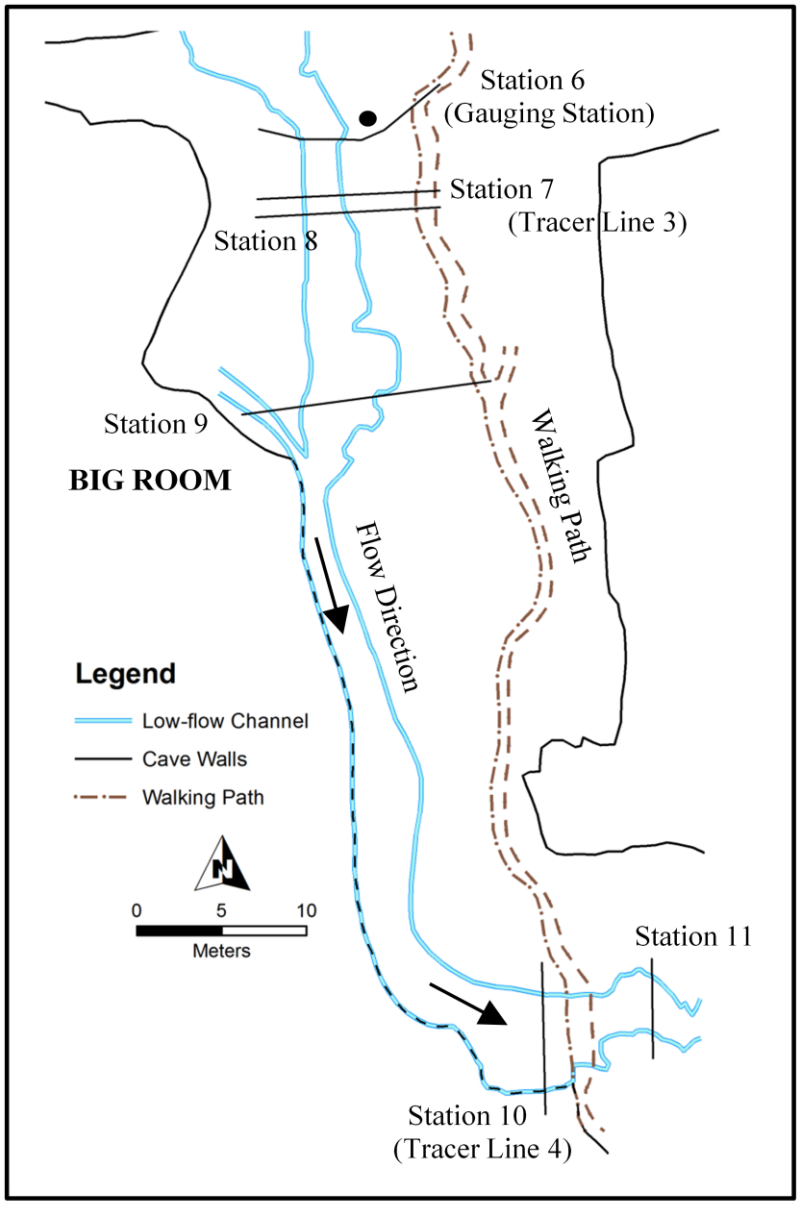

Figure 1.8. TCC study reach map showing the locations of cross-section stations and tracer lines (black lines across channel) and the location of the stilling well (black dot) at the gauging station. The entire length of the reach is ~ 70 m. Flow is to the south and east. [Modified from original cave survey in Thomson and Aley, 1971].

boulders originating from authigenic sources as breakdown within the cave. Both tracer seeding locations (discussed more in Chapter 3) are located atop riffles directly adjacent to pools on their upstream side. Tracer Line 3 (TCC-7) is located immediately downstream (~ 5 m) from the weir (see Figure 1.8) and a scour pit was created down to the bedrock on the downstream end of the weir after it was installed. The tracer line at this location may be influenced by turbulent eddies originating in the deep (~ 1 m) scour pit, and, in fact, three tracers have been observed to have moved upstream from their starting locations. However, under observed low flows, any presence of large turbulent eddies has dissipated once reaching the tracer line.

Tracer Line 4 (TCC-10) is located downstream of a small tributary entering the cave (see Figure 1.8) which is thought to increase discharge compared to that measured at the weir by less than 10% at any given time. This effect can be considered negligible and is not much larger than the error associated with discharge measurements themselves. No account for this increased discharge was considered for movement of tracers beyond its confluence with Tumbling Creek.

Prior Use of Tracers for Sediment Transport Studies

A commonly employed method for studying the dynamics of bed load movement involves introducing individual marked stones (tracer particles) to the stream bed and tracking their movements after high flows. This method has been developed in order to predict sediment travel distances (and therefore transport rates), selective sorting, critical entrainment thresholds, and deposition of bed material within stream reaches (e.g., Laronne and Carson, 1976; Hassan et al., 1992; Ferguson and Wathen, 1998; Church and Hassan, 1992, 2002; Ferguson et al., 2002). While their use for sediment transport studies has been extensive, with its beginnings in the mid-1960s (Hassan et al., 1984), the

use of tracer particles, however, has been limited to non-karst surface streams.

Tracer particles are ideal for studying sediment transport because of the logistical advantage and large quantity of information they provide (Wilcock, 1997a). They are well suited for studying the stochastic nature and spatial variability of bed load transport because they are based on a predetermined bed sample of individual grains, and they provide safety advantages because tracers can be seeded during low flows, thereby avoiding direct sampling during floods (Wilcock, 1997a). They have also been used to develop predictive models of sediment travel times, and therefore, virtual velocities, using a single critical discharge from peak flow estimates (e.g., Laronne and Carson, 1976; Hassan and Church, 1992; Ferguson and Wathen, 1998). For gravel-sized tracer particles, paint, magnets, and small radio transmitters have been used to track individual tracer particles (Hassan et al., 1992). Other methods used to measure bed load entrainment and transport are reviewed by Gomez (1991) and Hicks and Gomez (2003), and include the use of sampling devices, and bed load traps.

Determination of the entrainment threshold using tracer particles can be achieved by comparing the highest flows in which no displacement is observed and the smallest flows in which some displacement is observed (see Hassan et al., 1992). Calculation of transport rates using tracers requires an explicit statement of the relation between transport rate, entrainment and displacement length, or the virtual velocity of sediment (Hicks and Gomez, 2003). Wilcock (1997a, 1997b) presents a tracer particle-specific equation for steady-state transport rates, q_i, of individual sediment fractions of the form

$$q_i = M_i(N_i/T)L_i \qquad (1.1)$$

where M_i is the mass of fraction *i* entrained per unit bed area over the time period T, N_i is the number of times an individual grain of fraction *i* is entrained during T, and L_i is the mean length of a single displacement event. The expression of transport rate has units of

mass per length per time. At a single cross-section, the total transport rate can then be expressed as the sum of each fractional transport rate. If tracers are entrained only from the bed surface layer (assumed to be case in this study), then M_i is given by

$$M_i = m_i F_i Y_i / D_i^2 \qquad (1.2)$$

where m_i is the mass of a grain of fraction i, F_i is the proportion of fraction i on the bed surface before entrainment, D_i is fraction size, and Y_i is the proportion of surface grains of fraction i that are entrained over T. Because equation 1.2 represents entrainment from only the bed surface, it is likely to underestimate the entrainment of finer fractions at flows larger than those causing full mobilization (i.e., when $Y_i = 1$; Wilcock, 1997b).

Review of Sediment Transport Studies in the Ozarks

Past research on fluvial processes in the Ozarks have shown that streams tend to show similar characteristics, and that they are characterized by patterns of stable reaches followed by disturbance reaches (Jacobson, 1995; Horton, 2003). Stable reaches have trapezoidal shaped channels and are typically several kilometers long (on the larger rivers) with low sinuosities near 1.1, while disturbance reaches are areas of deposition and erosion with sinuosities near 1.5 over distances of a few hundred meters (Jacobson, 1995). Disturbance reaches are generally found along river segments with channels that are narrow relative to the valley width and may form as a result of collisions with the valley wall or because of sudden constrictions or expansions of valley width (McKenney and Jacobson, 1996).

Ozarks streams are likely affected by historical land-use factors that have resulted in gravel accumulations and their generally disturbed state (Jacobson, 1999; McKenney and Jacobson, 1996). Land-use factors include deforestation of the uplands during 1880 to 1920, open-range grazing, upland row-crop agriculture, riparian land-use changes, and

seasonal burning (Baumann, 1944; Saucier, 1983). The presence of sediment waves (resulting from land-use disturbance factors) has been observed by Jacobson (1995), Jacobson and Gran (1999), and McKenney and Jacobson (1996) from observations of stream bed elevation changes from 1920 to 1994. During that period, small drainage basins (<1400 km^2 area) had stream beds that generally stabilized, and elevations that generally decreased. Jacobson (1995) also hypothesized that the behavior of elevation changes related to gravel waves varied with reach-scale channel morphology and within channel network characteristics—disturbance reaches tending to show much more pronounced gravel waves than stable reaches (Jacobson, 1995).

Chapter 2

Theoretical/Empirical Basis

Critical Entrainment Threshold

Overview

The entrainment threshold is represented by equality between inertial forces (supplied by the flow of any fluid—water in this case) and gravity forces (given as the weight of the particle in question). When the entrainment threshold is met, conditions are considered critical and the initiation of motion results from any further increase in inertial forces. Shear stress (Du Boys, 1879), discharge (Schoklitsch, 1962; see Bathurst et al., 1987), and stream power (Bagnold, 1966, 1986) are commonly selected to represent flow conditions (as well as critical flow conditions) within open-channels (Gomez, 1991; Haschenburger and Church, 1998). Each of these three expressions can be incorporated into force-balance equations to express a relationship between flow conditions (hydraulic variables) and entrainment thresholds. The resulting relationships are sometimes referred to as flow competence equations. The competence of a flow is expressed as the diameter of the largest particle that can be entrained or eroded from a stream bed, and it increases with hydrodynamic forces of the flow, such as bed shear stress (Charlton, 2008). The concept of competence was originally introduced by Gilbert (1914) and has since been used by several researchers in constructing grain size entrainment threshold plots, based on the largest sampled bed load grain size transported (e.g., Baker and Ritter, 1975; Reid and Frostick, 1984; Komar, 1987; Lorang and Hauer, 2003; Thompson and Croke, 2008), or the largest displaced tracer particle moved after a storm event (e.g., Wilcock, 1971; Leopold and Emmett, 1981; Carling, 1983; Hassan et al., 1992; Wilcock, 1997a). Quantitatively defining competence, is most valuable for geologists as they attempt to

reconstruct ancient fluvial environments or events (e.g., Baker and Ritter, 1975) and for fluvial geomorphologists when evaluating the most effective or dominant flow conditions (i.e., bankfull channel forming flows), associated with a magnitude and frequency of sediment transport (Emmett and Wolman, 2001).

Shear Stress

Over the last several decades, many researchers studying gravel-bedded streams have used a standard or modified form of the critical dimensionless shear stress, termed the Shields parameter, to define the critical threshold condition for entrainment of a grain size of interest (Buffington and Montgomery, 1997). The standard Shields parameter, θ_{ci}, is defined as

$$\theta_{ci} = \tau_{ci}/[(\rho_s - \rho)gD_i] \qquad (2.1)$$

where τ_{ci} is the critical shear stress at the entrainment threshold for a grain size of interest, D_i (usually defined as the diameter of the intermediate (*b*-) axis of the median grain size, D_{50}; see Figure 2.1 for definition of grain axes), g is the gravitational acceleration, and ρ_s and ρ are the sediment and fluid densities, respectively. The Shields parameter, essentially the ratio of fluid motion and bed material stability forces at a critical value, has been shown to be fundamentally consistent with Coleman and Nikora's (2008) process-based expression of particle entrainment in describing averaged *en masse* threshold conditions.

Under quasi-uniform flow conditions (i.e., when flow depth is nearly constant with distance along the channel) the basal (bed, or boundary) shear stress, τ_0, or tractive force, averaged across the channel is expressed using the Du Boys (1879) equation as

$$\tau_0 = \rho gRS \qquad (2.2)$$

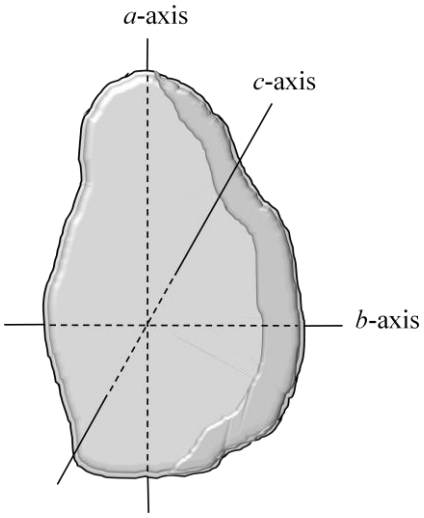

Figure 2.1. Illustration defining sediment particle axes and their mutually perpendicular angles of measurement.

where *R* denotes the hydraulic radius (ratio of cross-sectional area to wetted perimeter), and *S* the friction, or energy slope (typically approximated in field studies as the slope of the channel bed or water surface). Most investigators using the shear stress approach to assess entrainment replace *R* with the depth of water (*d*; depth-slope product approach) when calculating basal shear stress (e.g., Baker and Ritter, 1975; Andrews, 1983; Dogwiler and Wicks, 2004; Thompson and Croke, 2008). By using flow depth instead of hydraulic radius it can be shown that for a given unit area of the bed, or for various locations within a given cross-section, shear stress can be approximated using the depth-slope approach (Lorang and Hauer, 2003). Also, if width to depth ratios are large and therefore average flow depth closely approximates *R*, there is no difference between the two approaches. Furthermore, if channels have low width to depth ratios (i.e., streams are relatively narrow and deep), using the depth-slope approach is better suited to represent effective shear stress acting over bed materials, because the use of *R* includes stresses acting on the banks (as well as bed material) and represents total stream drag

(Komar, 1987). When flow depth is used, Andrews (1983) suggests that depth should be representative of the actual depth of the zone of maximum bed load transport when assessing entrainment threshold conditions.

Ashworth and Ferguson (1989) proclaim that the depth-slope product, using an average water surface slope and either the mean or thalweg depth is inappropriate in pool-riffle or braided channels because flow convergence and divergence causes local variations in shear stress, and because some of the total shear stress is dissipated as form drag associated with bars and pools. Bed form drag in natural rivers can comprise 10%-75% of the total channel roughness and if not accounted for, a significant difference between effective shear stress and actual shear stress, and overestimates of calculated θ_{ci} values, can result (Buffington and Montgomery, 1997). Strictly speaking, shear stress should be considered as the sum of two components: (1) the shear stress due to the resistance of the individual particles (effective, or grain, shear stress), the only one that should be considered in bed load entrainment, and (2) bed form resistance (Petit et al., 2005). Additionally, theoretical predictions of the Shields parameter are generally higher than field-obtained values, perhaps influenced by instantaneous, rather than time-averaged values (Buffington et al., 1992). To avoid these problems, Ashworth and Ferguson (1989) obtain at-a-point basal shear stress values from velocity profiles instead, calculated from friction, or shear, velocity, potentially improving estimates of effective shear stress.

The Shields parameter has been shown experimentally to be nearly constant ($\approx$ 0.060) on beds characterized by uniform materials in rough turbulent flow, with grain Reynolds numbers larger than 500 (Andrews, 1983; Bathurst, 1987a; Ferguson, 1994; Thompson and Croke, 2008); and the grain Reynolds (R_{e*}) number is expressed as

$$R_{e*} = (\tau_0/\rho)^{0.5} D_i/\nu \qquad (2.3)$$

where v is the kinematic viscosity of water, and D_i is a characteristic grain size of interest. However, a large body of literature exists, showing that values of the Shields parameter vary over a wide range (more than an order of magnitude) in natural gravel-bedded streams (e.g., Andrews, 1983; Komar, 1987; Buffington and Montgomery, 1997, Gordon et al., 2004). Thus, estimates of coarse bed load entrainment within natural streams characterized by non-uniform beds should not use a constant value of the Shields parameter for all grain sizes. This is due to many factors, many of which cannot be readily quantified in the field, including: grain size-specific friction angle, grain protrusion and hiding effects and mobility of neighboring grains (Buffington and Montgomery, 1997), as well as other factors, such as: the method used to define incipient motion (e.g., visual, competence, reference transport rate), grain characteristics (e.g., size, shape, orientation, density), bed packing arrangement (e.g., flood history, imbrication, and microtopography), and bed form resistance (Carling et al., 1992; Thompson and Croke, 2008).

The dependence of θ_{ci} on grain size is typically evaluated using a simple power-law regression of critical shear stress (τ_{ci}) against grain size (D_i), as

$$\tau_{ci} = a_1 D_i^x \qquad (2.4)$$

where x is the slope of the regression line and a_1 is the y-intercept on a log-log plot (Lorang and Hauer, 2003). Likewise, critical discharge, critical velocity, and critical stream power can be evaluated using the same analytical method. The relationship between hydraulic variables during entrainment and grain size, as presented in this way, is helpful in examining the difference in the overall bed material size as reflected in the coefficient a_1, and the degree of selective transport as reflected in the exponent x (Lorang and Hauer, 2003). Lower values of x represent a relatively larger degree of equal entrainment.

Using the standard Shields equation for estimating sediment entrainment, assuming a Shields parameter of 0.06 and a submerged weight density of sediment of 16,170 N m^{-3}, the critical shear stress required to move the median grain size, τ_{c50}, becomes

$$\tau_{c50} = 970 D_{50} \quad (2.5)$$

(with grain size measured in meters). This formulation relates to the movement of grains on a horizontal bed and is a simplification that does not apply to non-uniform beds with varying grain sizes. Several authors (e.g., Parker and Klingeman, 1982; Andrews, 1983; Komar, 1987) have demonstrated that variance in measured critical shear stress at the entrainment threshold of a grain size of interest can be reduced if normalized by the D_{50} of the bed; best quantified based on surface (rather than subsurface) grain size distributions (Buffington and Montgomery, 1997). This relationship is expressed by modifying the Shields parameter into the form

$$\theta_{ci} = \theta_{c50}(D_i/D_{50})^{-b} \quad (2.6)$$

(after Andrews, 1983), where θ_{c50} is the Shields parameter associated with movement of the median diameter bed material, D_{50}; and b is an empirical exponent found from the maximum particle size entrained in different flow conditions, measured using either bed load traps, tracer particles, or impact sensors. The relationship can be expanded to show shear stress in the equation, by incorporation with the traditional Shields equation, and after being modified algebraically (after Komar 1987), giving

$$\tau_{ci} = \theta_{c50}(\rho_s-\rho)g D_{50}^{\,b} D_i^{(1-b)} \quad (2.7)$$

Values for b have been found to range between 0.65 and 1 (Ferguson, 1994). When b equals 1 it means that the critical stress is entirely dependent on the relative size of particles rather than individual particle sizes, and the initial movement process is termed "equal mobility" by Parker and Klingeman (1982). In other words, the effect of hiding

and protrusion (whereby the larger grains on the bed act to hide smaller grains and the larger grains protrude into the flow increasing the exposed area of the grains) fully compensates for the effect of particle size (and weight) on particle mobility (Bathurst, 1987b). When values of b are less than 1, entrainment is size-selective and is expressed more closely by the traditional Shields curve (a value of b equal to 0 indicates pure selective entrainment). Observations from different streams and from different ranges of shear stress values have shown that entrainment is at least slightly size-selective at stresses up to twice the threshold for motion (Ashworth and Ferguson, 1989, Wilcock, 1992).

Several authors have empirically parameterized different values of θ_{c50} and b (see Buffington and Montgomery, 1997), based on data from flume studies and natural rivers with varying processes affecting entrainment. For natural channel beds, Komar (1987), suggests $\theta_{c50} = 0.045$ and $b = 0.60$, while Church and Hassan (2002) suggest $\theta_{c50} = 0.044$ and $b = 0.75$. For comparison, the standard Shields curve corresponds to values of $\theta_{c50} = 0.060$ and $b = 0.0$, while Dingman (1984) suggested parameter values $\theta_{c50} = 0.044$ and $b = 0.0$ (representing a mixture between the standard Shields values and what has been parameterized to include transport affected by hiding and protrusion. Buffington and Montgomery (1997) suggest a value of $\theta_{c50} = 0.040$ based on an extensive review of entrainment equations (Figure 2.2). The Shields parameter (θ_{ci}) plotted against relative grain size (D_i/D_{50}) using values from these investigators provides an indication of the variability observed in the entrainment process from stream to stream; it also has the benefits of being dimensionally homogeneous and it accounts for the particle density (in the θ_{ci} term; see equation 2.1), as well as the D_{50} of the bed material, thus making it easily transferable to other streams. Higher values for the θ_{c50} than those above are suggested where channel gradients are steep and where low relative depth (d/D_i) occurs because of

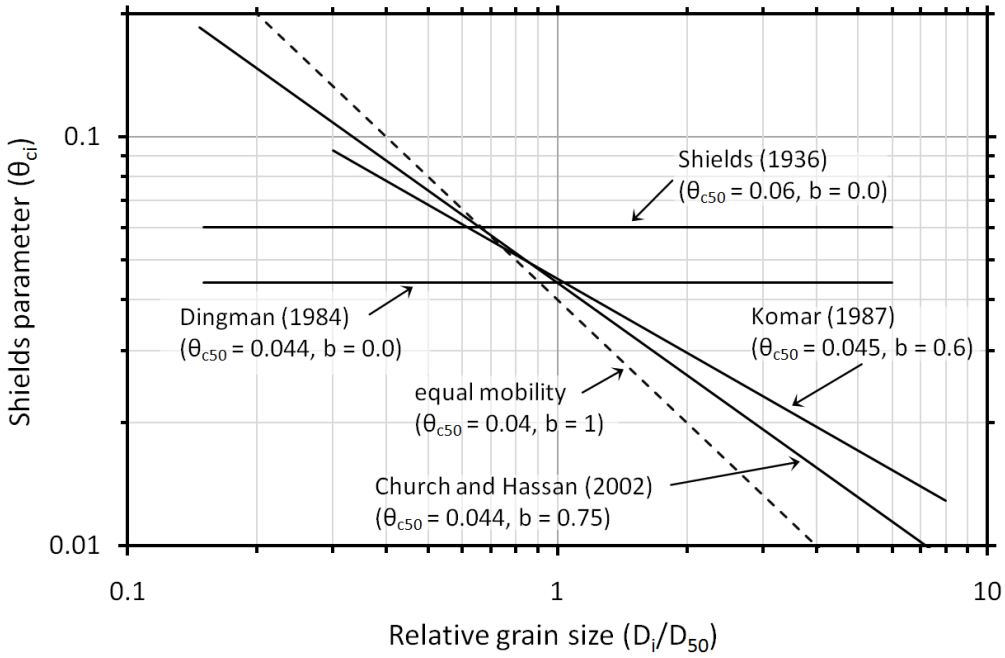

Figure 2.2. Relationships between the Shields parameter and observed maximum grain sizes entrained by the flow scaled by the median grain size of the bed material (dotted line is a theoretical relationship for an equally mobile bed where $\theta_{c50} = 0.04$ as suggested by Buffington and Montgomery, 1997). Church and Hassan (2002) use D_{50s}, while Komar (1987) use D_{50ss} data to characterize the median grain size. Dingman's form of the equation is included here because of its continued use. Both the Dingman (1984) and Shields (1936) equations represent fully size-selective entrainment ($b = 0.0$). Notice the logarithmic scaling of axes.

the development of surface structure and high flow resistance (Ferguson, 2005). Counter to this, when individual grains protrude from the bed by almost a complete diameter, Fenton and Abbot (1977) have shown experimentally that θ_{c50} values can be as low as 0.010.

Discharge

An evaluation of critical flow conditions based on discharge has been sought as a means of reconciling difficulties associated with monitoring mean flow depth accurately in shallow streams, and because discharge can immediately be estimated from gauged stream reaches (Ferguson, 1994). Bathurst (1987a) and Bathurst et al. (1987) argue that because entrainment conditions are not accurate using the traditional Shields approach (i.e., a constant value of θ_{ci}) where there is a low ratio between flow depth and grain size (d/D_i), entrainment criteria based on critical unit discharge (i.e., critical discharge per unit width) may provide more accurate predictions. For upland, or mountain stream reaches, characterized by steeply sloping beds, and cobble to boulder sized bed material with bed slopes ranging from 0.0025-0.1 (0.25%-10%), Bathurst et al. (1987) proposes an empirical relationship for the calculation of critical unit discharge expressed in dimensionless form as

$$q_c^* = q_c/[(gD_{16}^3)^{1/2}] = 0.21S^{-1.12} \qquad (2.8)$$

where q_c is the general critical unit discharge, D_{16} is the 16th percentile of the surface grain size distribution, and S is channel (bed) slope. This equation does not apply to the full range of grain sizes if it is large, meaning that it may only apply to the finer fractions (Bathurst, 1987b), and relative size effects are not included in the empirical relation.

As an improvement to the equation presented by Bathurst et al. (1987), Ferguson (1994) derives a generalized size-specific critical unit discharge for poorly sorted gravel-bedded streams that incorporates a flow-resistance relationship (Darcy-Weisbach) for critical discharge (after Schoklitsch, 1962), and the effects of hiding and protrusion of neighboring grains (relative size effects; after Andrews, 1983) that takes on the following form

$$q_{ci} = a_2 D_{50}^{3/2}(D_i/D_{50})^{(1-b)(c+3/2)}/S^{c+1} \qquad (2.9)$$

where q_{ci} is the critical unit discharge of a grain size of interest, a_2 is given by

$$a_2 = m_1(8g)^{1/2}(R_s\theta_{c50})^{c+3/2} \quad (2.10)$$

R_s is defined as the submerged specific gravity of the grains (usually = 1.65), c and m_1 are constants, derived from the power-law dependence of the Darcy-Weisbach friction factor on the relative flow depth d/D_{50} given as

$$(1/f)^{1/2} = m_1(d/D_{50})^c \quad (2.11)$$

and b is a hiding factor as before (parameterized following Andrews' (1983) equation). Following assumptions as described by Ferguson (1994), including $m_1 = 1.14$, $c = 0.37$ (parameterized from the modified Keulegan flow resistance equation after Thompson and Campbell, 1979), $b = 0.9$, $\rho_s = 2650$ kg m^{-3}, and $\theta_{c50} = 0.06$, this equation becomes

$$q_{ci} = 0.134D_{50}^{1.5}(D_i/D_{50})^{0.187}/S^{1.37} \quad (2.12)$$

Using four data sets from two reaches of a boulder-bedded tributary stream of the Roaring River, in Colorado (see Bathurst, 1987a), Ferguson (1994) tests the validity of equation 2.12 finding good agreement. Sensitivity analysis shows that the value of a_2 (and therefore q_{ci}) increases as almost the square of θ_{c50} (the variable in equation 2.9 corresponding with the highest degree of uncertainty). Figure 2.3 shows the trends of data plotted using a critical shear stress approach (Figure 2.2) determined by fitting trend lines to the data sets by log-log least-squares regression and solving for the values of θ_{c50} and b (these values are also presented in Buffington and Montgomery, 1997). Figure 2.3 also shows the same four data sets plotted using a critical discharge approach by taking the best fit values for θ_{c50} to solve for q_{ci} using equations 2.9 and 2.10.

It is also worth mentioning that Bathurst (1987a), when introducing a form for critical unit discharge, that incorporates relative size effects on entrainment, replaces D_{50} by D_r, the diameter of sediment that is unaffected by the hiding and protrusion effect. However, D_{50} is used ubiquitously, although there has been no consensus about whether

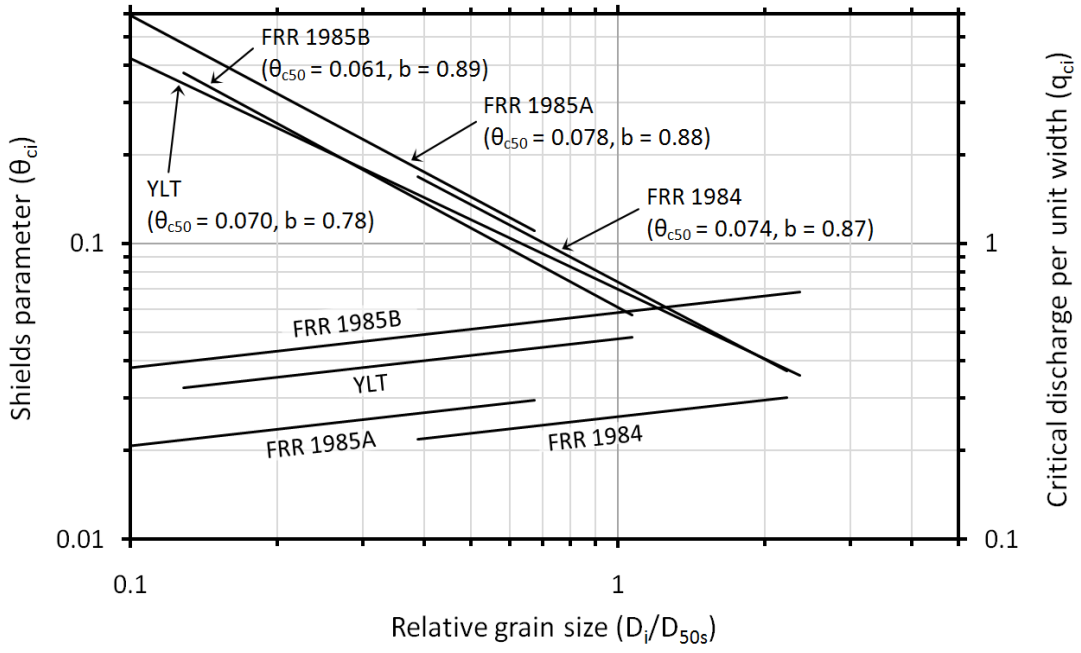

Figure 2.3. Relationships between the Shields parameter and observed maximum grain sizes entrained by the flow scaled by the median grain size of the surface bed material using data from Bathurst (1987a) for two reaches of the boulder-bedded Fall River in Colorado. YLT = Ypsilon Lake Trail, FRR = Fall River Road, and the year in which data was collected is indicated. Lines with a negative exponent (slope) are plotted using the scale on the left ordinate axis (θ_{c50}), and for each the θ_{c50} and b (hiding factor) values are given (plotted using equations 2.6; values are least-squares best fit after Ferguson, 1994). Lines with a positive exponent (slope) are plotted using the scale on the right ordinate axis (q_{ci}) and are obtained using the least-squares best fit values for θ_{c50} and then calculating q_{ci} using equations 2.9 and 2.10. Notice the logarithmic scaling of axes.

or not it should be taken to be the D_{50} of the surface layer (D_{50s}), or the D_{50} of the subsurface stream bed material (D_{50ss}). Also, Bathurst (1987a) suggests that the discharge be scaled by the active width of sediment transport rather than the flow width to obtain good results with his derived relationships (similar to relationships plotted in Figures 2.2 and 2.3), and Ferguson (1994) finds that a better agreement is found between field data and equation 2.12 if this is adhered to.

Stream Power

Bagnold (1966), in studies of sediment transport, originally defined stream power per unit area of the stream bed as

$$\omega = \rho g Q S / w = \rho g d S V = \tau_0 V \qquad (2.13)$$

where Q is mean cross-sectional discharge, w is water top width, and V is the mean velocity in the stream cross-section, and it has units of N m^{-1} s^{-1} (watts m^{-2}). Stream power can also be defined as the rate of potential energy expenditure or the ability of the stream to perform work (i.e., erode and carry sediments). A simple relation between the grain size entrained and critical stream power (ω_{ci}) was proposed by Bagnold (1980) and has been evaluated using tracer particles in natural streams by such authors as Hassan et al. (1992), and Petit et al. (2005). The Bagnold (1980) relation is given by

$$\omega_{ci} = \alpha_1 D_i^{1.5} \log_{10}(\alpha_2 d / D_i) \qquad (2.14)$$

where α_1 and α_2 are numerical constants, d is mean flow depth, and D_i is the diameter of mobilized particles; and d and D are in meters. Using $D_i = D_{50}$, Bagnold (1980) derived the following constants: $\alpha_1 = 290$, and $\alpha_2 = 12$. The units, however, are not watts m^{-2} because Bagnold failed to include gravity acceleration (Ferguson, 2005). Reid and Frostick (1985) observed in a river in southern England that (ω_{c50}) was 35-40 W m^{-2} for a gravel-bed stream with a D_{50} = 28 mm.

In order to obtain relations for critical stream power that could prove to be more useful, and are thought to be more representative of the physical processes occurring during entrainment (when compared to the relation of Bagnold), Ferguson (2005) derives two new general forms that (1) specify the grain size transported by the flow and the grain size which characterizes the bed roughness, (2) do not include depth as an independent variable, and (3) include a formulation for shear stress which incorporates the effects of hiding and protrusion. The relation based on the logarithmic flow resistance law, as presented by Ferguson (2005) can be written as

$$\omega_{\mathrm{ci}} = \frac{2.30}{\kappa}\rho(\theta_{\mathrm{cr}}R_{\mathrm{s}}gD_{\mathrm{r}})^{1.5}\log_{10}\left[\frac{30\theta_{\mathrm{cr}}R_{\mathrm{s}}}{em_2S}(D_i/D_{\mathrm{r}})^{1-\mathrm{b}}\right](D_{\mathrm{i}}/D_{\mathrm{r}})^{1.5(1-\mathrm{b})} \quad (2.15)$$

where κ is the von Karman constant (≈ 0.4), e is the base of the natural logarithm ($\approx$ 2.718), m_2 is treated as a numerical constant multiplied by D_{84}, (usually taken to be equal to 3 or 3.5 in gravel-bedded streams; Bettess, 1999; Recking et al., 2008) the product of which is used to denote roughness height (k_s) arising from the logarithmic flow resistance equation, and θ_{cr} is the Shields parameter for the grain size D_r unaffected by the hiding and protrusion effect (usually $D_r = D_{50}$, as was implied by Bagnold). Bagnold's (1980) equation for critical stream power was compared against field data using magnetic tracer particles in a natural stream by Hassan et al. (1992), who found that observed values were very close to the predicted values. Ferguson's (2005) form of the equation has not previously been tested against field data, but the incorporation of hiding and protrusion (relative size) effects and the replacement of depth with channel slope in the entrainment threshold relation are thought to improve the performance of the equation.

Grain Shape Adjustment for Entrainment

In order to objectively adjust the θ_{c50} for the effects of shape, and therefore, bed packing arrangement, Thompson and Croke (2008) use a lithology-averaged shape factor called the Corey shape factor (CSF; Corey, 1949). The shape factor is calculated as

$$\mathrm{CSF} = \mathrm{c}/(\mathrm{ab})^{0.5} \quad (2.16)$$

where the letters represent the length of the *c*-, *a*-, and *b*-axes of a representative sample of grains (all measured in the same units; see Figure 2.1). Once a base dimensionless critical shear stress (Shields parameter) is determined (i.e., estimated), that value is adjusted by multiplying it by the inverse of the CSF. Writing the equation introduced by Komar (1987) in terms of the CSF yields

$$\tau_{ci} = \theta_{c50b}/[\mathrm{CSF}(\rho_s-\rho)gD_{50}{}^{b}D_i{}^{(1-b)}] \quad (2.17)$$

where θ_{c50b} is a base Shields parameter for the D_{50} grain size and is approximately 0.03 for unpacked natural beds (Buffington and Montgomery, 1997). This value has been proposed by Parker (2008) as well when a pebble count (see Wolman, 1954) is used to measure the grain sizes on the bed surface.

Bed Slope Adjustment for Entrainment

The effects of bed slope may play an important role in the entrainment process in upland streams having high bed slopes, as was discussed above. This effect can be evaluated by using a correction to the Shields parameter (like grain shape) that involves an estimation of the angle of repose of the sediments in question. Smart (1984) found it necessary to use a correction factor to the Shields parameter only if the bed slope is greater than 2 or 3% (0.02, 0.03), assuming an angle of repose equal to 33°. The angle of repose generally varies from 30° for sand to 40° for gravel and may increase if grains are tightly packed (Garcia, 2008). Equations for entrainment on steeply sloping channel beds have been developed by Bathurst and Ferguson, among others, and were presented above.

Bed Load Transport

Bed load transport is the process by which sediment is mobilized by the flow and the particles move by sliding and rolling, and by saltation (when the particles hop up from the bed following ballistic-type trajectories; Garcia, 2008). The bed load is the fraction of the bed material load (Figure 2.4) that can only be suspended by the flow for intermittent periods (saltation) and may also be referred to as the traction load. The categorization of fluvial sediments can be dynamic and is dependent upon flow

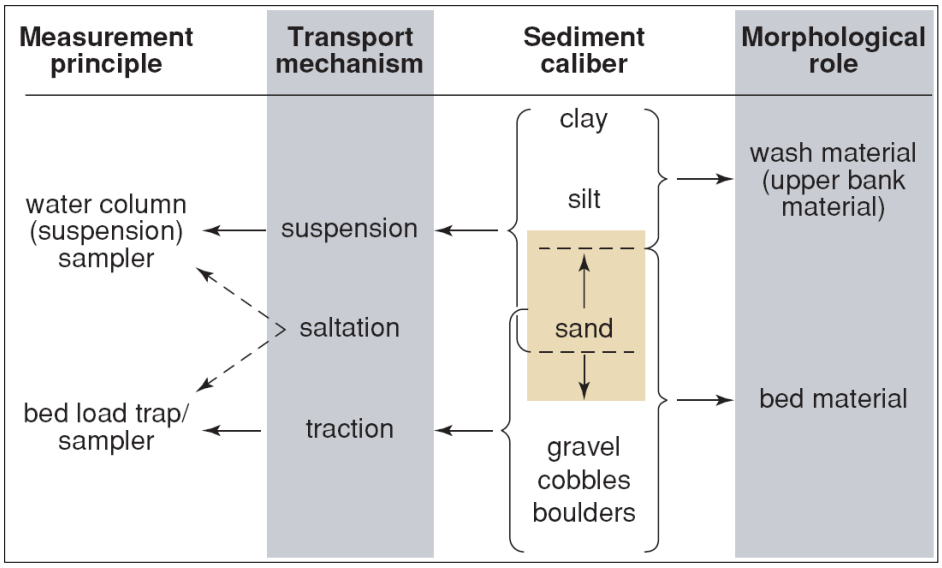

Figure 2.4. Categorization of fluvial sediments (sediment caliber/size) according to transport process, measurement principle, and morphological/sedimentary association [after Church, 2006]. Bed material is made up of the coarser sediment transported by a river and may move as bed load or intermittently as suspended load.

conditions, but large particles require rather rare and large flow events to become a part of the suspended load.

For both the development and testing of new bed load transport equations, the best information can be obtained through direct field observations (Garcia, 2008). It is apparent from a brief search of the literature on bed load transport, that many theoretical and empirical equations have been derived to describe and predict transport rates for coarse stream bed material. The most practical and common equations are empirical (although mechanistic forms produce similar results—same as for entrainment threshold equations) enabling prediction based on measurable features in the field. In the majority of transport equations, bed load transport rate scales either with basal shear stress to the 3/2 power or linearly with unit stream power beyond the critical entrainment threshold for motion (Whipple and Tucker, 2002). Other types of bed load transport equations

have been developed as functions of other hydraulic variables, including particle densimetric Froude number (dimensionless mean velocity; Aguirre-Pe et al., 2003), and discharge (Bathurst et al., 1987).

Bed load transport in gravel-bed streams is an intermittent, spatially variable, and stochastic process (Wilcock et al., 2009), causing estimates to generally have large uncertainties. Sources of uncertainty in estimating transport rates may arise from the use of a single threshold for motion (based on any measurable hydrodynamic force) for any given size of bed material, and the effects of partial transport, as well as when transport occurs in part of the channel even though the section-average basal shear stress is used (Wilcock et al., 1996). Partial transport occurs when some grains within an individual size fraction are active (entrained at least once during a transport event), and the remainder are immobile (Wilcock, 1997b). This partial mode of transport is accounted for by the use of the fractional transport rates presented here as equations 1.1 and 1.2 after Wilcock (1997a, 1997b). Another source of error may arise because of differences in channel geometry (across the stream), although this can generally be considered low within small streams when compared with the lateral heterogeneity inherent within larger streams.

Chapter 3

Methods

Field Procedures

Hydrological Measurements

In TCC, discharge has been monitored since the fall of 2002 at a 90-degree V-notch weir located in the Big Room (Thomson and Aley, 1971), at the upstream end of the study reach (Figures 1.8 and 3.1). The logger has been programmed to record temperature and water height (among other water quality parameters), at an interval of 10 seconds with 2-minute averaging during rapid changes in discharge (i.e., during storm events). During periods of low flow, the logger records at intervals no longer than 60 minutes, typically between 2 and 10 minutes.

In BCH, near the center of the study reach (Figures 1.7 and 3.2), a gauging station was installed on April 11, 2009 and has since been recording water height and temperature when stage values change by more than the instrument precision of ± 0.003 m. The pressure transducer and logger were manufactured by Global Water Instrumentation, Inc., and the sensor corrects for atmospheric pressure automatically. The logger was programmed to record measurements every 5 minutes during the beginning of the study period until July 31, 2009 when it was decided that hydrograph detail would be better observed by changing the recording interval to 1 minute (the interval used following July 31, 2009).

Rainfall data were taken from weather stations nearby TCC to correlate discharge with rainfall in order to carry out a frequency analysis, thereby providing a proxy for a historical discharge record. Within the TCC recharge area daily rainfall records from the MO-TY-15 Protem 3.0 NE rain gauge (36.57°N, -92.83°W; see Figure 1.1 for location)

A

B

Figure 3.1. (A) The TCC gauging station showing staff gauge and stilling well at the weir, directly upstream from study reach. A pressure transducer and data logger was used to record water height and temperature. (B) High flow event at the V-notch weir in TCC used to correlate stage with discharge. The discharge during the time the picture was taken was approximately 2.5 $m^3 s^{-1}$.

Figure 3.2. View of the BCH gauging station located approximately 10 m from the upstream end of the study reach, looking downstream to the east. A Global Water Instrumentation, Inc. WL16 pressure transducer was used to record water height and temperature during flow events. The sensor sits ~ 10 cm below the surface of the stream bed within the depicted 15 cm diameter PVC pipe (stilling well) installed in the thalweg of the channel. The stilling well is secured in place by a fence post attached to a tree trunk laid perpendicular across the channel. The average bank height here is approximately 0.71 m.

were obtained from the Community Collaborative Rain, Hail, and Snow Network (CoCoRaHS; see Cifelli et al., 2005), available on-line at http://www.cocorahs.org. Data sheets of precipitation provided by the CoCoRaHS volunteer, Dr. Richard Meyers were also used because they provided a longer record than is available on-line. A small percentage (6.9%) of record from the gage was missing daily rainfall measurements so

data from another nearby CoCoRaHS station (MO-FSA-213 Protem; 36.51°N, -92.80°W) were used to complete the record. Historical daily rainfall data were taken from the Lead Hill, AR (36.42°N, -92.90°W; U.S. Cooperative Network Station 034106) weather station; data are available from the National Climatic Data Center on-line at http://www.ncdc.noaa.gov/oa/ncdc.html. 5 to 30 minute interval rainfall data were also taken from the Forsyth, MO (36.68°N, -93.11°W; DanO's Place) weather station; data are available from the Weather Underground on-line at http://www.wunderground.com. The distances between the MO-TY-15 Protem 3.0 NE rain gauge (located within the TCC recharge area) and the other weather stations is as follows: to Forsyth—27.9 km; to Lead Hill—17.8 km; and to MO-FSA-213 Protem—7.2 km.

Stream Channel Surveys

Cross-section data were gathered at five stations in the BCH study reach, and six stations in the TCC study reach, using standard surveying techniques with the use of a measuring tape, stadia rod, pocket transit, and automatic level and total station. At the gauging stations, stream cross-section data were gathered for the estimation of in-channel flows in BCH, and for estimating flows that exceed the capacity of the weir (i.e., when water spills over its top) in TCC. Several stations were surveyed more than once to capture the effects of flow events capable of rearranging the channel bed, and to observe differences in channel geometry associated with seeding tracer particles (see Appendix A). Each cross-section survey line was conducted as close to perpendicular to the stream banks as possible and every break in slope was identified. The original cave survey completed in 1971, by Ken Thomson, Don Rimbach and members of the Heart of the Ozarks Grotto (Thomson and Aley, 1971), has been utilized as the base map for the locations of cross-sections surveyed during this study (see Figure 1.8). A survey of the

BCH study reach was also conducted using a Sokkia SET300 Total Station with a mean point precision of better than ± 0.005 m. The total station survey was conducted on October 3, 2009 and provided a high resolution topographic map of the channel geometry, and cross-sections. It was also utilized as the base map for the locations of cross-sections (see Figure 1.7) and made it possible to get more precise measurements of channel slope.

Along the thalweg of the study reaches, channel bed slope was measured with a tape and automatic level. In BCH, bed slope averages from point measurements made during the total station survey were compared against those measured using the tape and it was determined that the total station measurements would be most accurate. Slope measurements of the bed extended 2 to 3 channel widths in BCH and only 0.5 to 1.5 channel widths in TCC, due to abrupt changes in slope. In TCC water surface slope measurements were also made at the two tracer line stations. Water surface slope measurements were used for all calculations of hydraulic variables in TCC, as they are preferred over bed slope because the water slope usually represents the slope of the energy line more closely.

Grain Size Distributions

Stream bed sediments found on the surface at each tracer line and at three more selected cross-sections downstream of the tracer lines (see Figure 1.5) were measured to determine the D_{84s}, D_{50s}, and D_{16s} sediment sizes, to provide estimates of channel roughness, and to select grain size distributions for tracer particles that closely represent the sediments naturally occurring on the bed. The length of the intermediate (*b*-) axis of 100 clasts was measured to the nearest millimeter using calipers and a tape measure for

larger grains. Sediment particles were selected from the bed using the pebble-count method (Wolman, 1954), centered over the cross-sections.

In order to determine the Corey shape factor (CSF) for the tracer particles, measurements (using a caliper) of three mutually perpendicular particle axes: the longest (*a*-axis), the intermediate (*b*-axis), and the shortest (*c*-axis; Figure 2.1), of a small sample (50 grains) of bed material selected randomly from the bed of BCH, were made.

Grain size data for subsurface stream bed material (clasts found directly beneath the surface layer of the bed) were sampled from BCH, directly downstream of the study reach (~ 10 m below BCH-5). Sediments from the sampling site are similar to sediments found within the study reach itself. Subsurface sediments sampled from TCC were gathered from within the study reach (~ 2 m above TCC-10). Although, the subsurface sediment samples were taken from a pool and a bar, whereas surface grain size data were taken from riffles and a bar. Each sample was taken from the active stream bed at depths no greater than 0.5 meters beneath the surface layer.

Subsurface grain size distributions were obtained by using a Ro-Tap Testing Sieve Shaker (Model B) with standard mesh sizes in order to obtain D_{84ss}, D_{50ss}, and D_{16ss}, sediment sizes, enabling comparison between the subsurface and surface grain sizes, and between study reaches. Shaking commenced for 10 minutes for all samples. Three samples of approximately equal weight were analyzed from each study reach (BCH and TCC) and average weight values for each grain size were calculated for analysis and used to determine D_{84ss}, D_{50ss}, and D_{16ss} sediment sizes. Total weight of sediment sieved was 4.22 kg and 6.65 kg for TCC and BCH, respectively. Grain size distributions from sieving were truncated on the smaller end at a mesh size of 2 mm and at the larger end at a mesh size of 32 mm. Grain size distributions were extended by one phi-size class (mesh size equal to 32 mm) by measuring the *b*-axis of the largest grains after sieving.

During the sieve analysis, particles were weighed dry by phi-size class and their volumes were obtained by submerging them in a known volume of water. Density was calculated for each phi-size class using these measurements. Sediment density for the largest two phi-size classes (clasts with *b*-axis diameters between 16 and 64 mm) were then used as the basis for the density of the tracer particles. Instrument precision resulted in density values with errors of approximately ± 5%, accurate to ± 0.12 kg m^{-3}.

Tracer Particles

Painted tracers were selected over other tracing techniques because the primary interest is the entrainment from the bed surface layer and because flow depths were low or non-existent (in BCH) during displacement measurements allowing for thorough searches of the channel. Tracer particles seeded in both BCH and TCC were randomly selected from the BCH stream bed (downstream of the study reach) and measured to be separated into half-phi size classes (Table 3.1). The selection of the grains used as tracers from within the watershed is ideal because tracers are supposed to represent the natural sediment and its movement. The original tracer particle distributions were designed to include several half-phi sized classes, representative of the local bed surface grain sizes extending from below the D_{50} at least up to the D_{84}. Figures 3.3 and 3.4 are plots of grain size distributions for tracers at each tracer line along with distributions of the naturally occurring sediment for comparison.

Once tracers were collected, they were transported to the on-site field house (owned by the OUL) where they were painted with a single coat of reflective red paint and marked on one side using white paint with either a letter, or a number, as an identifier. The paint used was reflective safety paint and is non-toxic so that no aquatic

Table 3.1. Number of tracer particles in each half-phi size class and the total number of tracers seeded at each tracer line.

Reach-Station	>128 mm > -7 ϕ	>90 mm > -6.5 ϕ	>64 mm > -6 ϕ	>45 mm > -5.5 ϕ	>32 mm > -5 ϕ	>23 mm > -4.5 ϕ	>16 mm > -4 ϕ	Number of Tracers
BCH-1			20	40	40	40	60	200
BCH-3			10	20	20	20	40	110
TCC-7	20	20	40	40	40	60	60	280
TCC-10			10	15	15	20	20	80

organisms inhabiting the cave system were harmed. At Tracer Line 1 (BCH-1), Tracer Line 3 (TCC-7), and Tracer Line 4 (TCC-10), tracers were labeled using letters, while at Tracer Line 2 (BCH-3) tracers were labeled using numbers to avoid the possibility of misinterpreting the source of tracers, because Tracer Line 2 is so close to Tracer Line 1. The white identifier was the same for each tracer in a given half-phi size class. The use of red paint for tagging tracer particles worked very well in this study even in the poor lighting of the cave. Other more elaborate methods of tracing individual particles involve the use of magnets and radio frequency identification (RFID) techniques. Their development has generally been attributed to the desire to increase recovery rates. For this study, however, it was decided that the possibility of decreased recovery rates was outweighed by the increased time and money required to drill and insert small magnets or radio identification tags. For shorter study periods (less than one year), like this one, it was believed that the recovery rates would not significantly affect the results.

Because recovery rates for painted tracers have been observed to be lower for small fractions due to their preferential burial (e.g., Laronne and Carson, 1976; Ferguson and Wathen, 1998), the number of tracers in the smallest fraction was increased relative

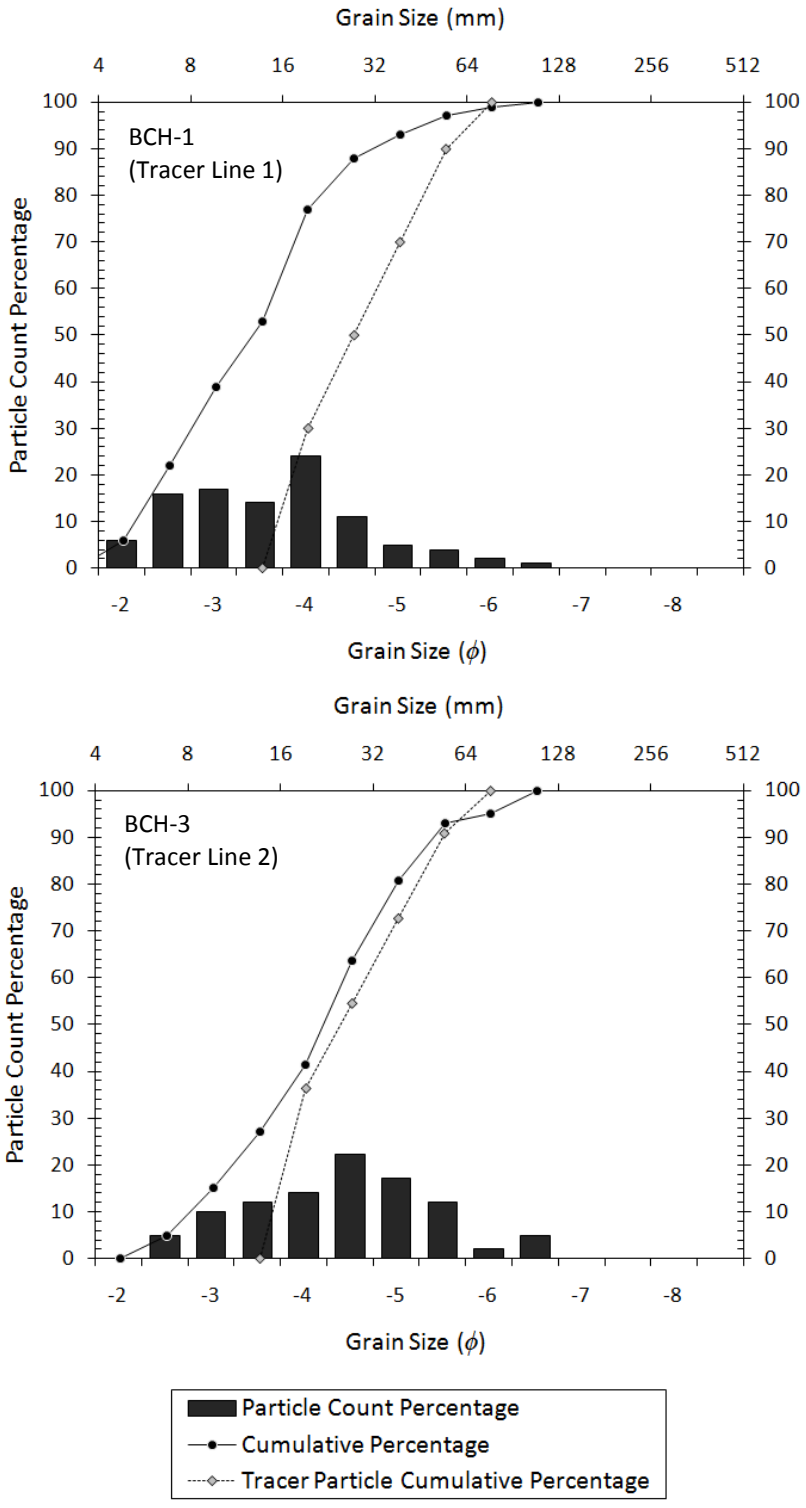

Figure 3.3. Grain size distributions for tracer particles and naturally occurring sediments at tracer lines within the BCH study reach. Only the cumulative curve is shown for tracers.

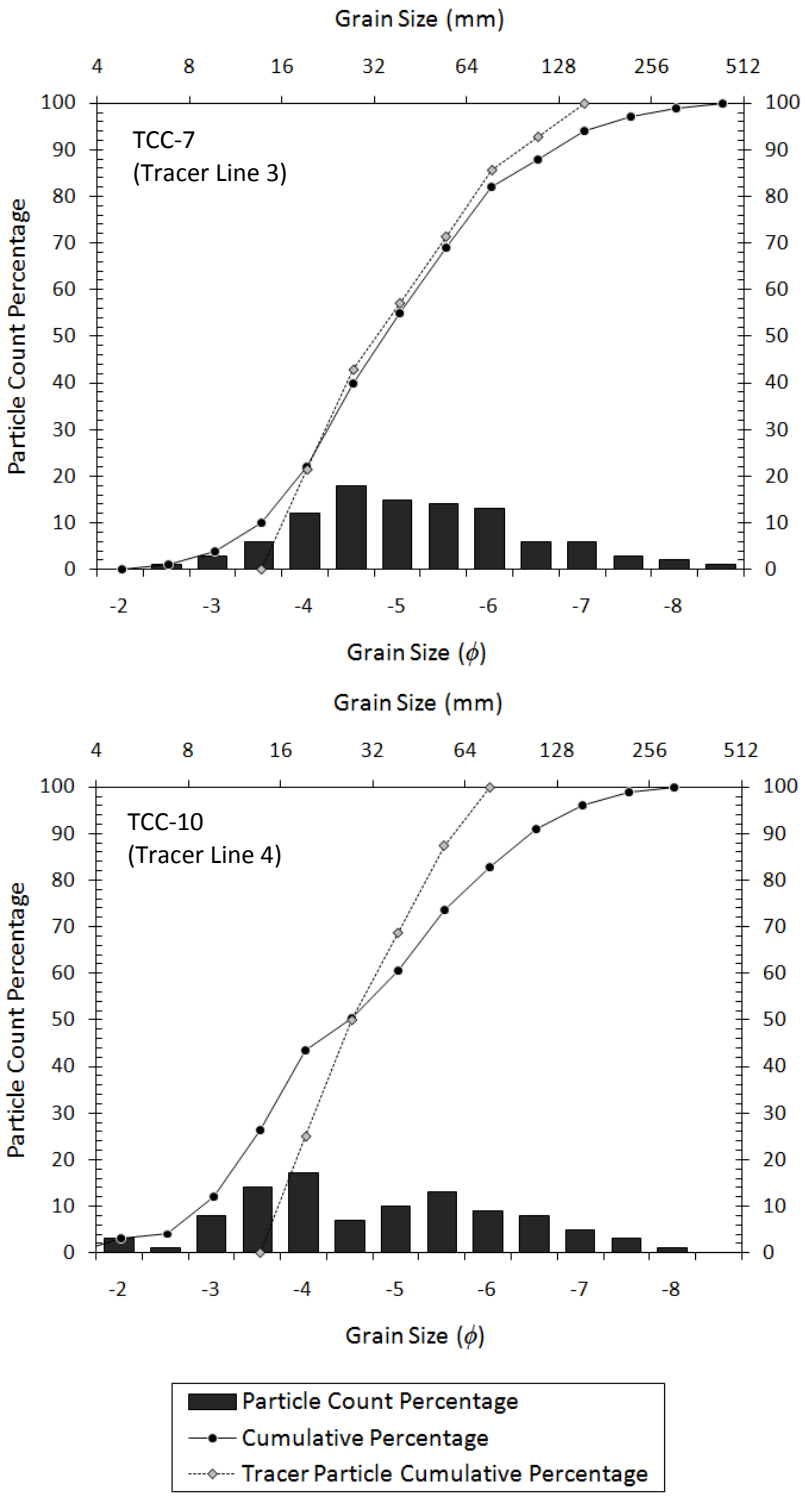

Figure 3.4. Grain size distributions for tracer particles and naturally occurring sediments at tracer lines within the TCC study reach. Only the cumulative curve is shown for tracers.

to the larger fractions. Likewise, the number of tracers in the largest fractions was decreased relative to the smaller fractions in the middle of the grain size distributions (see Table 3.1 for tracer distributions). In all, a total of 670 tracers were utilized during the study at four tracer line cross-section stations. This number is likely to represent the movement of the natural stream sediment because the streams studied are small (Hassan and Church, 1992), armoring is observed (i.e., the surface grain sizes are larger than the subsurface grain sizes), and the number of tracers per half-phi size class is comparable to the population sizes used by Ferguson and Wathen (1998) who studied a larger river (Allt Dubhaig in the Scottish Highlands with a peak discharge of greater than 20 $m^3 s^{-1}$ during their study). Ferguson and Wathen (1998) used 40 tracer particles per half-phi size class because it was estimated in a previous study, by Drew (1992), that a mean travel distance standard error of ~ 15% could be achieved and that any systematic effects of grain size on mobility could be detected.

Tracer particles were seeded loosely on the surface along the length of a single cross-section (tracer line) in each study reach (BCH-1, and TCC-7) on May 9, 2009. While it is common to replace a volume of sediment from the bed with tracers, that approach was avoided here, because within TCC there are several benthic organisms living on the stream bed material, including the endangered cavesnail that is known only to TCC. Second tracer lines were seeded on August 30, 2009 and November 7, 2009 at TCC-10 and BCH-3, respectively. Each particle was placed more or less randomly while also trying to achieve an even distribution of half-phi size classes across the width of the channel. In TCC, tracer line stations were chosen where it was likely that moderate to high floods would result in the movement of tracers, and also in locations where plenty of downstream passage existed that was open enough to conduct surveys of tracer displacements. In the BCH study reach, sites were chosen randomly as the channel

geometry and bed materials were rather homogeneous. The study reach was selected because of its rather straight channel and the presence of a thick ($\geq$ 0.5 m) bed of sediment.

Field measurements of tracer movement distances (displacements, or step-lengths) were conducted using a tape measure either held in place, or laid across the stream bed (for large displacements in BCH), and were made in the longitudinal (parallel with the channel) direction only. Some tracer displacements were also measured using the Analysis Tool within Adobe Photoshop CS3 and stitched-together photo mosaics created using a digital camera with vertical pictures taken across tracer lines. Displacements (step-lengths) of transported tracers were referenced to tracer starting lines marked by two red reflective metal stakes at the ends of the station cross-sections. The starting lines have been defined to be lines on the downstream side of all seeded tracers (no more than 10 cm from the nearest tracer) prior to a competent flow event. In TCC the starting line locations have not changed during the study period, while at BCH-1, the starting line has been relocated approximately 0.5 m downstream after two large flow events (October 8th and 29th, 2009) that transported nearly all tracers. The starting line in the BCH was then defined as a line connecting the end points of the cross-section that was later surveyed on December 18th, 2009.

Measurements of the movement of tracers identified in the field to have moved since the last site visit (movement past the starting line) were made with a precision of 1 cm with a tape measure and Adobe Photoshop CS3. Some site visits were made after two flow events occurred, in which case it was assumed that the largest flow event before the survey date had caused all of the observed sediment transport. Once a competent flow event occurred tracers were typically returned to the starting line where they were re-seeded in the same manner that they were at first seeding. Although, in two cases (flow

events of May, 26th and October 8th, 2009) tracers were not returned to the starting line in order to provide an indication of the effects of seeding tracers loosely, and unnaturally, on the bed. Some investigators have argued that grains placed unnaturally on the stream bed have a higher propensity to be mobilized, and that once they have moved to more natural locations higher flows will be required to entrain them (e.g., Hassan et al., 1992). The random seeding on the bed in a group (centered over the cross-section) is thought to have acted to make initial movement reflective of natural transport of surface grains.

Data Analysis

Estimation of Hydraulic Variables

Evaluating entrainment and transport based on hydraulic variables first required estimates of cross-sectional velocity (V) and discharge (Q) from water height measurements. The approach used was necessary because low to moderate flows with minimal bed load transport were observed during site visits. Within TCC, Q was calculated at the gauging station as a function of water height (based on a weir coefficient) by staff of the OUL. During the study period, some flow events were not recorded in TCC, so a linear least-squares trend line was fitted to flow data from TCC, plotted against corresponding estimated flow within BCH (Figure 3.5) in order to provide estimates of peak flows for missing data. Within BCH the function used to estimate Q is based on field data from several natural stream channels at 50 sites in California during varying flow conditions, in which Manning's n (roughness coefficient) was determined by Limerinos (1970). The incorporation of Limerinos' equation into the logarithmic flow resistance equation was derived algebraically by Bettess (1999), and is written as

$$Q = VA = [(31.9gRS)^{0.5}\log_{10}(11.4R/k_s)]A \qquad (2.18)$$

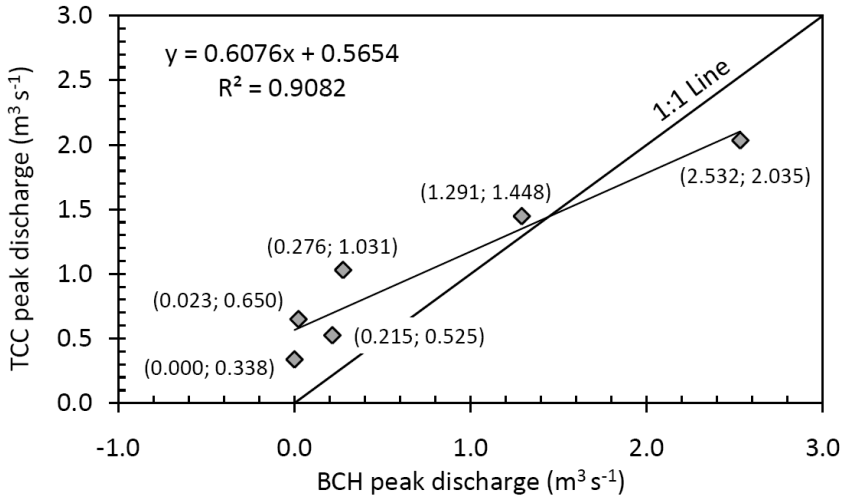

Figure 3.5. Relationship between six available peak discharge measurements from TCC matched with estimated peak discharge from BCH for the same flow events during the period from 9/22/2009 – 3/21/2009. The linear function fitted to the data is used to estimate discharge in TCC where data are missing (May – January, 2009). The figure also shows that Tumbling Creek continues to flow when BCH is dry, and when flow in BCH becomes greater than approximately 1.5 $m^3 s^{-1}$, its flow exceeds that in Tumbling Creek. The x and y values, respectively, are provided for each point in parentheses.

where all variables have previously been defined. Roughness height (k_s) was set equal to $3.5D_{84s}$. This equation was also used to determine flow height during peak flows at tracer line cross-sections in TCC (explained later in this section). The form of equation 2.18 provides identical estimates of Q if the Limerinos-Manning equation, with a roughness height = $3.0D_{84s}$, is used. When roughness height is larger than $3.0D_{84s}$, it indicates the presence of a smaller laminar sublayer and relatively large turbulent viscosity due to increased channel roughness (caused by channel bank curvature, woody debris, or other flow obstructions). In both study reaches the average cross-sectional velocity is thought to be approximated best when k_s equals $3.5D_{84s}$, because of the presence of vegetation and woody debris within BCH and abrupt channel contractions and expansions as well as more drastic channel curvature in TCC. The Limerinos (1970) equation was selected

because it has performed well against tests using experimentally and field derived data from a variety of streams (Bray, 1979; Recking et al., 2008), and because other empirically derived equations applied to low-order streams (e.g., Jarrett, 1984), give very low discharges due to an over estimation of roughness (Thompson and Croke, 2008). Furthermore, other equations that are used to predict mean velocity from knowledge of the hydraulic radius, bed material size distribution, and slope, give similar results (see, Bettess, 1999).

Discharge per unit flow width (q), bed shear stress (τ_0), and stream power per unit area (ω) were calculated for each tracer line cross-section from the reach discharge (determined using equation 2.18 at the gauging station in BCH) and input from measured channel geometry, hydraulic roughness and local bed slope, and the assumption that water mass is conserved (i.e., Q is constant throughout the study reach). The technique used was a trial-and-error approach, where water height within the surveyed cross-section of interest was varied and discharge was solved using equation 2.18 until the computed discharge was in close agreement ($< \pm 0.01$ m^3 s^{-1}) with the discharge at the gauging station (for both BCH and TCC). Using survey data, cross-sections were digitized in ArcGIS v. 9.2 and hydraulic radius, wetted perimeter, mean depth, and flow width were determined for the optimum flow heights. This process was carried out for peak flow event discharges only, because it was assumed that entrainment occurs during peak flow. Bankfull discharge was also calculated using equation 2.18, with bankfull determined as the minimum width to depth ratio of the cross-section (break in slope at top of channel), except at TCC-10 where it is taken to be at the maximum height of fine-grained deposits.

Once water height was determined, discharge was divided by flow width to determine q, and divided by the active width (width of the bed actively transporting sediment) to determine q_{aw}. Bed shear stress was computed using equation 2.2. The

hydraulic radius approach to shear stress was used (in place of the depth-slope approach) because the width to depth ratio was large (> 11) for all measured peak flow events and the percentage difference between R and d was low ranging from -2.9 to -9.0%. Also, because R was always lower than d, the use of R acts to minimize differences between the effective shear stress acting to entrain material from the bed and the average bed shear stress (τ_0). Stream power (ω) was defined earlier as given by equation 2.13 and was calculated using the product of the bed shear stress and the estimated mean cross-sectional velocity, calculated from equation 2.18 and divided by the cross-sectional area. The stream power used reflects the choice of the shear stress (R instead of d), so that the values for ω are somewhat lower than they would be if mean depth (d) was used.

Flow Competence

The largest grain size of observed mobilized tracer particles was paired with peak flow estimates of hydraulic variables, including discharge per unit width, bed shear stress, and stream power per unit area to determine competence at each tracer line cross-section. Competent flow conditions were defined here to be the flow capable of moving tracer particles beyond the starting line, although entrainment of grains that did not move past the starting line was also determined from semi-vertical photographs. A least-squares regression of the competence data for each hydraulic variable was carried out to quantify the scatter in the observations and to make comparisons of how well each hydraulic variable performed. Grain size was taken to be half-way between phi-sizes, for instance, if the largest tracer entrained was between 64 and 90 mm, it was assumed that the clast had a b-axis of 77 mm. Because of the division into half-phi size classes, there is some uncertainty as to the actual size of entrained tracers, and the uncertainty increases with entrainment of larger fractions (because of the logarithmic scaling of half-phi size).

Rainfall and Discharge Correlation

Rainfall and peak discharge data were examined to determine if a correlation exists, and to provide the basis for estimates of the frequency of sediment transporting flow events in the studied stream reaches using an 81 year rainfall record. Four variables of rainfall were obtained for rain events during the study period coinciding with each flow event in the surface and cave streams, and then were regressed against the magnitude of the peak flow. The four variables examined were (1) total event rainfall (using daily rainfall totals, from between 1 to 3 days), (2) peak rainfall intensity (5 to 30 minute interval data from Forsyth weather station), (3) daily rainfall, and (4) previous 30 day total rainfall. Daily values of rainfall were taken from the MO-TY-15 Protem 3.0 NE rain gauge within the TCC recharge area when making the correlations.

Bed Load Transport Rate

Bed load transport rates were assessed using field observations of tracer displacement lengths (from photographs and field measurements) which were determined from equations 1.1 and 1.2 (Chapter 1) at each tracer line cross-section after competent flow events. Equation 1.1, defines transport rate for any grain size of interest as

$$q_i = M_i(N_i/T)L_i \qquad (1.1)$$

where M_i is the mass of fraction *i* entrained per unit bed area over the time period *T*, N_i is the number of times an individual grain of fraction *i* is entrained during *T*, and L_i is the mean length of a single displacement event. Since observations were taken from only the bed surface layer, M_i is represented by equation 1.2 as

$$M_i = m_i F_i Y_i / D_i^2 \qquad (1.2)$$

where m_i is the mass of a grain of fraction *i*, F_i is the proportion of fraction *i* on the bed surface before entrainment, D_i is fraction size (*b*-axis dimension), and Y_i is the proportion of surface grains of fraction *i* that are entrained over *T*.

Although equations 1.1 and 1.2 are written to allow for transport rates of a grain size fraction of interest, only the average transport rate (including all transported size classes) was calculated. The mass of the tracers (m_i) was calculated by assuming that each clast has a volume represented by a rectangular solid with relative dimensions given by the average grain dimensions relative to the *b*-axis, with the *b*-axis equal to the half-way point of tracer phi-size, and then multiplied by the average density of the grains measured during the sieve analysis. On average (from 50 grains), tracer particles have *c*-axis dimensions of 0.66 and *a*-axis dimensions of 1.48 times the *b*-axis, giving an average volume of sediment equal to 0.98 times that of 1 ml water at 20°C. Tracer phi-size in this case was taken as the modal grain size entrained. Representing the grains as rectangular solids will tend to increase transport rates because the grains are somewhat rounded, but most grains can be approximated as such, because they are subangular.

The number of tracers entrained during flow events (N_i) was determined from comparison of vertical photographs taken over the starting line before and after competent flow and counted using Adobe Photoshop CS3. Mean displacement length over a single tracer event was determined from both photographs and field measurements and was defined using tracers that were transported past the starting line.

Flow event duration (T) was originally approximated as the period of time spanning the entire flow event (defined as the beginning of flow to a flow rate of zero in BCH, and the beginning of flow to a flow rate equal to one-third of peak flow in TCC). However, it was decided that a flow duration T of 5 hours be used for the calculation of transport rate (for any given event) for easy comparison of events, and because hydrograph peaks generally lasted about 5 hours. This choice of T is better representative of the period of competent flow because it has been observed that bed load transport does

not carry on for the entire period of the flow event in upland gravel-bedded streams (e.g., Reid and Frostick, 1984; Thompson and Croke, 2008).

F_i and Y_i values were calculated by including all entrained tracers (only tracers that were transported past the starting line) and the tracers available for entrainment from the bed. In this case, the value of F_i was always equal to one, as all tracer particle size fractions are considered together. The data collected could be analyzed by grain size individually, but only an average transport rate was calculated because of the interest in the average denudation rate of the watershed, and not necessarily in the transport regimes of individual sizes classes. However, the transport rates reflect the size of material moved because of the choice of grain size. Also, the degree of partial transport can be observed in the transport rate as calculated in this way (i.e., the value for Y_i—when $Y_i < 1$, partial transport exists).

Flow event frequency multiplied by event duration yields transport rates that may apply to a longer time frame than those observed during the study period of 10 months. A frequency analysis was carried out with a rainfall record from the beginning of 1928 to the end of 2008 from the Lead Hill, AR weather station in order to obtain event frequencies. The record was analyzed with MATLAB and Microsoft Excel. Rainfall events were defined as days of record with rainfall amounts greater than zero and bounded by days before or after with no rainfall. The minimum duration of a rainfall event as analyzed in this way is one day, while the actual duration of the rainfall that produces a peak flow in the stream reaches may be less than 24 hours. Additionally, rainfall totals may be better represented by totals from more than one day if rainfall producing peak flow happened during days split by the time measurements are recorded. This is accounted for by using a regression equation of rainfall with discharge that includes multiple days of rainfall.

Results and Discussion

Flow Competence

The impacts of increased turbidity and suspended sediments caused by increased agriculture within Tumbling Creek are likely to have had a minimal impact on the frequency and magnitude of bed load transport observed during this study because agriculture is considered light (Elliott and Aley, 2005), and because 23.7% of the recharge area's riparian areas were returned to forests by 2004. However, because of the presence of clay- and silt-sized sediments deposited within a framework of coarse-grained sediments (i.e., siltation) sometime after the conversion from forest to pasture, there is the possibility that cohesion has affected the force necessary to entrain natural sediments found within TCC. Kothyari and Jain (2008) have experimentally determined that the shear stress needed to entrain particle gravel mixtures containing 10, 20, 30, 40, and 50% clay, ranges from approximately 1.0 to 3.3 times that which is needed to entrain non-cohesive gravels. The percentage clay found in the sediment along the reach studied was low in the riffles and higher in the pools, but not directly quantified. An objective way to evaluate the spatial distribution of clay in the stream channel would be to make visual estimates of embeddedness (taken from the aquatic ecology discipline), as defined by the amount of clay or silt covering the substrate.

The flashiness of karst stream hydrographs depends on the developmental stage of the conduit system and on the fraction of autogenic recharge (water fed to the karst system via discrete points) in the drainage basin, which is large for TCC (see Thomson and Aley, 1971). Flashy drainage systems are generally more effective at clastic sediment transport (Bosch and White, 2004). The flashiness of the karst system will vary transiently and is difficult to represent mathematically (e.g., Whipple and Tucker, 2002). Flow at the gauging stations during relatively large flow events ($> \sim 0.3\ m^3\ s^{-1}$) had steep

rising and falling limbs, while smaller events were less flashy with longer and more drawn out peaks, especially in BCH. Observed (and estimated) peak discharge while tracers were deployed varied from 0.02 to 2.53 $m^3 s^{-1}$ in BCH, and from 0.34 to 2.04 $m^3 s^{-1}$ in TCC. The dates of the lowest flow do not coincide between TCC and BCH, but the date of the largest flow event does.

Considering only the largest tracers transported (competence approach, see Buffington and Montgomery, 1997), a total of 23 measurement pairs (flow events and tracer movements) were produced during the study at four tracer lines, including flows that did not transport any sediments. Figures 3.6 and 3.7 are hydrographs during the study period for BCH and TCC, respectively. Six flow events (1, 3, 4, 6, 7, and 10) at BCH-1 (from Figure 3.6) have corresponding tracer transport observations, and flow event 2 is paired with an observation of no tracer transport. At BCH-3, tracers were only deployed over four flow events (7-10), and transport was observed once after two tracer surveys. That transport observation is paired with transport by flow event 10, and flow event 7 is paired with an observation of no tracer transport. Eight flow events (1, 2, 3, 4, 6, 7, 8, and 11) at TCC-7 (from Figure 3.7) all have corresponding tracer transport observations from eight surveys. At TCC-10, tracers were only deployed over nine flow events (3-11), and transport was observed five times after six tracer surveys. Flow event 7 is paired with an observation of no tracer transport.

Table 3.2 displays peak hydraulic variables at the four tracer lines (and the dates of tracer surveys) during flow events occurring while tracer particles were deployed. Figure 3.8 is a plot of each tracer line cross-section and the corresponding modeled flow heights at peak flow (see Appendix A for other cross-sections). Observed competent flow events had flow depths varying from 15.1 to 63.2% of bankfull, and grain Reynolds numbers varying from 2510 to 18200, well above the laminar-turbulent transition. Calculated

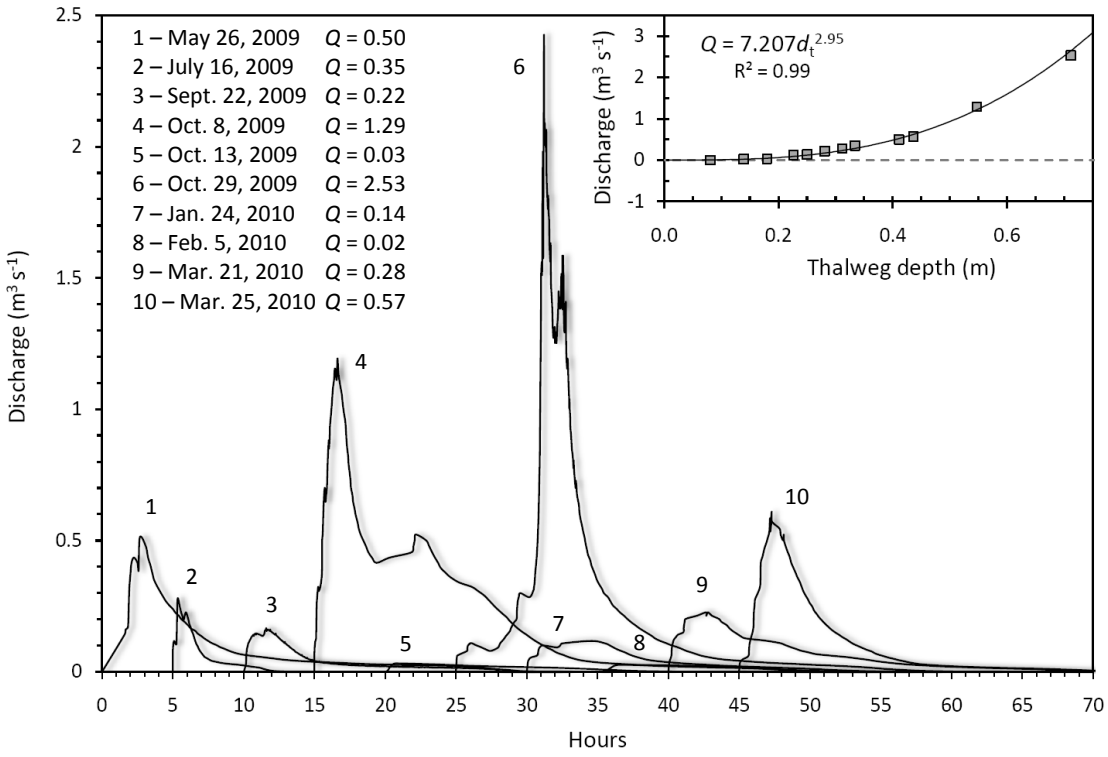

Figure 3.6. Hydrographs of flow events at the gauging station in BCH from May, 2009 through April, 2010. Discharge was determined by fitting a power function to calculated peak discharge (using equation 2.18) plotted against flow depth measurements in the thalweg (d_t), as shown in the inset. Hydrographs are spaced by five hours and ordered so that flow event dates increase to the right (numbered according to flow event date as shown in the upper left, along with corresponding peak discharges). The July 16th event (2) did not transport any tracers in BCH, but they were not returned to the starting line following the competent event before it. Events 5, 8, and 9 do not have any corresponding tracer transport observations because surveying of tracers was not done until after a subsequent flow event had occurred.

Manning roughness coefficients ranged from 0.039 at the highest observed flow to 0.096 at the lowest observed flow (consistent with values from small gravel-bedded streams; Bray, 1979).

Measured flow depth at TCC-7 coincided closely with modeled flow depth using equation 2.18 (measured exceeded modeled by approximately 0.05 m) with a resulting percent difference between modeled discharges of 8.7% (within the precision of field

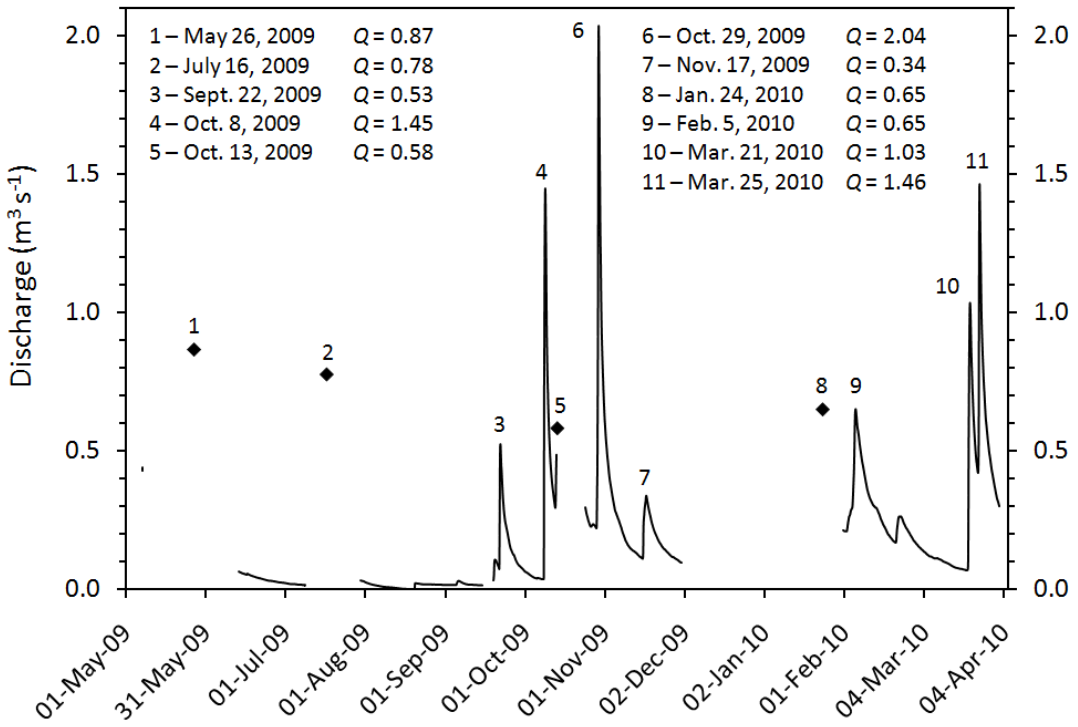

Figure 3.7. Discharge record in TCC from May, 2009 through April, 2010. Missing data appear as gaps in the record. Estimated peak flow values (see Figure 3.5 for regression equation) are plotted as black diamonds at times equal to nine hours past the time of peak flow in BCH (the average lag time between peak flows between BCH and TCC). Flow events are numbered according to event date as shown in the upper half, along with corresponding peak discharges. Events 5, 9, and 10 do not have any corresponding tracer transport observations because surveying of tracers was not done until after a subsequent flow event had occurred.

measured water depths). A much larger discrepancy exists between measured flow depth and modeled flow depth at TCC-10 (measured exceeded modeled by approximately 0.17 m) with a resulting percent difference in discharges of 59%. This could have resulted from the complicated geometry of the cave cross-section, particularly because of the presence of a small natural bridge at TCC-10 (see Figure 3.8).

The maximum grain size entrained (and transported past the starting line) was plotted against hydraulic variables of interest for each tracer line (Figures 3.9 and 3.10),

Table 3.2. Hydraulic variables during peak flow at BCH and TCC tracer line cross-sections, with corresponding tracer survey dates. Dates of tracer surveys are shown between the two flow events before it when two flow events had occurred prior.

Reach-Station	Flow event date	Tracer survey date	Reach peak discharge Q ($m^3 s^{-1}$)	Bettess-Limerinos-Manning n	Discharge per unit flow width q ($m^2 s^{-1}$)	Discharge per unit active flow width q_{aw} ($m^2 s^{-1}$)	Bed shear stress τ_0 ($N m^2$)	Stream power per unit bed area ω ($W m^2$)	Grain Reynolds number for D_{50s} R_{e*}	Relative roughness d/D_{50s}	Percent of bankfull depth (%)
BCH-1	5/26/2009	7/11/2009	0.496	0.047	0.119	0.234	15.7	9.94	4280	5.07	26.6
	7/16/2009	8/1/2009	0.349	0.050	0.086		13.4	7.27	4290	4.32	22.6
	9/22/2009	10/3/2009	0.215	0.054	0.056	0.203	10.9	4.71	3660	3.49	18.3
	10/8/2009	10/25/2009	1.291	0.042	0.278	0.552	24.3	23.1	4880	7.90	41.4
	10/13/2009		0.028	0.084	0.011		5.30	0.922	2270	1.70	8.90
	10/29/2009	11/7/2009	2.532	0.039	0.518	0.993	33.4	42.1	5900	11.1	58.2
	No flow	12/18/2009	0		0		0	0	0	0	0
	1/24/2010	2/6/2010	0.140	0.059	0.037	0.103	9.00	3.13	2510	2.87	15.1
	2/5/2010		0.023	0.088	0.010		5.00	0.81	1740	1.62	8.50
	3/21/2010	3/27/2010	0.276	0.052	0.070		12.1	5.87	2780	3.87	20.3
	3/25/2010		0.569	0.047	0.134	0.306	16.7	11.2	3560	5.40	28.3
BCH-3	1/24/2010	2/6/2010	0.140	0.058	0.026		6.48	1.90	1540	3.07	11.9
	2/5/2010		0.023	0.053	0.038		7.87	2.87	1840	3.59	13.9
	3/21/2010	3/27/2010	0.276	0.047	0.073		10.8	5.45	2060	4.98	19.3
	3/25/2010		0.569	0.042	0.145	0.162	15.2	10.78	2670	7.06	27.3
TCC-7	5/26/2009	7/11/2009	0.867††	0.073††	0.150††	0.202††	58.8††	46.9††	15100††	2.65††	32.3††
	7/16/2009	8/1/2009	0.777††	0.075††	0.134††	0.181	56.4††	42.6††	14700††	2.53††	30.9††
	9/22/2009	10/3/2009	0.525	0.084	0.092	0.122	47.7	28.9	13600	2.14	26.1
	10/8/2009	10/25/2009	1.448	0.065	0.245	0.338	73.4	76.1	14200	3.31	40.4
	10/13/2009		0.582††	0.081††	0.102††		49.9††	32.1††	13900††	2.22††	27.1††
	10/29/2009	11/7/2009	2.035	0.061	0.338	0.474	85.3	105	18200	3.88	47.4
	11/17/2009	12/18/2009	0.338	0.096	0.060	0.090	40.1	18.9	12500	1.80	22.0
	1/24/2010	2/6/2010	0.650††	0.079††	0.114††	0.152††	52.2††	35.7††	14200††	2.34††	28.6††
	2/5/2010		0.650	0.079	0.114		52.2	35.7	13900	2.34	28.6
	3/21/2010	3/27/2010	1.031	0.070	0.177		63.5	55.6	15200	2.86	34.8
	3/25/2010		1.463	0.065	0.247	0.341	73.8	77.0	16400	3.34	40.7
TCC-10	9/22/2009	10/3/2009	0.525	0.053	0.084	2.625	9.09	3.86	3260	5.05	33.6
	10/8/2009	10/25/2009	1.448	0.045	0.210	7.240	14.5	9.73	3470	8.00	53.3
	10/13/2009		0.582††	0.054††	0.079††		8.4††	3.27††	3130††	5.09††	33.9††
	10/29/2009	11/7/2009	2.035	0.043	0.289	2.544	17.0	13.3	4470	9.49	63.2
	11/17/2009	12/18/2009	0.338	0.054	0.082		8.59	3.43	3170	5.18	34.5
	1/24/2010	2/6/2010	0.650††	0.051††	0.102††	3.250	10.1††	4.74††	3420††	5.58††	37.2††
	2/5/2010		0.650	0.051	0.102		10.1	4.74	3350	5.58	37.2
	3/21/2010	3/27/2010	1.031	0.047	0.158		12.5	7.27	3690	6.93	46.2
	3/25/2010		1.463	0.045	0.144	7.315	14.5	9.81	3990	5.46	36.4

††Hydraulic variables estimated using regression in Figure 3.5.

producing flow competence plots. Several different magnitude flow events were competent to entrain the largest tracer size class, which has led to a large degree of scatter in the relationship between grain size and hydraulic variable. The goodness of fit to a linear trend line was low overall. However, it does reveal which hydraulic variables can provide the best means of prediction for a flow-competence relationship based on the simple relation between peak flow and largest grain size entrained. The r^2 values at BCH-1 were nearly identical falling between 0.126 and 0.136. At TCC-7 the r^2 values were very poor, ranging from 0.0004 to 0.0016, from discharge per unit active width (q_{aw}) having the lowest r^2 value. At TCC-10 the largest r^2 value was 0.689 with unit discharge (q) as the regressed variable. BCH-3 could not be evaluated in this way because only two data points were generated from field data.

If entrainment of bed material is size-selective, as was observed in laboratory experiments by Shields (1936) and in field tracer experiments by Ferguson and Wathen (1998), among others, then a positive correlation should be observed when hydraulic variables are regressed against grain size. Linear least-squares regressions reveal that a significant positive correlation (slope of the regression equation $\neq 0$) does not exist between any of the tested hydraulic variables at any tracer line at the 5% ($\alpha = 0.05$) level. *P*-values for tests of significance of the slope of the regression lines are between 0.47 and 0.55 at BCH-1, between 0.93 and 0.97 at TCC-7, and between 0.08 and 0.75 at TCC-10. The *P*-value could not be evaluated at BCH-3 because of too few data points. The low *P*-value at TCC-10 is from regression of q, which has the most significantly non-zero slope out of all the variables and cross-sections tested. In order to make a true empirical relationship between sediment and water discharges, however, a much larger number of samples are needed over a complete range of flows (e.g., Emmett, 1980; Hubbell, 1987; Wilcock, 2001).

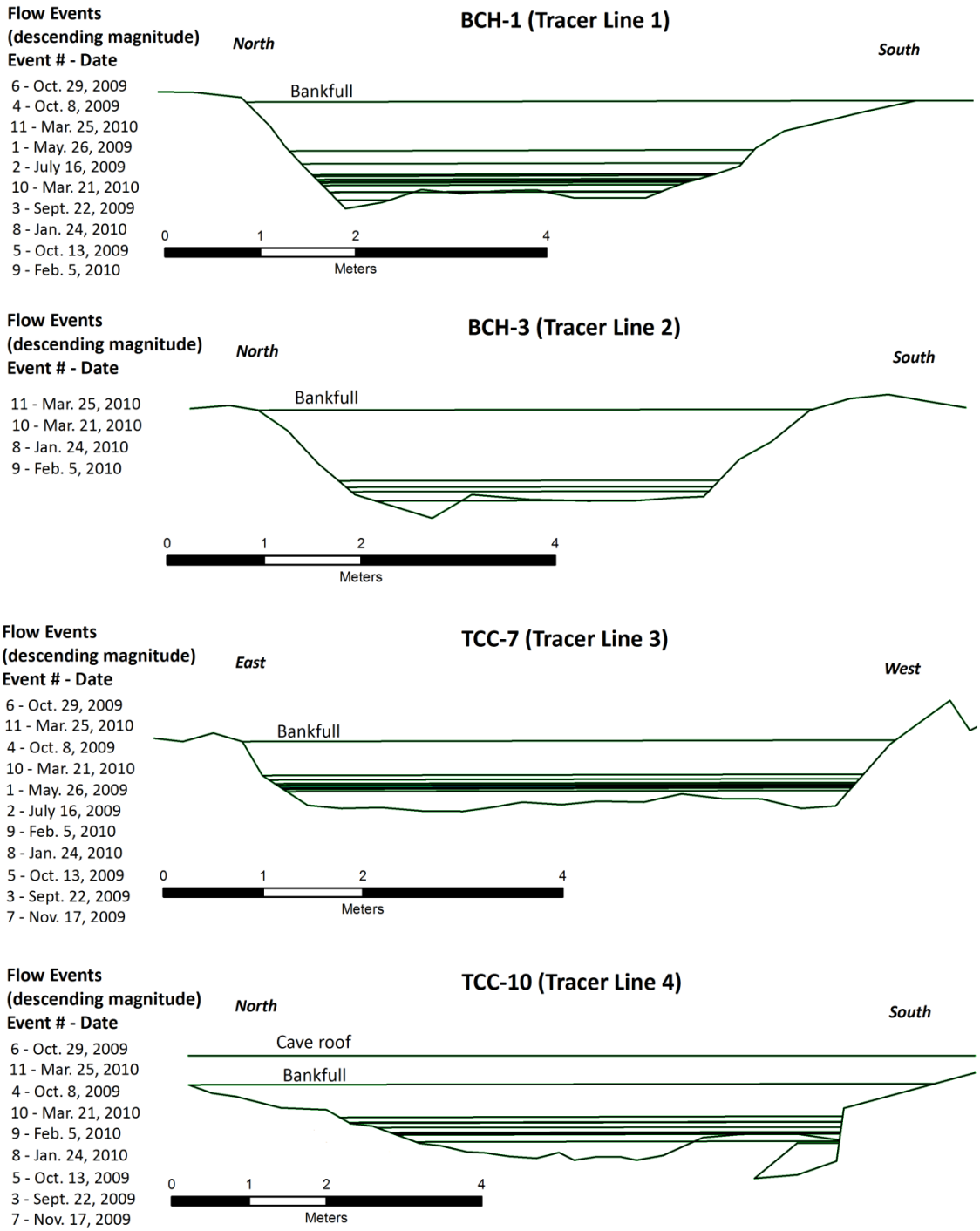

Figure 3.8. Cross-sections at tracer particle seeding locations (tracer lines) looking downstream, with bankfull and modeled peak flow heights during the period when tracer particles were deployed. Flow event numbers (see Figures 3.6 and 3.7) and dates are also given in descending order by peak flow magnitude.

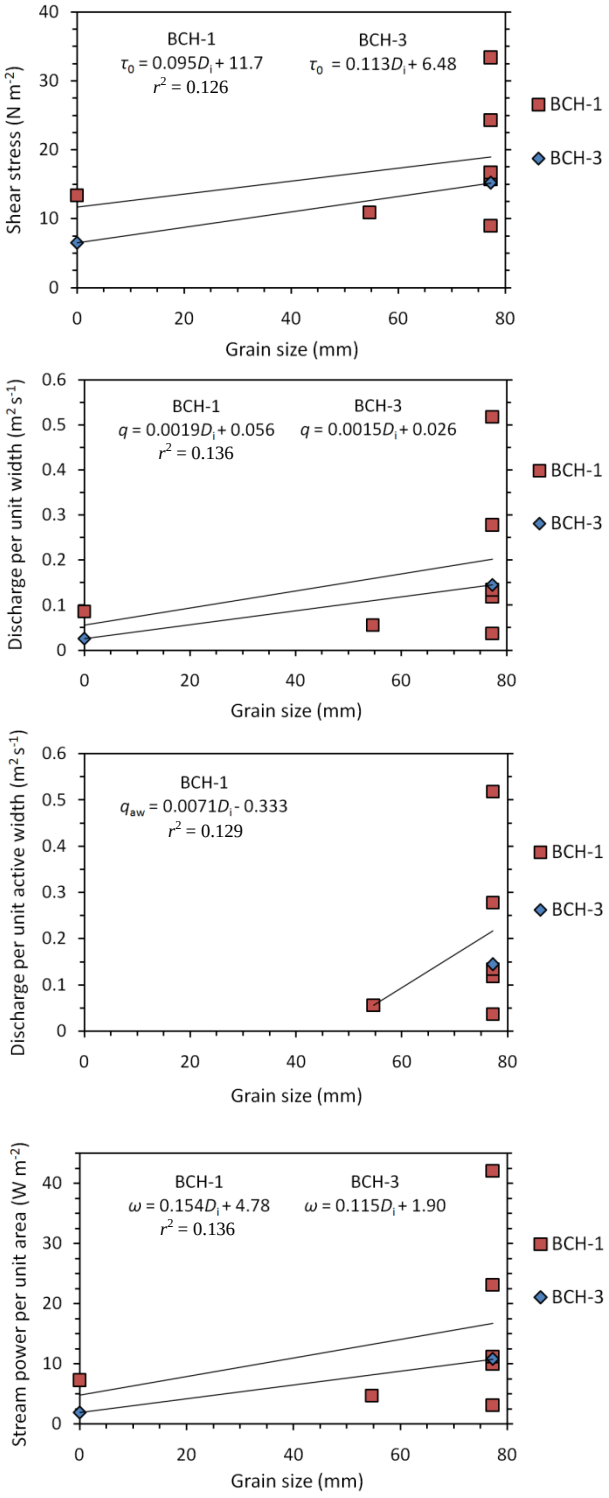

Figure 3.9. Flow competence plots for observed peak flows in BCH (seven at BCH-1, and two at BCH-3) with trend lines and their equations.

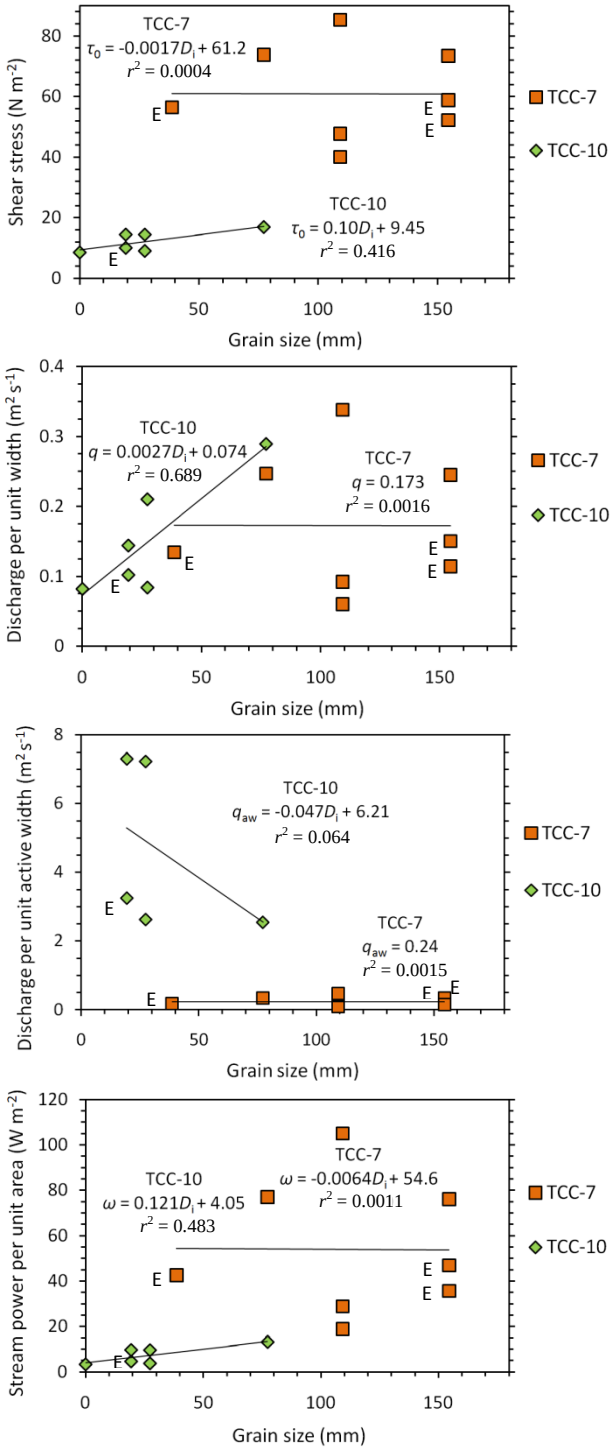

Figure 3.10. Flow competence plots for peak flows in TCC (eight at TCC-7, and six at TCC-10) with trend lines and their equations. Data points marked with an 'E' were estimated using the regression equation in Figure 3.5.

Flow competence relationships based on the observed critical shear stress were originally parameterized using the least-squares best fit regressions between shear stress and grain size from each tracer line and include the use of all available data (including estimated peak basal shear stress values in TCC). The resulting linear regression equations (provided in Figures 3.9 and 3.10) could be used to calculate the magnitude of the peak critical hydraulic variable necessary to entrain any given grain size on the bed. From that, then a relationship between the Shields parameter (θ_{ci}) and critical unit discharge (q_{ci}) as a function of the relative grain size (D_i/D_{50s}) could be determined. However, more data and larger r^2 values would be needed to employ this type of analysis.

From Figures 3.9, and 3.10, and Tables 3.2 and 3.3, it can be seen that flow competence is not similar at all four tracer lines. At BCH-1, BCH-3, and TCC-10, entrainment occurs at much lower shear stresses and lower Shields parameters than those at TCC-7. These limited data indicate that at TCC-7, the equations provided by Bathurst (1987a) obtained from the boulder-bedded Fall River in Colorado provide a better match to the observations from this study. Bathurst's equations were derived from steeply sloping channels with high roughness and a wide range in grain sizes. The equation fitted to the second set of data sampled at Fall River Road in 1985 (FRR 1985B; Figure 2.3) by Ferguson (1994), gives $\theta_{c50} = 0.061$, and $b = 0.89$. A simple comparison of the channel slope and the grain size distribution at TCC-7 with data from Bathurst (1987a) provide a physical explanation for the close match. The channel slope, width and grain size distribution data collected by Bathurst (1987a) was done in the same manner (standard surveying and 100 particle Wolman pebble count), and Bathurst matches the largest mobilized bed load particle with the largest magnitude of the flow during sampling, as was done in this study. At FRR 1985B, Bathurst reports $w = 6.1$ m, $S_b = 0.047$, $D_{16} = 32$, $D_{50} = 77$, and $D_{84} = 156$ (with grain size in mm), surprisingly similar to the data collected

Table 3.3. Tracer entrainment, displacement, and transport rates from tracer surveys in BCH and TCC. Dates of tracer surveys are shown between the two flow events before it if two flow events had occurred prior.

Reach-Station	Flow event date	Tracer survey date	Largest tracer entrained (mm)	Total number of tracers entrained	Largest tracer transported past starting line (mm)	Number of tracers transported past starting line N_i	Proportion of entrained tracers Y_i	Modal entrained grain size (m)	Calculated mass of transported tracers m_i (g)	Mean displacement length† L_i (m)	Bed load transport rate q_i (g m^{-1} hr^{-1})
BCH-1	5/26/2009	7/11/2009	64-90	33*	64-90	33*	0.165	0.0195	0.018	0.64*	5.84
	7/16/2009	8/1/2009	No entrainment§								
	9/22/2009	10/3/2009	64-90	10	45-64	7	0.037	0.0195	0.018	0.18	0.0787
	10/8/2009 10/13/2009	10/25/2009	64-90	122	64-90	44	0.277	0.0545	0.392	1.11*	63.3
	10/29/2009	11/7/2009	64-90	80§	64-90	59§	0.468	0.0545	0.392	2.02	262
	No flow	12/18/2009	No entrainment								
	1/24/2010 2/5/2010	2/6/2010	64-90	8	64-90	4	0.0345	0.0385	0.138	0.20	0.0913
	3/21/2010 3/25/2010	3/27/2010	64-90	32	64-90	29	0.190	0.0195	0.018	1.52*	14.0
BCH-3	1/24/2010 2/5/2010	2/6/2010	No entrainment								
	3/21/2010 3/25/2010	3/27/2010	64-90	65	64-90	65	0.591	0.0195	0.018	0.63	40.6
TCC-7	5/26/2009	7/11/2009	128-180	6*	128-180	6*	0.021	0.077	1.106	0.52*	0.443
	7/16/2009	8/1/2009	32-45	26*	32-45	26*	0.093	0.028	0.050	0.10*	0.571
	9/22/2009	10/3/2009	90-128	76	90-128	32	0.114	0.020	0.018	0.22	1.349
	10/8/2009 10/13/2009	10/25/2009	128-180	59	128-180	37	0.132	0.039	0.138	0.39	6.313
	10/29/2009	11/7/2009	128-180	21§	90-128	18§	0.066	0.054	0.381	0.72‡	3.953
	11/17/2009	12/18/2009	90-128	5	90-128	5	0.018	0.055	0.392	0.51‡	0.218
	1/24/2010 2/5/2010	2/6/2010	128-180	13	128-180	8	0.0292	0.0545	0.392	0.37	0.405
	3/21/2010 3/25/2010	3/27/2010	64-90	13	64-90	13	0.0474	0.0545	0.392	0.65*	1.879
TCC-10	9/22/2009	10/3/2009	23-32	5	23-32	4	0.0500	0.0195	0.018	0.05*	0.017
	10/8/2009 10/13/2009	10/25/2009	23-32	2*	23-32	2*	0.025*	0.0235*	0.031	0.065	0.007
	10/29/2009	11/7/2009	64-90	4§	64-90	4§	0.05	0.0406	0.162	0.0625	0.044
	11/17/2009	12/18/2009	No entrainment								
	1/24/2010 2/5/2010	2/6/2010	16-23	2§	16-23	2§	0.025	0.0195	0.018	0.04	0.003
	3/21/2010 3/25/2010	3/27/2010	16-23	1§	16-23	1§	0.0125	0.0195	0.018	0.07	0.001

†Includes all half-phi size classes transported past starting line.
*No photographs used in analysis.
§Tracers were not returned to starting line prior to transporting event or survey date.
‡Negative displacements were not included in the analysis.

at TCC-7 (Table 1.1). Bathurst, however, was examining critical discharge, and he found that a much larger q_{ci} is required to initiate motion of bed material in the Fall River, Colorado ($q_{c50} \approx 0.60$ m^2 s^{-1}) than the magnitude of q_{ci} observed at TCC-7 from this study ($q_{c50} = 0.17$ m^2 s^{-1}). This may be a result of the slightly larger bed slope present at the Fall River Road reach and a better developed structural packing arrangement of the bed.

At TCC-10, where a large range in grain sizes is also observed, the largest number of tracers transported was four (out of 80) during any one flow event. Therefore, differences between the entrainment thresholds at TCC-10 and TCC-7 may be minimal at larger flow events. With that said, the high bed slope and large overall grain sizes at TCC-7 are the likely culprits for the relatively higher flow competence relationship observed.

Other estimates for the critical hydraulic variables for entrainment were calculated and compared against observed tracer transport data. Commonly applied assumptions that are used when only basic channel and sediment information can be attained, such as: sediment density, grain size distributions and channel slope, were used. Without using the regression equations from Figures 3.9 and 3.10, the performance of predictive entrainment threshold equations as compared against the "raw" field data can be made with the variability of the flow competence data preserved. Figure 3.11 shows the observed hydraulic variables versus the critical hydraulic variables as estimated by using the predictive equations of Shields (1936) for shear stress, Bagnold (1980) for stream power, and Ferguson (1994) for discharge. While some of the observed flow events were not competent to mobilize bed load sediment, the data is useful in describing the flow conditions for entrainment, and so they are plotted in Figure 3.11 as well (distinguished by a larger symbol size). When values plot above the entrainment threshold (1 to 1 line) as predicted, the bed should be observed to be mobile (if the equation is accurate in

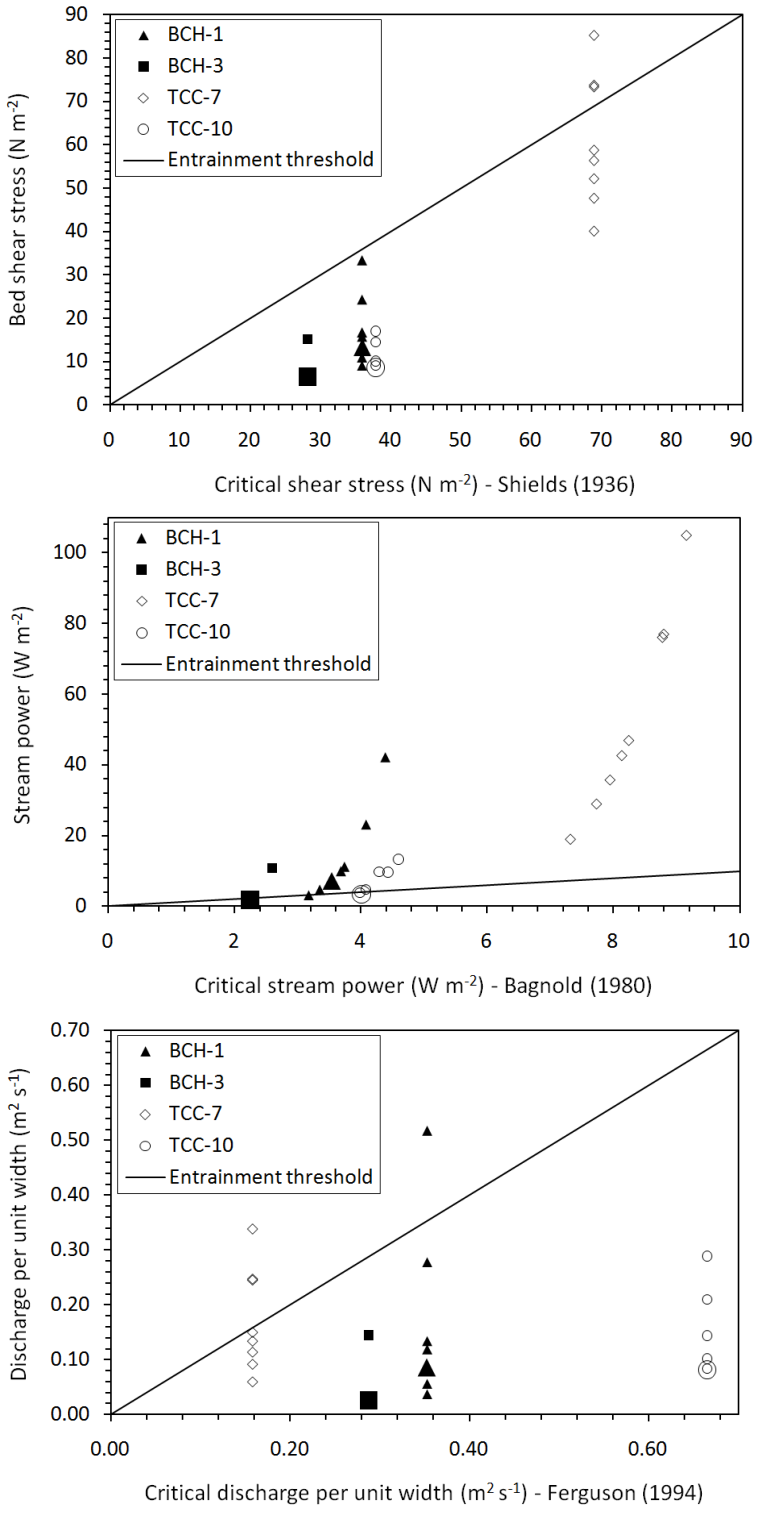

Figure 3.11. Comparison of observed and predicted peak hydraulic variables from the equations of Shields (1936), Bagnold (1980), and Ferguson (1994). Enlarged symbols indicate no observed transport, while all other symbols indicate observed transport.

predicting entrainment threshold flow conditions). The Bagnold (1980) equation is seen to perform best.

The estimated critical shear stress using the Shields (1936) equation (equation 2.5) did not perform well against observational data, as critical shear stress was overestimated at all tracer lines, although at TCC-7, only a slight overestimate was observed. When deriving critical entrainment thresholds, other investigators (e.g., Komar, 1987; Buffington and Montgomery, 1997) suggest using lower values of the Shields parameter than that predicted by Shields himself, which leads to more accurate predictions when compared with our observations (equations 2.6 and 2.7). The Bagnold (1980) equation (equation 2.14) performs very well for the D_{84} sized material and the best overall, while it under predicts critical flow conditions slightly, except at TCC-7 where the Ferguson (1994) equation (equation 2.9) may provide better predictions of entrainment.

An adjustment to the base dimensionless critical shear stress (Shields parameter) can be made in order to objectively account for the effects of grain shape on bed packing arrangement (e.g., imbrication and pebble clusters) by using a lithology-averaged grain shape factor (i.e., the Corey shape factor –CSF). Following Thompson and Croke (2008), the base Shields parameter ($\theta_{c50b} = 0.03$) is divided by the CSF to obtain a new Shields parameter that can be used to solve for the critical shear stress for entrainment using equation 2.1. Analysis of grain shape of tracers gave an average CSF of 0.56 (and standard deviation of 0.15). The adjusted Shields parameter is 0.054. While this method is useful for comparisons from reach to reach it does not necessarily imply that the adjusted Shields parameter is more accurate than those proposed by other investigators, (discussed earlier). The value of 0.054 is very close to the average value of 0.059 determined as the best-fit Shields parameter at TCC-7 where large hydraulic roughness and a wide range of grain sizes are observed. This provides independent evidence for a

strong packing arrangement of the bed. However, the packing arrangement is structural, and cannot be easily described by the presence of imbricated grains or pebble clusters. Also, the best-fit Shields parameter is very near to the θ_{c50b} at the other three tracer lines, indicating that bed packing is negligible, at least for the mobile tracers.

Rainfall and Discharge Correlation

Rainfall data during the study period showed significant ($\alpha = 0.05$) trends when regressed against observed peak discharge data from both TCC and BCH. Of the four rainfall variables tested, including—(1) total event rainfall (using daily rainfall totals from 1 to 3 days), (2) peak rainfall intensity (5 to 30 minute interval data from Forsyth weather station), (3) daily rainfall, and (4) previous 30 day total rainfall—peak rainfall intensity had the highest correlation coefficient for BCH ($r = 0.742$) and TCC ($r = 0.710$). Rainfall intensity is expected to give the best estimates of discharge because peak flows are generated by periods of high rainfall intensity (with some lag time between peaks) and because rainfall intensity data have a much finer temporal resolution than daily rainfall totals. However, frequency analysis of rainfall that utilizes historical rainfall records relies on daily observations, so peak rainfall intensity cannot be used for that purpose. When compared against the other three rainfall variables, daily rainfall has a correlation coefficient that is second lowest for both BCH discharge ($r = 0.599$) and TCC discharge ($r = 0.496$), while the correlation for the previous 30 day total rainfall was the worst ($r = 0.334$, and 0.286 for BCH and TCC, respectively). Total event rainfall showed a much better correlation than the previous 30 day total rainfall, and daily rainfall, with $r = 0.675$ for BCH and $r = 0.713$ for TCC. All correlation coefficients may be low due to the small number of events available for the analysis (13 events from BCH, and 6 from

TCC). The resulting linear least-squares best fit equations using the total event (daily) rainfall and peak discharge data are, for BCH

$$Q = 0.0219R_d - 0.5356 \quad (3.1)$$

and for TCC

$$Q = 0.0172R_d + 0.0876 \quad (3.2)$$

where R_d denotes the total event (daily) rainfall in units of mm observed at the rain gauge in the TCC recharge area, and Q is discharge in units of $m^3\ s^{-1}$.

Rainfall/Discharge Frequency Analysis

A frequency analysis of 81 years (beginning of 1928 through the end of 2008) of daily rainfall data from the Lead Hill, AR weather station (U.S. Cooperative Network Station 034106; 17.8 km SW of TCC), was performed (Figure 3.12). The flow frequency associated with the observed entrainment of coarse bed material during the study occurs with return periods between 2.41 and 3.59 years in BCH and between 2.14 and 3.10 years in TCC as indicated from the historic record of rainfall and the correlation of rainfall with peak discharge. Bankfull flow events have return periods of approximately 10 years in BCH and TCC. The relationship between rainfall event total (summed over consecutive days with rainfall) and discharge is not perfect (r = 0.675 for BCH and r = 0.713 for TCC), and much variability exists in the rainfall record, so these values are only viewed as first-order approximations.

Additionally, rainfall during the study period was higher than the mean rainfall when rainfall data from the Protem 3.0 NE rain gauge from March 29, 2009 through March 29, 2010, was compared with yearly rainfall data from Ozark Beach, MO weather station (27.4 km from TCC). The difference between observed total rainfall for one year prior to March 28th, 2010 and mean yearly rainfall was about + 243 mm (22% more

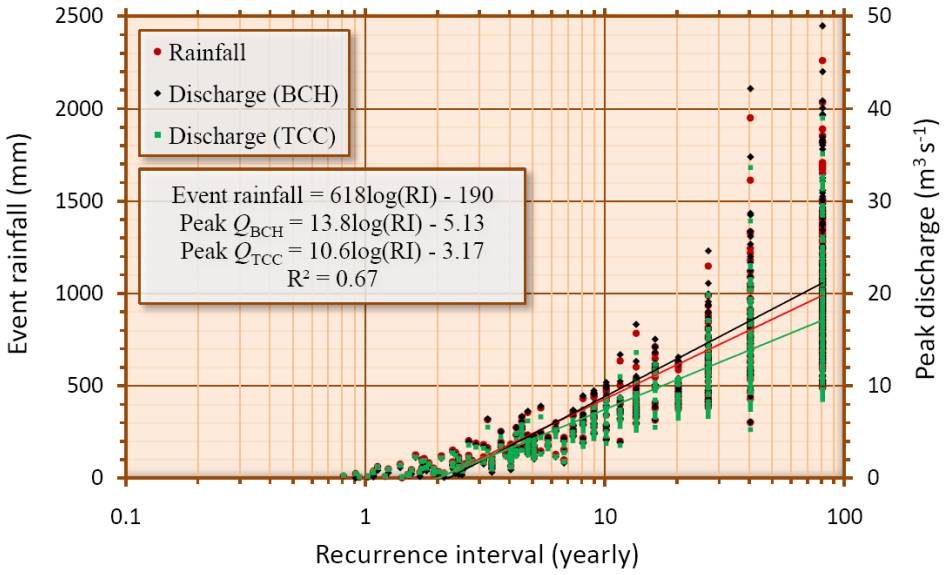

Figure 3.12. Yearly recurrence intervals for rainfall and peak discharge magnitude found using the daily rainfall record at Lead Hill, AR and correlations with total event rainfall with peak discharge at BCH and TCC. Rainfall event frequency (per year) is the inverse of the recurrence interval. Red dots represent rainfall, black dots represent BCH discharge, and green dots represent TCC discharge. Best fit logarithmic equations are provided and used in analysis. The r^2 value applies to all regressions.

rainfall). Based on these data, it can tentatively be stated that the observed frequency for sediment entrainment during this study is not representative of normal conditions, but can be expected to be higher. If we define entrainment frequency as the number of days from the initial seeding date at a tracer line until March 29, 2010 (two days after final tracer survey) divided by the number of observed competent flow events during that period, then sediment entrainment was observed with maximum frequencies between 40 days (TCC-7), and 140 days (BCH-3). These are much more frequent than what is predicted by the frequency of entrainment in a normal year from the rainfall/discharge frequency analysis, even when the lowest competent flow magnitude is considered (2.41 years in BCH, and 2.14 years in TCC).

While the frequency of entrainment observed during this study is likely higher than what is typical (as indicated by the frequency analysis), it still provides a basis for comparisons with other karst stream systems. A surface stream reach located at the outlet of the Devil's Icebox fluviokarst system near Columbia, MO has been estimated by Dogwiler and Wicks (2004) to transport median size bed material with a frequency of 2.4 months (approximately 73 days), very similar to the observed frequencies of transport using tracers in Tumbling Creek Cave and one of its surface drainages (BCH). However, Dogwiler and Wicks (2004) based their analysis on a shear stress approach employing the Shields (1936) equation, and, as the observations made during this study have shown, the Shields (1936) equation has the potential to over predict the critical shear stress necessary for entrainment. Therefore, the frequency of entrainment may well actually be higher than they predicted.

Bed load Transport Rate

Analysis of bed load transport rates using equations 1.1 and 1.2 (after Wilcock 1997a, 1997b) reveal that travel distances of tracers, and transport rates, are variable from one reach to the next and from cross-section to cross-section within the same reach, even during the same flow events (Table 3.3, Figure 3.13). Figure 3.13 shows quartile (box) plots of the entire observed sample of tracer displacements (including all grain sizes transported past the starting line) per event at each tracer line, while Appendix C shows the maximum, mean, and minimum number of tracers transported past the starting line in each half-phi grain size class per event at each tracer line.

Transport rates are observed to be low to non-existent most of the time, with measureable bed load transport rates (using tracers) occurring only during storm-induced flow events. Transport rates are much larger in BCH than they are in TCC, with the

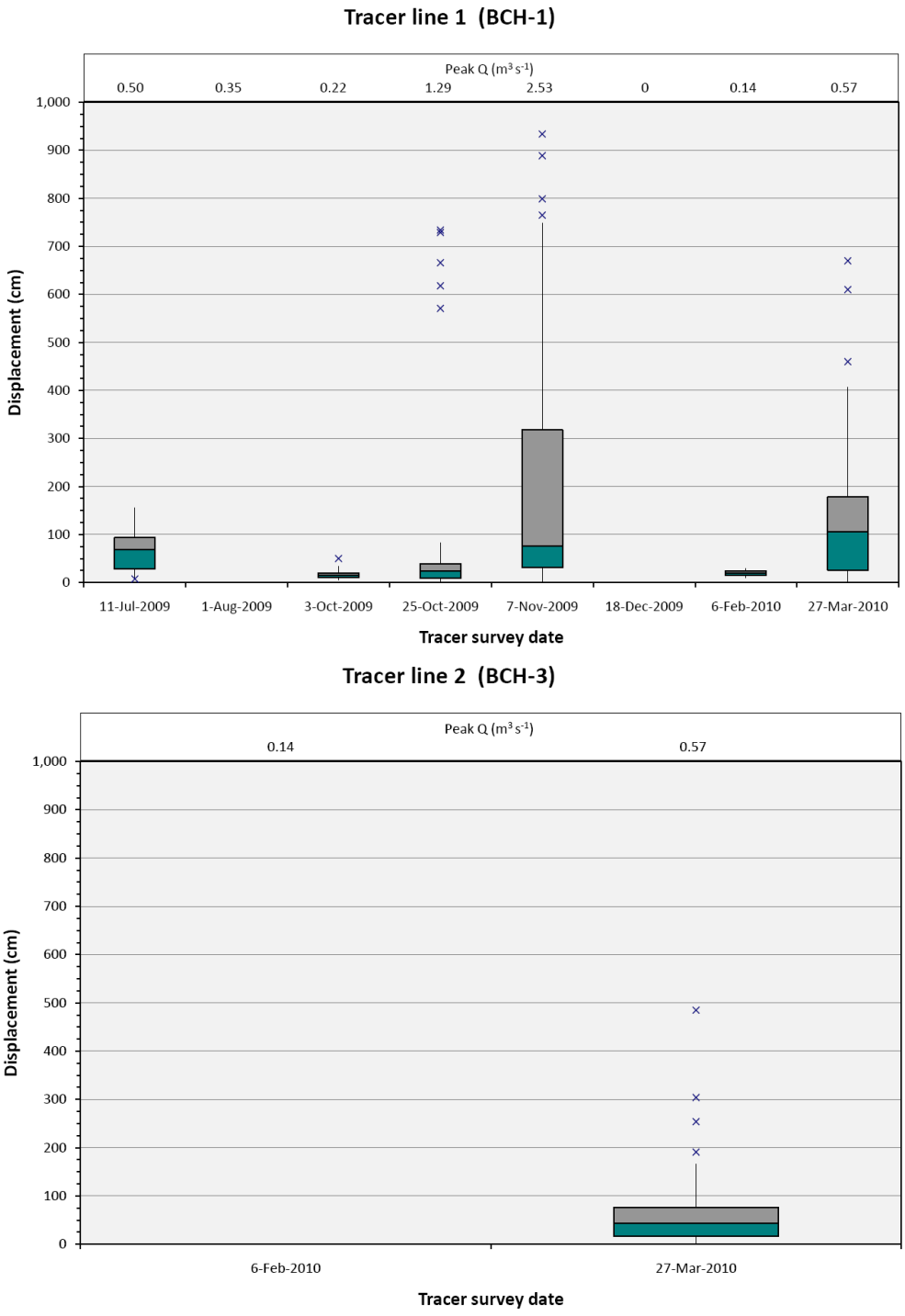

Figure 3.13. Box plots of tracer displacement distances for tracers (all grain sizes) transported past the starting line from each tracer survey (survey date increases to the right). The magnitude of the peak discharge paired with tracer movement is provided at the top of the each plot (Cont…).

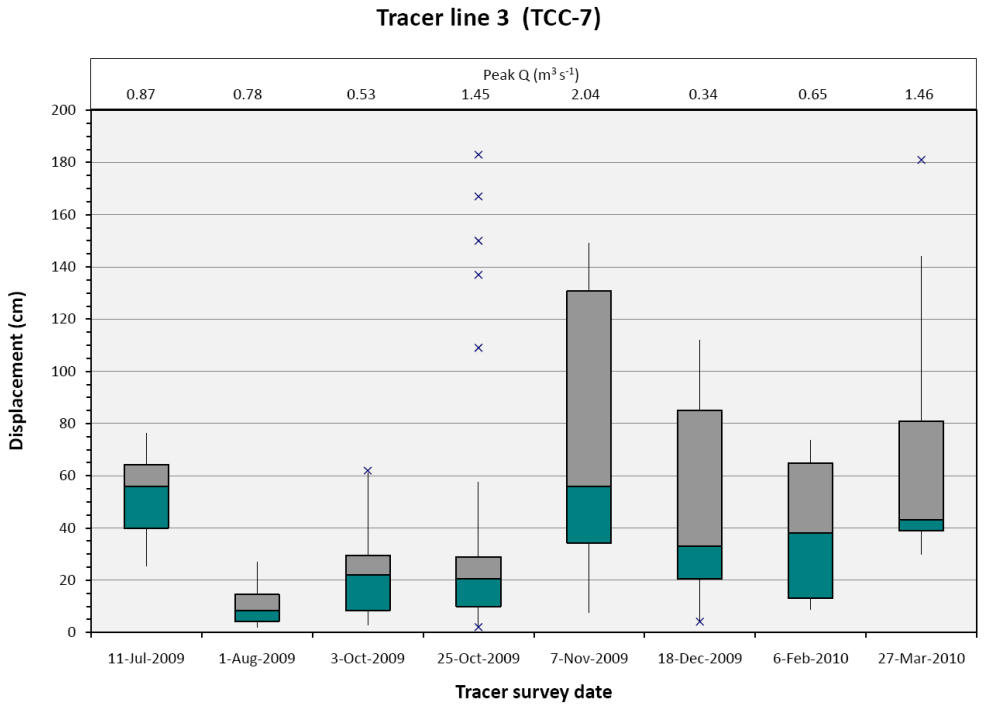

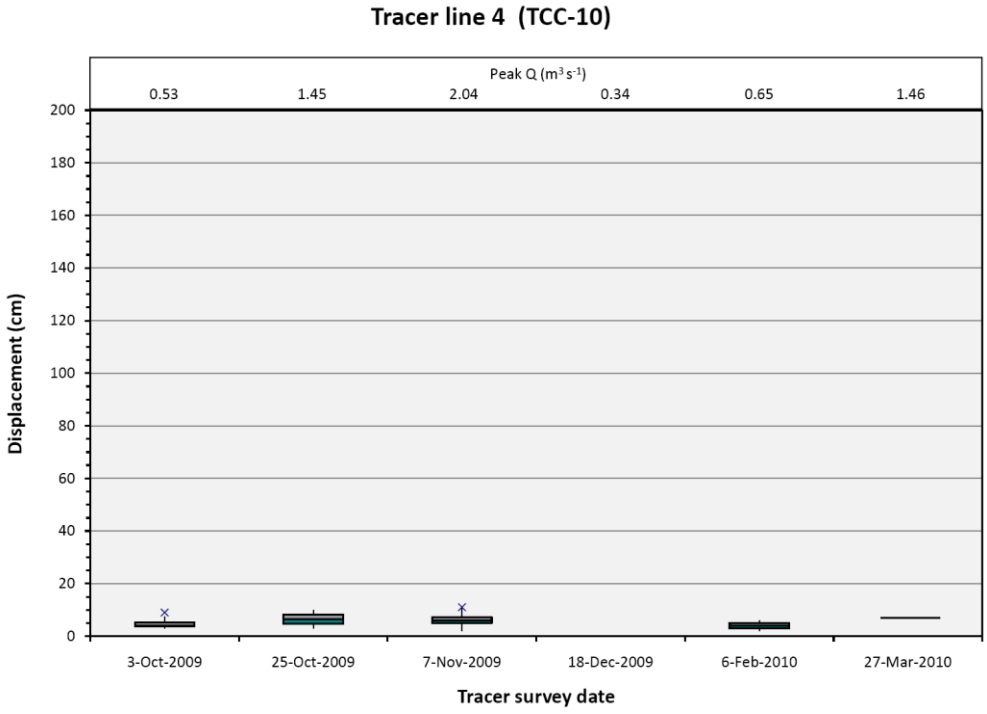

Figure 3.13 (Cont…).

largest calculated bed load transport rates being 262 g m^{-1} hr^{-1}, and 6.3 g m^{-1} hr^{-1}, respectively (Table 3.3). Moderate flow events (> 1 m^3 s^{-1}) are required to mobilize large fractions (> 20%) of the bed material in BCH, while much larger flow events (on the order of 3-5 m^3 s^{-1}) are required to mobilize that amount of material in TCC (the highest flow observed in TCC was 2.04 m^3 s^{-1}) coinciding with Y_i values of 13.2% at TCC-7 and only 5.0% at TCC-10. The discrepancies in transport rates and the fraction of material transported, is likely to do with a stronger bed packing arrangement of grains in TCC.

The recovery rate for tracers was relatively high compared with other painted tracer particle studies (Hassan and Ergenzinger, 2003). Over the entire study period, 77% of grains were recovered at BCH-1 (with six competent flow events), 97% recovery at BCH-3 (over one competent flow event), and 100% at TCC-10 (with five competent flow events). The final tracer pebble count was not conducted at TCC-7, although recovery rates are thought to be higher than 90% based on photographs.

Reed et al. (2010), report values of total suspended solids (TSS) flux normalized by basin area at several karst springs during storm flow in Kentucky and Tennessee, which have similar climate and geology). The range they report is from 0.000225 to 44.5 kg ha^{-1} hr^{-1}, and they report an average from four basins within the Inner Bluegrass Physiographic Province, Kentucky as 0.0460 kg ha^{-1} hr^{-1}. Bed load flux as determined from tracers during this study, calculated by normalizing drainage basin area above gauging stations and multiplying by the length of the channel, yield minimum values of 0.00166 kg ha^{-1} hr^{-1} and 0.000000390 in BCH and TCC, respectively, while maximum observed values obtained are 4.78 kg ha^{-1} hr^{-1} and 0.00246 kg ha^{-1} hr^{-1}.

From this analysis, the data from this study indicate that bed load flux is an important component of the mass being transferred through the karst subsurface. Although the rate for bed load and suspended load transport is highly variable,

comparisons with other studies show that bed load transport rates may vary from negligible to more than one-order of magnitude less than suspended load transport rates. Bed load transport rates may very well be an order of magnitude higher during larger flow events (e.g., bankfull).

Table 3.3 also provides the number of tracers entrained, including both the number entrained and transported past the starting line and the number of tracers moved at least one grain diameter. Generally, there are more tracers that are entrained and transported a short distance than there are transported past the starting line. These movement are considered negligible in the study and tracers that did not move past the starting line were not returned to their original positions.

The underlying physical controls of bed load transport can be ascertained from the calculated bed load transport rates and the flow competence relationship, and knowledge of the channel and sediment characteristics. The availability of sediment on the bed that can be entrained by the flow is controlled strongly by an armoring layer of coarse-grained sediment. This occurs when the surface grain size distribution is coarse compared to the subsurface grain size distribution. Discrete bedforms such as pebble clusters, and imbricated grains were not observed at any high density in the studied channels, (probably because clasts were generally not disc-shaped). However, sheltering (e.g., hiding) of the smaller grains by the larger grains was observed and is reflected in many of the short displacement distances measured at TCC-7 (Figure 3.13). As smaller grains become mobile and then dropped out of the flow and into the bed framework created by the larger grains, transport of the individual grains ceased. This process is sometimes referred to as trapping. The short observed displacements at TCC-10 (Figure 3.13) might be attributed to the effect of sheltering and trapping, but most of the mobilized sediment was moving from the bar on the north side of the channel, which is composed mostly of

fine material, so this cannot be the case. In BCH, trapping may have had an influence on the deposition of finer-grained material, but its effects were minimized under moderate flow conditions as the armor layer began to break up. The process of breakup of the armor layer is referred to as "phase 2" transport by Bathurst (1987b), and coincides with increased rates of bed load transport as the finer grained material becomes available to the flow. Under all observed flow conditions, except the largest, the armor layer in BCH had a noticeable sheltering effect on transport distances and bed load transport rates.

Some investigators of sediment transport who utilize tracer particles (e.g., Hassan et al., 1992) have argued that transport after an initial seeding does not represent the natural movement of the bed sediment. While this argument has merit, much information may still be gained from employing the use of tracers in this fashion. For this study, the two primary tracer lines (BCH-1 and TCC-7) were setup with tracers relatively close together, which may have acted to increase the flow required for entrainment because of particle-to-particle interaction, and actually may have acted to replicate the natural sediment structure quite well. This assumption holds best at tracer lines BCH-1 and TCC-7 where the width of the tracer lines was more than the width of four tracer particle diameters, whereas at BCH-3 and TCC-10 the tracer line width was only the width of one particle across most of the tracer line distance.

TCC sediments are typically covered by a thin coating of a dark black mineral (most likely manganese oxide) that may indicate that those sediments are immobile for extended periods of time. The rate of mineral deposition on those grains has become something of interest during the course of this study because it could be a useful way to discern whether or not cave substrate is being transported or not. While no conclusive evidence was drawn from this study, some observations from repeat trips to TCC provide

insight. There was not any large clasts coated black that were noticeably transported at TCC-7 or TCC-10 during the study.

Conclusions

The painted tracer particle experiment during the ~ 10 month study period provide evidence that bed load material in the Tumbling Creek Cave fluviokarst watershed is mobilized frequently (several times per year). In humid climates with regular rainfall, hydrological and sediment transport fluctuations will occur on a frequent basis (Dogwiler, 2002). Fluviokarst systems in similar climates with similar gradients will respond to rainfall events in a similar fashion and on similar time scales.

The absolute flow competence for Tumbling Creek is higher (on average) than one of its surface stream counterparts, Bear Cave Hollow. This provides evidence against the hypothesis that the critical entrainment threshold will be similar for surface (non-karst) and subsurface (karst) stream reaches. This is likely due to a greater hiding and protrusion effect (leading to equal mobility of the grains) caused by a strong structural bed packing arrangement developed in TCC (especially in riffles). The short travel distances of entrained and transported tracers provides further evidence for structural arrangement of the bed material and lends to the interpretation that the transporting capacity is not exceeded by the supply of coarse sediments to the studied stream reach in TCC (Church, 2002). This interpretation is consistent with tracer experiments conducted by Church and Hassan (1992) and Hassan and Church (1992), who describe the process of trapping. In BCH, the surface material is only slightly larger than the subsurface material indicating an armoring layer, but the mean travel distances of tracers is much more related to flow magnitude than it is in TCC (which has a surface layer that is much larger than the subsurface material). This would also indicate that the armor layer is not

as tightly packed in BCH and perhaps that sediment supply to the channel is greater. This is consistent with the observation of a small amount of aggradation and burial of *in situ* tracer particles at BCH-1 by the end of the study.

Data reveal that the entrainment threshold is particularly well estimated by the Bagnold (1980) empirical critical stream power equation, as was observed by Hassan et al. (1992). The frequency of entrainment is grossly under estimated when the Shields (1936) equation is used with a $\theta_{c50} = 0.06$, thus supporting the primary hypothesis of this study. All but three of the 20 competent flow events (having at least one tracer entrained by the flow) would be estimated to have shear stresses below critical using the simple Shields equation. Thus, studies basing the frequency of bed load entrainment and transport on a 'sediment entrainment potential' may want to consider choosing an adjusted Shields parameter and perhaps using an equation for the Shields parameter that accounts for relative size effects (e.g., the equations of Andrews, 1983 or Komar, 1987), as sediment grain size distributions are fairly easy to obtain. Adjusting the Shields equation for relative size effects is more important in streams having high bed slopes and packed beds with large grain sizes. On the other hand, the choice of the hiding factor is not easy to predict, as other studies suggest (*b* values range from 0.65 to 1.0). The choice of *b* is also related to the grain size distribution and any structural packing arrangement of the grains on the bed (e.g., Bathurst 1987a found high *b* values in a cobble to boulder-bedded stream).

The incorporation of an adjustment to the base Shields parameter, using a lithology-averaged grain shape factor (i.e., the CSF), has been shown to provide good results with data from TCC-7, but does not seem to be beneficial to the approximation of the Shields parameter at the other tracer line cross-sections. This is likely an aspect of the degree of structural packing, or armoring of the bed, and the overall range in grain

sizes (similar to the interpretation of the resulting short travel distances). Samples of the surface and subsurface grain sizes and relatively simple characterization of the bed structure (perhaps just a visual estimation of density of structure elements) may provide better estimates for entrainment in karst streams than the use of the CSF adjusted Shields parameter.

While the frequency of transported bed load sediments in the studied fluviokarst system is relatively high, the bed load transport rates remains small, especially in the studied cave reach (TCC). However, only low to moderate flows were observed, whereas during high bankfull flows (recurring roughly every 10 years) should be capable of causing the breakup of the armor layer and the occurrence of "phase 2" transport, even in TCC. This phase of transport was thought to have been occurring during the largest observed event (2.53 $m^3 s^{-1}$) in BCH because of nearly complete mobilization of grains in a single half-phi size class (i.e., $Y_i \approx 1$). High sediment transport rates during bankfull flows may be sufficient to physically weather exposed bedrock through abrasion within discrete segments along the cave stream channel. Future studies in karst streams could expand the time period of sediment tracing in order to capture the effects of high flow events on the transport rates of coarse sediments, and to gain more insight into the possibility that mechanical abrasion plays a role in the development of karst landscapes.

The observed high frequency of transport has implications for physical aquatic habitat stability, and the likelihood of channel bed reconfiguration. While the habitat created by the presence of coarse stream bed material in TCC has been undermined by the deposition of fine sediment into the interstices of the substrate, the high frequencies of bed load transport has the potential to increase the population of the endangered cave snail (*Antrobia culveri*) through the reestablishment of its physical habitat. Frequent flows which are competent to transport large grain sizes may soon dispel those fine

sediments in a few short years to decades as long as riparian forest cover is maintained around surface drainage channels, such as Bear Cave Hollow, and methods of conservation land use are practiced. On the other hand, since bankfull flows may be required to completely breakup the armor layer, fine material may require extreme floods and several decades to dispel fines.

REFERENCES CITED

Aguirre-Pe, J., Olivero, M.L., and Moncada, A.T., 2003, Particle densimetric Froude number for estimating sediment transport: Journal of Hydraulic Engineering, v. 129, p. 428-437, doi: 10.1061/(ASCE)0733-9429(2003)129:6.

Aley, T., Aley, C., Moss, P., and Hertzler, E., 2007, Hydrogeological characteristics of delineated recharge areas for 40 biologically significant cave and spring systems in Missouri, Arkansas, Oklahoma, and Illinois: National Cave and Karst Management Symposium, p. 154-167.

Aley, T., and Thomson, K.C., 1971, Ozark Underground Laboratory part 2: Ozark Caver, v. 3, p. 1-18.

Andrews, E.D., 1983, Entrainment of gravel from naturally sorted riverbed material: Geological Society of America Bulletin, v. 94, p. 1225-1231.

Ashworth, P.J., and Ferguson, R.I., 1989, Size-selective entrainment of bed load in gravel bed streams: Water Resources Research, v. 25, p. 627-634.

Bagnold, R.A., 1966, An approach to the sediment transport problem from general physics: United States Geological Survey Professional Paper 422-I, 37 p.

Bagnold, R.A., 1980, An empirical correlation of bedload transport rates in flumes and natural rivers: Proceedings of the Royal Society of London, Series A, v. 372, p. 453-473.

Bagnold, R.A., 1986, Transport of solids by natural water flow: evidence for a world-wide correlation: Proceedings of the Royal Society of London, Series A, v. 405, p. 369-374.

Baker, V.R., and Ritter, D.F., 1975, Competence of rivers to transport coarse bedload material: Geological Society of America Bulletin, v. 86, p. 975-978.

Bathurst, J.C., 1987a, Critical conditions for bed material movement in steep, boulder-bed streams: International Association of Hydrological Sciences Publication, no. 165, p. 309-318.

Bathurst, J.C., 1987b, Measuring and modelling bedload transport in channels with coarse bed materials, *in* Richards, K.S., ed., River Channels: Environment and Process: Cambridge, Blackwell Publishers, p. 272-294.

Bathurst, J.C., Graf, W.H., and Cao, H.H., 1987, Bed load discharge equations for steep mountain rivers, *in* Thorne, C.R., Bathurst, J.C., and Hey, R.D., eds., Sediment Transport in Gravel Bed Rivers: New York, John Wiley & Sons, p. 453-491.

Bauman, A., 1944, Prescription for a sick stream: Missouri Conservationist, p. 2-3, 14-15.

Bettess, R., 1999, Flow resistance equations for gravel bed rivers: Graz, Austria, XXVIII International Association for Hydro-Environmental Engineering and Research Congress, p. 6.

Beylich, A.A., and Warburton, J., eds., 2007, Analysis of source-to-sink-fluxes and sediment budgets in changing high-latitude and high-altitude cold environments, SEDIFLUX Manual: Trondheim, Norway, Norges Geologiske Undersokelse, 158 p.

Bosch, R.F., and White, W.B., 2004, Lithofacies and transport of clastic sediments in karstic aquifers, *in* Sasowsky, I.D., and Mylroie, J.E., eds., Studies in Cave Sediments: New York, Kluwer Academic/Plenum Publishers, p. 1-22.

Bottrell, S., Hardwick, P., and Gunn, J., 1999, Sediment dynamics in the Castleton karst, Derbyshire, U.K.: Earth Surface Processes and Landforms, v. 24, p. 745-759.

Bray, D.I., 1979, Estimating average velocity in gravel-bed rivers: Proceedings of the American Society of Civil Engineers, Journal of the Hydraulics Division, v. 105 HY9, p. 1103-1122.

Buffington, J.M., and Montgomery, D.R., 1997, A systematic analysis of eight decades of incipient motion studies, with special reference to gravel-bedded rivers: Water Resources Research, v. 33, p. 1993-2029.

Buffington, J.M., Dietrich, W.E., and Kirchner, J.W., 1992, Friction angle measurements on a naturally formed gravel streambed: Implications for critical boundary shear stress: Water Resources Research, v. 28, p. 411-425.

Bunte, K., and Abt, S., 2001, Sampling surface and subsurface particle-size distributions in wadable gravel- and cobble-bed streams for analysis in sediment transport, hydraulics, and streambed monitoring: Fort Collins, CO, U.S. Department of Agriculture, Forest Service, Rocky Mountain Research Station, General Technical Report RMRS-GTR-74, 428 p.

Carling, P.A., 1983, Threshold of coarse sediment transport in broad and narrow natural streams: Earth Surface Processes and Landforms, v. 8, p. 1-18.

Carling, P.A., Kelsey, A., and Glaister, M.S., 1992, Effect of bed roughness, particle shape and orientation on initial motion criteria, *in* Billi, P., Hey, R.D., Thorne, C.R., and Tacconi, P., eds., Dynamics of Gravel-bed Rivers: New York, John Wiley & Sons, p. 23-39.

Charlton, R., 2008, Fundamentals of Fluvial Geomorphology: New York, Routledge, 234 p.

Church, M., 2002, Geomorphic thresholds in riverine landscapes: Freshwater Biology, v. 47, p. 541-557.

Church, M., 2006, Bed material transport and the morphology of alluvial river channels: Annual Review of Earth and Planetary Science, v. 34, p. 325-354.

Church, M., and Hassan, M.A., 1992, Size and distance of travel of unconstrained clasts on a streambed: Water Resources Research, v. 28, p. 299-303.

Church, M., and Hassan, M.A., 2002, Mobility of bed material in Harris Creek: Water Resources Research, v. 38, 1237, doi:10.1029/2001WR000753.

Cifelli, R., Doesken, N., Kennedy, P., Carey, L.D., Rutledge, S.A., Gimmestad, C., and Depue, T., 2005, The Community Colaborative Rain, Hail, and Snow Network: informal education for scientists and citizens: Bulletin of the American Meteorological Society, v. 86, p. 1069-1077.

Coleman, S.E., and Nikora, V.I., 2008, A unifying framework for particle entrainment: Water Resources Research, v. 44, W04415, doi:10.1029/2007/WR006363.

Corey, A.T., 1949, Influence of shape on the fall velocity of sand grains[MS Thesis]: Fort Collins, CO, Colorado A & M College, 102 p.

Davis, L., 2009, Sediment entrainment potential in modified alluvial streams: implications for re-mobilization of stored in-channel sediment: Physical Geography, v. 30, p. 249-268.

Dingman, S.L., 1984, Fluvial Hydrology: New York, W.H. Freeman and Company, 383 p.

Dodd, J.A., and Dettman, E., 1996, Soil Survey of Taney County, Missouri: Washington, D.C., U.S. Department of Agriculture, Natural Resources Conservation Service, 122 p.

Dogwiler, T., 2002, Fluvial disturbances in karst systems [PhD Dissertation]: Columbia, MO, University of Missouri-Columbia, 146 p.

Dogwiler, T., and Wicks, C.M., 2004, Sediment entrainment and transport in fluviokarst systems: Journal of Hydrology, v. 295, p.163-172.

Drew, I.B., 1992, Bedload transport, vertical exchange and sediment storage in two Scottish Highland gravel-bed streams [PhD Dissertation]: St. Andrews, U.K., St. Andrews University.

Du Boys, M.P., 1879, Etudes du regime et l'action exerce par les eaux sur un lit a fond de gravier indefiniment affouiable: Annales des Ponts et Chaussees, v. 5, p. 141-195.

Elliott, W.R., and Aley, T.J., 2005, Karst conservation in the Ozarks: forty years at Tumbling Creek Cave: National Cave and Karst Management Symposium, p. 204-214.

Elliott. W.R., and Echols, K., 2007, Waterborne contaminants in Tumbling Creek Cave, Missouri: National Cave and Karst Management Symposium, p. 107-123.

Emmett, W.W., 1980, A field calibration of the sediment trapping characteristics of the Helley-Smith bed load sampler: U.S. Geological Survey Professional Paper, v. 1139, p. 44.

Emmett, W.W., and Wolman, M.G., 2001, Effective discharge and gravel-bed rivers: Earth Surfaces Processes and Landforms, v. 26, p. 1369-1380.

Farrant, A., 2004, Paleoenvironments: clastic cave sediments, *in* Gunn, J., ed., Encyclopedia of Caves and Karst Science: New York, Fitzroy Dearborn, p. 553-555.

Fenton, J.D., and Abbott, J.E., 1977, Initial movement of grains on a stream bed: The effect of relative protrusion: Proceedings of the Royal Society of London, Series A, Mathematical and Physical Sciences, v. 352, p. 523-537.

Ferguson, R.I., 1994, Critical discharge for entrainment of poorly sorted gravel: Earth Surface Processes and Landforms, v. 19, p. 179-186.

Ferguson, R.I., 2005, Estimating critical stream power for bedload transport calculations in gravel-bed rivers: Geomorphology, v. 70, p. 33-41.

Ferguson, R.I., Bloomer, D.J., Hoey, T.B., and Werritty, A., 2002, Mobility of river tracer pebbles over different timescales: Water Resources Research, v. 38, 1045, doi:10.1029/2001WR000254.

Ferguson, R.I., and Wathen, S.J., 1998, Tracer-pebble movement along a concave river profile: virtual velocity in relation to grain size and shear stress: Water Resources Research, v. 34, p. 2031-2038.

Garcia, M.H., 2008, Sediment transport and morphodynamics, *in* Garcia, M.H., ed., Sedimentation engineering: processes, measurements, modeling, and practice: Reston, VA, American Society of Civil Engineers, p. 21-163.

Gilbert, G.K., 1877, Report on the geology of the Henry Mountains: Geographical and geological survey of the Rocky Mountain region: Washington, D.C., Government Printing Office, 106 p.

Gilbert, G.K., 1914, The transportation of debris by running water: United States Geological Survey Professional Paper, v. 86, 263 p.

Gillieson, D., 1996, Caves: Processes, Development, Management: Oxford, Blackwell Publishers, 324 p.

Gomez, B., 1991, Bedload transport: Earth-Science Reviews, v. 31, p. 89-132.

Gordon, N.D., McMahon, T.A., Finlayson, B.L., Gippel, C.J., and Nathan, R.J., 2004, Stream Hydrology: An introduction for ecologists: Chichester, U.K., John Wiley & Sons, 2nd ed., 429 p.

Haschenburger, J.K., and Church, M., 1998, Bed material transport estimated from the virtual velocity of sediment: Earth Surface Processes and Landforms, v. 23, p. 791-808.

Hassan, M.A., and Church, M., 1992, The movement of individual grains on the streambed, *in* Billi, P., Hey, R.D., Thorne, C.R., and Tacconi, P., eds., Dynamics of Gravel-bed Rivers: New York, John Wiley & Sons, p. 159-173.

Hassan, M.A., and Ergenzinger, P., 2003, Use of tracers in fluvial geomorphology, *in* Kondolf, G.M., and Piegay, H., eds., Tools in Fluvial Geomorphology: Chichester, U.K., John Wiley & Sons, p. 397-423.

Hassan, M.A., Church, M., and Ashworth, P.J., 1992, Virtual rate and mean distance of travel of individual clasts in gravel-bed channels: Earth Surface Processes and Landforms, v. 17, p. 617-627.

Hassan, M.A., Schick, A.P., and Laronne, J.B., 1984, The recovery of flood dispersed coarse sediment particles, a three dimensional magnetic tracing method: Catena Supplement, v. 5, p. 153-162.

Hicks, D.M., and Gomez, B., 2003, Sediment transport, *in* Kondolf, G.M., and Piegay, H., eds., Tools in Fluvial Geomorphology: Chichester, U.K., John Wiley & Sons, p. 425-461.

Horton, J.M., 2003, Channel geomorphology and restoration guidelines for Springfield Plateau streams, South Dry Sac Watershed, southwest Missouri [MS Thesis]: Springfield, MO, Southwest Missouri State University, 151 p.

Hubbell, D., 1987, Bed load sampling and analysis, *in* Thorne, C.R., Bathurst, J.C., and Hey, R.D., eds., Sediment Transport in Gravel Bed Rivers: New York, John Wiley & Sons, p. 89-118.

Jacobson, R.B., 1995, Spatial controls on patterns of land-use induced stream disturbance at the drainage-basin scale—an example from gravel-bed streams of the Ozark Plateaus, Missouri: American Geophysical Union Monograph, v. 89, p. 219-239.

Jacobson, R.B., and Gran, K.B., 1999, Gravel sediment routing from widespread, low-intensity landscape disturbance, Current River Basin, Missouri: Earth Surface Processes and Landforms, v. 24, p. 897-917.

Jarrett, R.D., 1984, Hydraulics of high-gradient streams: American Society of Civil Engineers, Journal of the Hydraulics Division, v. 110, p. 1519-1539.

Komar, P.D., 1987, Selective gravel entrainment and the empirical evaluation of flow competence: Sedimentology, v. 34, p. 1165-1176.

Kothyari, U.C., and Jain, R.K., 2008, Influence of cohesion on the incipient motion condition of sediment mixtures: Water Resources Research, v. 44, W04410, doi:10.1029/2007WR006326.

Laronne, J.B., and Carson, M.A., 1976, Interrelationship between bed morphology and bed-material transport for a small, gravel-bed channel: Sedimentology, v. 23, p. 67-85.

Leopold, L.B., Wolman, M.G., and Miller, J.P., 1964, Fluvial Processes in Geomorphology: San Francisco, W.H. Freeman and Company, 522 p.

Limerinos, J.T., 1970, Determination of the Manning coefficient from measured bed roughness in natural channels: Federal Centre, CO, U.S. Geological Survey Water-Supply Paper 1898-B, p. 47.

Lorang, M.S., and Hauer, F.R., 2003, Flow competence and streambed stability: an evaluation of technique and application: Journal of the North American Benthological Society, v. 22, p. 475-491.

Montgomery, D.R., and Buffington, J.M., 1997, Channel-reach morphology in mountain drainage basins: Geological Society of America Bulletin, v. 109, p. 596-611.

Nash, D.B., 1994, Effective sediment-transporting discharge from magnitude-frequency analysis: Journal of Geology, v. 102, p. 79-95.

Neill, H., Gutierrez, M., and Aley, T., 2004, Influences of agricultural practices on water quality of Tumbling Creek cave stream in Taney County, Missouri: Environmental Geology, v. 45, p. 550-559.

Nelson, J.M., Bennett, J.P., and Wiele, S.M., 2003, Flow and sediment-transport modeling, *in* Kondolf, G.M., and Piegay, H., eds., Tools in Fluvial Geomorphology: Chichester, U.K., John Wiley & Sons, p. 539-576.

Newson, M.D., 1971a, A model of subterranean limestone erosion in the British Isles based on hydrology: Transactions, Institute of British Geographers, v. 54, p. 55-70.

Newson, M.D., 1971b, The role of abrasion in cavern development, Symposium on the Origin and Development of Caves: London, British Cave Research Association, p. 101-107.

Noltie, D.B., and Wicks, C.M., 2001, How hydrogeology has shaped the ecology of Missouri's Ozark cavefish, *Amblyopsis rosae*, and southern cavefish, *Typhlichthys subterraneus*: insights on the sightless from understanding the underground: Environmental Biology of Fishes, v. 62, p. 171-194.

Overstreet, R.B., Oboh-Ikuenobe, F.E., and Gregg, J.M., 2003, Sequence stratigraphy and depositional facies of lower Ordovician cyclic carbonate rocks, southern Missouri, U.S.A.: Journal of Sedimentary Research, v. 73, p. 421-433.

Palmer, A.N., 1991, Origin and morphology of limestone caves: Geological Society of America Bulletin, v. 103, p. 1-21.

Parker, G., 2008, Transport of gravel and sediment mixtures, *in* Garcia, M.H., ed., Sedimentation engineering: processes, measurements, modeling, and practice: Reston, VA, American Society of Civil Engineers, p. 165-251.

Parker, G., and Klingeman, P.C., 1982, On why gravel bed streams are paved: Water Resources Research, v. 18, p. 1409-1423.

Peterson, E.W., Sickbert, T.B., and Moore, S.L., 2008, High frequency stream bed mobility of a low-gradient agricultural stream with implications on the hyporheic zone: Hydrological Processes, v. 22, p. 4239-4248.

Recking, A., Frey, P., Paquier, A., Belleudy, P., and Champagne, J.Y., 2008, Feedback between bed load transport and flow resistance in gravel and cobble bed rivers: Water Resources Research, v. 44, W05412, doi:10.1029/2007WR006219.

Reed, T.M., McFarland, J.T., Fryar, A.E., Fogle, A.W., and Taraba, J.L., 2010, Sediment discharges during storm flow from proximal urban and rural karst springs, central Kentucky, USA: Journal of Hydrology, v. 383, p. 280-290.

Reid, I., and Frostick, L.E., 1984, Particle interaction and its effect on the thresholds of initial and final bedload motion in coarse alluvial channels, *in* Koster, E.H., and Steel, R.J., eds., Sedimentology of gravels and conglomerates: Calgary, Canada, Canadian Society of Petroleum Geologists, Memoir 10, p. 61-68.

Reid, I., and Frostick, L.E., 1985, Dynamics of bedload transport in Turkey Brook, a coarse-grained alluvial channel: Earth Surface Processes and Landforms, v. 11, p. 143-155.

Renault, P., 1970, La Formation des Cavernes: Paris, Presses Universitaires de France, 126 p.

Saucier, R.T., 1983, Historic changes in Current River meander regime: Proceedings of Conference, Rivers '83, American Society of Civil Engineers, p. 180-190.

Schoklitsch, A., 1962, Handbuch des wasserbaues [Manual of water engineering]: Vienna, Springer-Verlag, 3rd ed., 475 p.

Schwendel, A.C., Death, R.G., and Fuller, I.C., 2009, The assessment of shear stress and bed stability in stream ecology: Freshwater Biology, doi:10.1111/j.1365-2427.2009.02293.x.

Shields, A., 1936, Anwendung der aehnlichkeitsmechanik und der turbulenzforschung auf die geschiebebewegung [Application of similarity principles and turbulence research to bedload movement]: Heft Berlin, Mitteilungen der Preussischen Versuchsanstalt fur Wasserbau Schiffbau, 26 p.

Sklar, L.S., and Dietrich, W.E., 2001, Sediment and rock strength controls on river incision into bedrock: Geological Society of America Bulletin, v. 29, p. 1087-1090.

Smart, G.M., 1984, Sediment transport formula for steep channels: Journal of Hydraulic Engineering, v. 110, p. 267-276.

Thompson C., and Croke, J., 2008, Channel flow competence and sediment transport in upland streams in southeast Australia: Earth Surface Processes and Landforms, v. 33, p. 329-352.

Thompson, S.M., and Campbell, P.L., 1979, Hydraulics of a large channel paved with boulders: Journal of Hydraulic Research, v. 17, p. 341-354.

Thomson, K.C., and Aley, T., 1971, Ozark Underground Laboratory part 1: Ozark Caver, v. 3, p. 1-25.

Van Gundy, J.J., and White, W.B., 2009, Sediment flushing in Mystic Cave, West Virginia, USA, in response to the 1985 Potomac Valley flood: International Journal of Speleology, v. 38, p. 103-109.

Whipple, K.X., and Tucker, G.E., 2002, Implications of sediment-flux-dependent river incision models for landscape evolution: Journal of Geophysical Research, v. 107, doi:10.1029/2000JB000044.

White, W.B., 1988, Geomorphology and Hydrology of Karst Terrains: New York, Oxford University Press, 464 p.

White, E.L., and White, W.B., 1968, Dynamics of sediment transport in limestone caves: The National Speleological Society Bulletin, v. 30, p. 115- 129.

White, W.B., and Deike, G.H., III, 1989, Hydraulic geometry of cave passages, *in* White, W.B., and White, E.L., eds., Karst Hydrology: Concepts from the Mammoth Cave Area: New York, Van Nostrand Reinhold, p. 223-258.

Whiting, P.J., and Bradley, J.B., 1993, A process-based classification system for headwater streams: Earth Surface Processes and Landforms, v. 18, p. 603-612.

Wilcock, D.N., 1971, Investigation into the relations between bedload transport and channel shape: Geological Society of America Bulletin, v. 82, p. 2159-2176.

Wilcock, P.R., 1992, Experimental investigation of the effect of mixture properties on transport dynamics, *in* Billi, P., Hey, R.D., Thorne, C.R., and Tacconi, P., eds., Dynamics of gravel-bed rivers: Chichester, U.K., John Wiley & Sons, p. 109-139.

Wilcock, P. R., 1997a, Entrainment, displacement and transport of tracer gravels: Earth Surface Processes and Landforms, v. 22, p. 1125-1138.

Wilcock, P.R., 1997b, The components of fractional transport rate: Water Resources Research, v. 33, p. 247-258.

Wilcock, P.R., 2001, Toward a practical method for estimating sediment-transport rates in gravel-bed rivers: Earth Surface Processes and Landforms, v. 26, p. 1395-1408.

Wilcock, P.R., Barta, A.F., Shea, C.C., Kondolf, G.M., Graham Matthews, W.V., and Pitlick, J., 1996, Observations of flow and sediment entrainment on a large gravel-bed river: Water Resources Research, v. 32, pg. 2897-2909.

Wilcock, P., Pitlick, J., and Yantao, C., 2009, Sediment transport primer: estimating bed-material transport in gravel-bed rivers, General Technical Report RMRS-GTR-226: Fort Collins, CO, U.S. Department of Agriculture, Forest Service, Rocky Mountain Research Station, 78 p.

Williams, G.P., 1978, Bank-full discharge of rivers: Water Resources Research, v. 16 p. 1141-1154.

Wolman, M.G., 1954, A method of sampling coarse river-bed material: Transactions – American Geophysical Union, v. 35, p. 951-956.

Wolman, M.G., and Miller, J.P., 1960, Magnitude and frequency of forces in geomorphic processes: Journal of Geology, v. 68, p. 54-74.

Worthington, S.R.H., 1984, The paleodrainage of an Appalachian fluviokarst: Friars Hole, West Virginia [MS Thesis]: Hamilton, Ontario, Canada, McMaster University, 218 p.

Yalin, M.S., 1977, Mechanics of Sediment Transport: New York, Pergamon, 2nd ed., 298 p.

APPENDIX A

Each of the surveyed cross-sections in Bear Cave Hollow and Tumbling Creek Cave has been plotted in this section. Bankfull stage is marked with a dashed line. Cross-sections used in analysis are marked with a star when consecutive cross-sections are shown at a single station. Cross-sections are presented in upstream to downstream order in each of their respective streams, and by date when consecutive cross-sections were made. The date of survey is also listed for each cross-section. All cross-sections have been plotted with a vertical exaggeration of 5 times.

Bear Cave Hollow

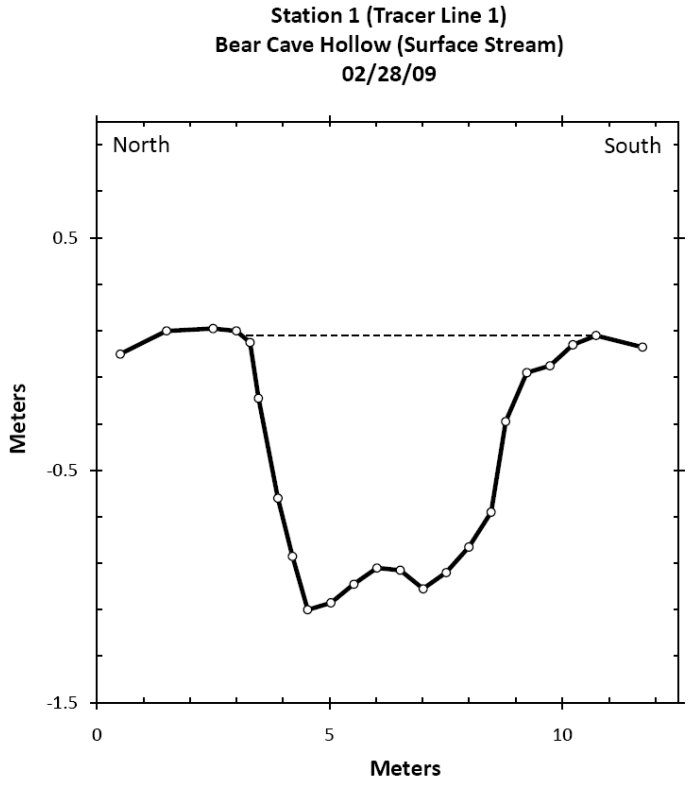

Station 1 (Tracer Line 1)
Bear Cave Hollow (Surface Stream)
10/03/09

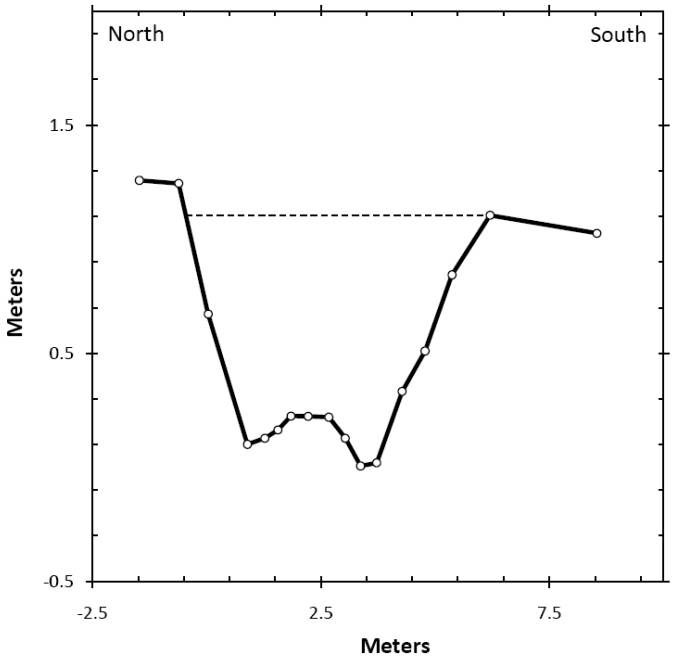

Station 1 (Tracer Line 1)
Bear Cave Hollow (Surface Stream)
12/18/09

★ *Used in analysis*

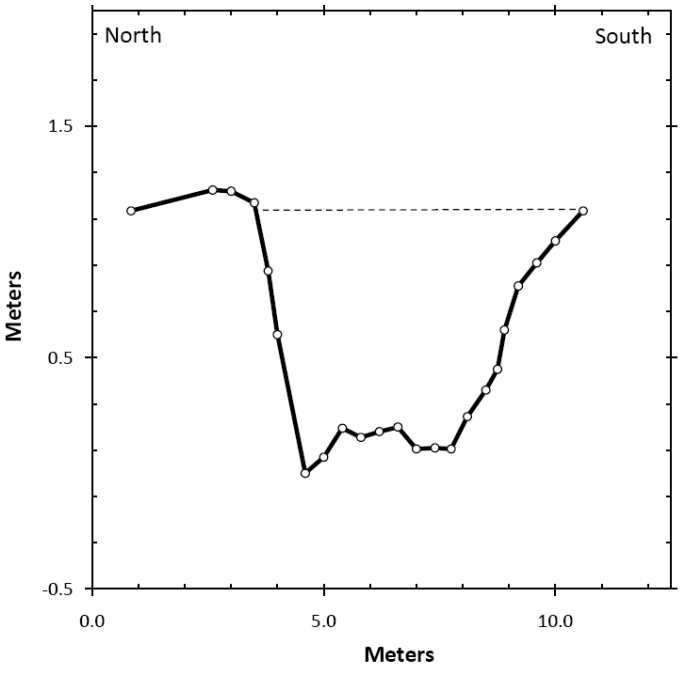

Station 2 (Gaging Station)
Bear Cave Hollow (Surface Stream)
12/18/09

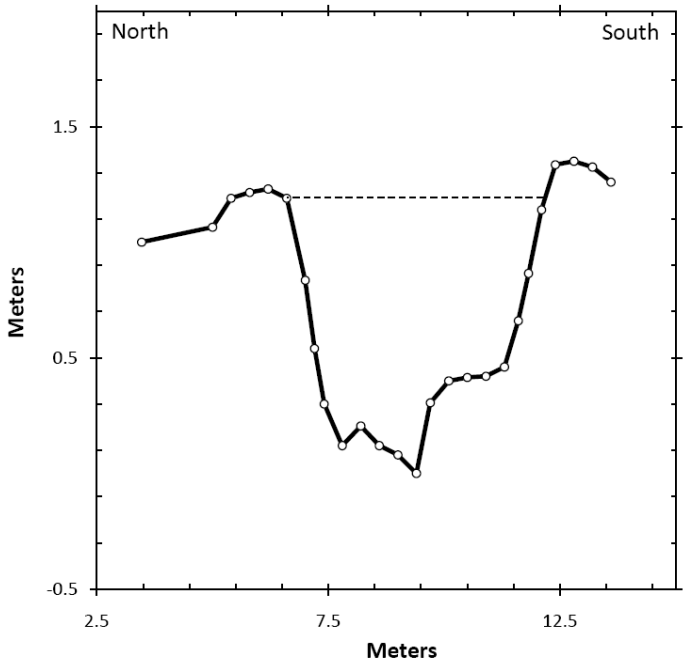

Station 3 (Tracer Line 2)
Bear Cave Hollow (Surface Stream)
02/28/2009

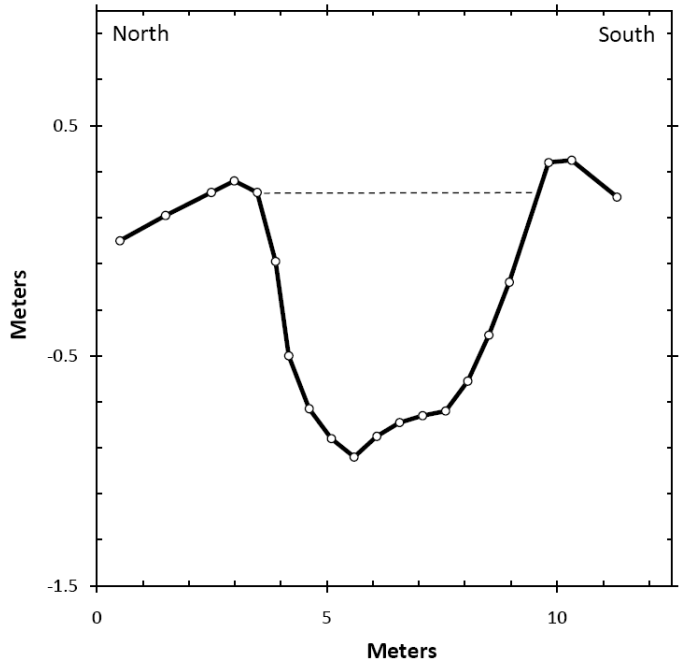

Station 3 (Tracer Line 2)
Bear Cave Hollow (Surface Stream)
10/03/2009

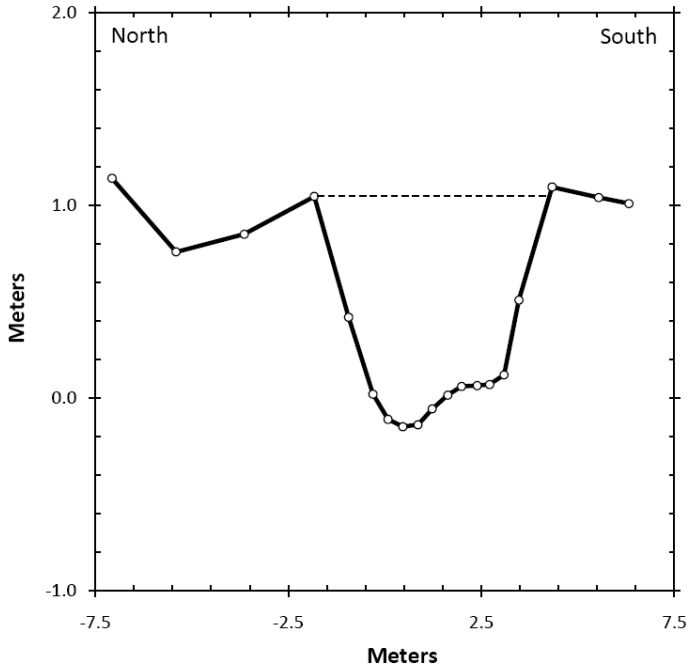

Station 3 (Tracer Line 2)
Bear Cave Hollow (Surface Stream)
12/18/09

★ *Used in analysis*

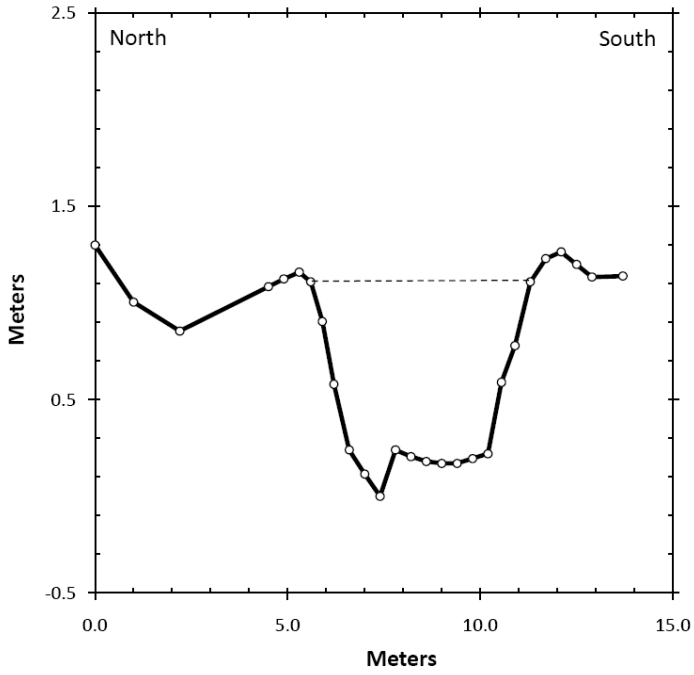

Station 4
Bear Cave Hollow (Surface Stream)
10/03/2009

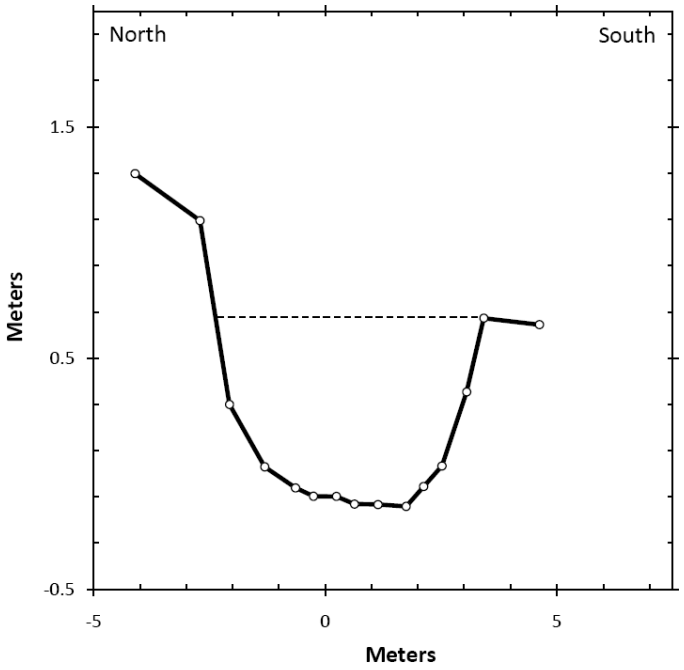

Station 5
Bear Cave Hollow (Surface Stream)
02/28/2009

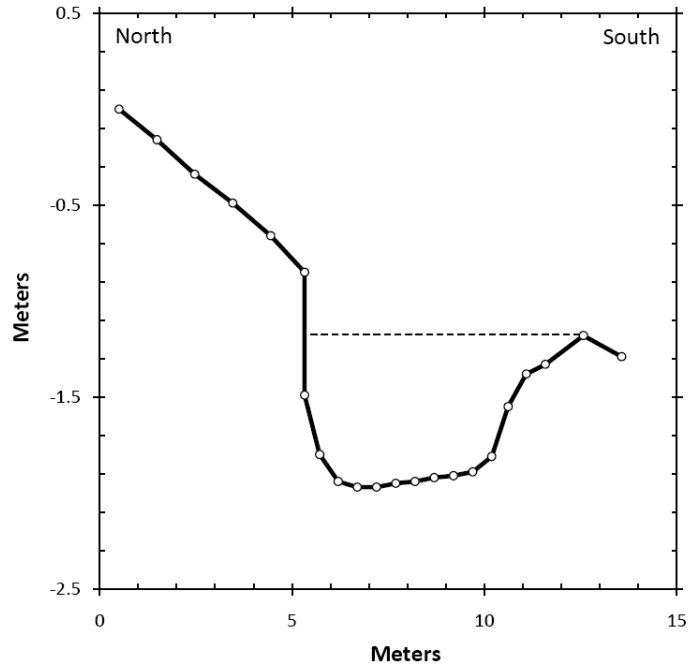

Tumbling Creek Cave

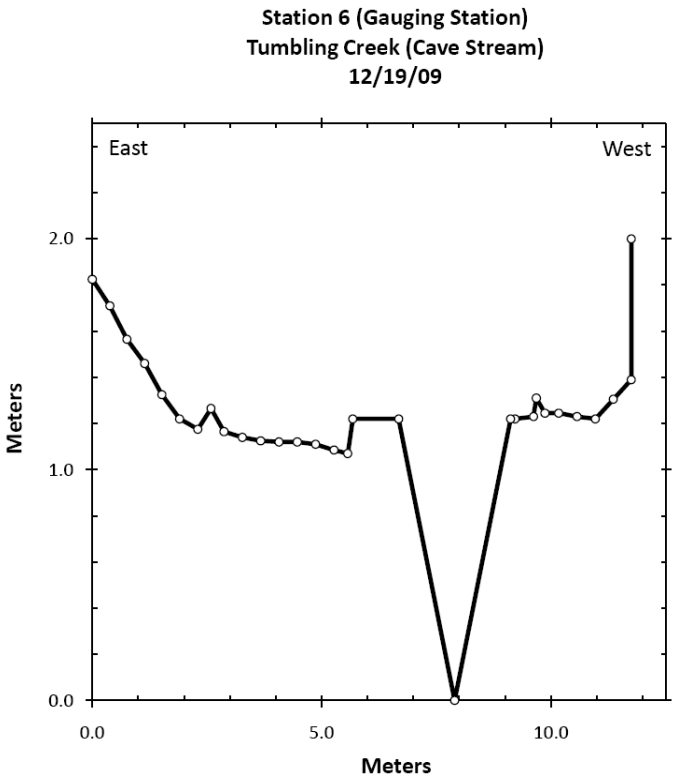

Station 7 (Tracer Line 3)
Tumbling Creek (Cave Stream)
12/19/09

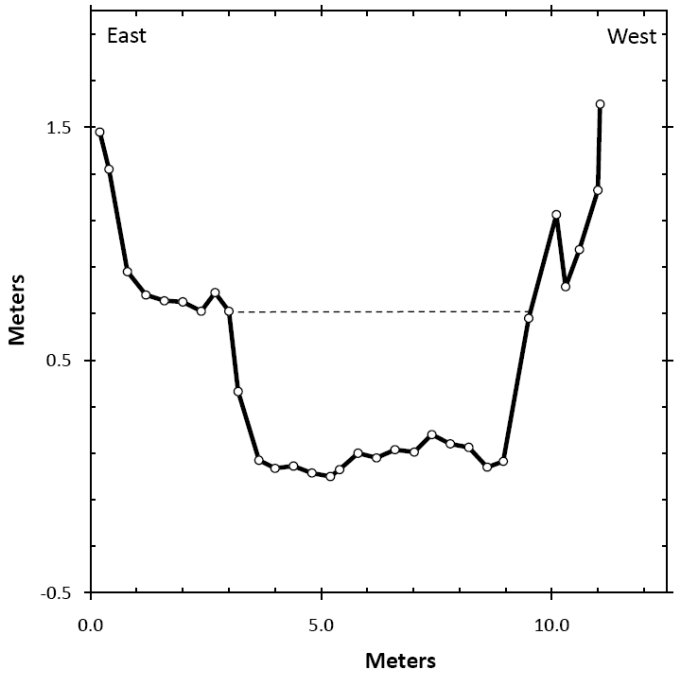

Station 8
Tumbling Creek (Cave Stream)
02/28/09

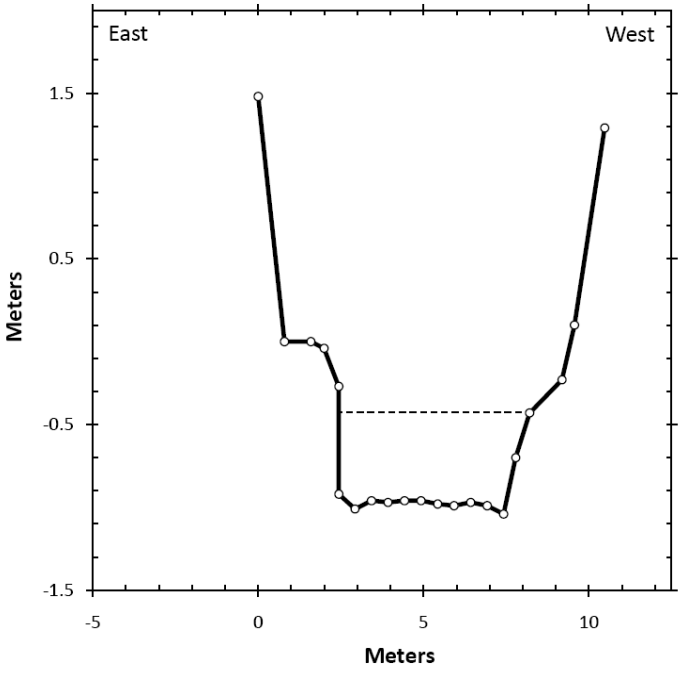

Station 9
Tumbling Creek (Cave Stream)
02/28/09

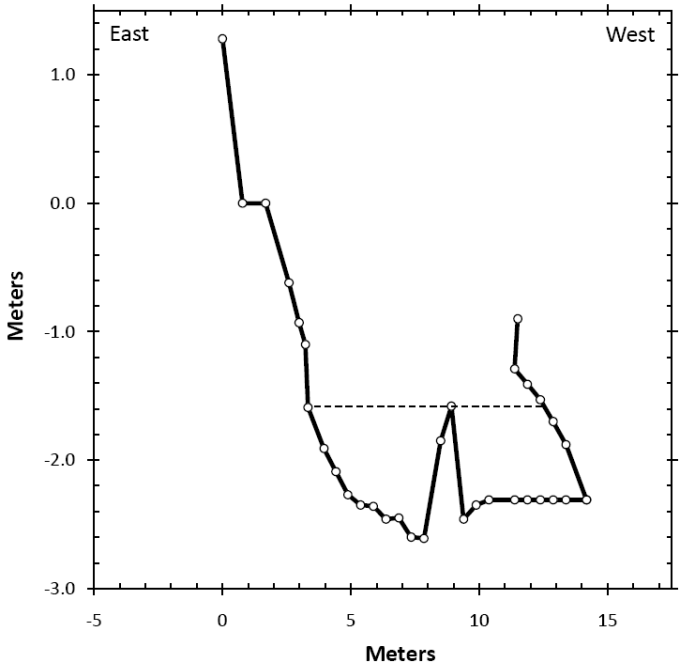

Station 10 (Tracer Line 4)
Tumbling Creek (Cave Stream)
08/01/09

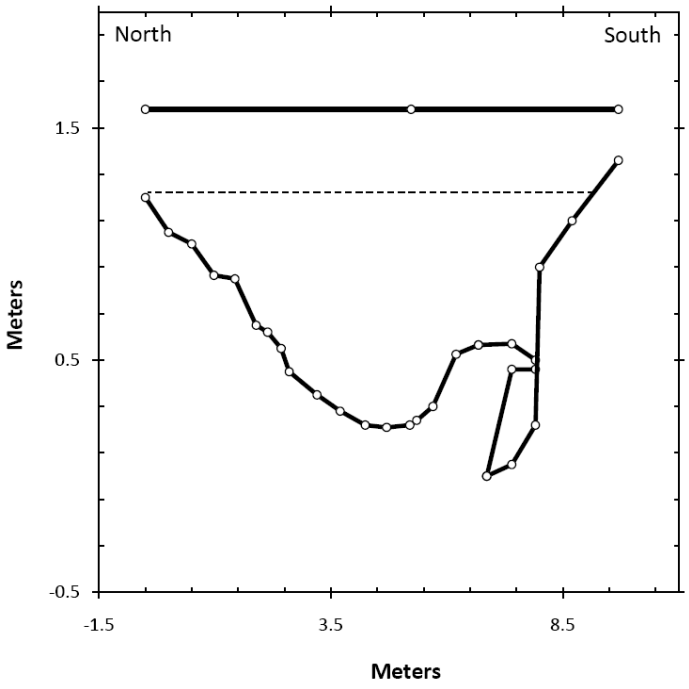

Station 10 (Tracer Line 4)
Tumbling Creek (Cave Stream)
02/06/10

★ *Used in analysis*

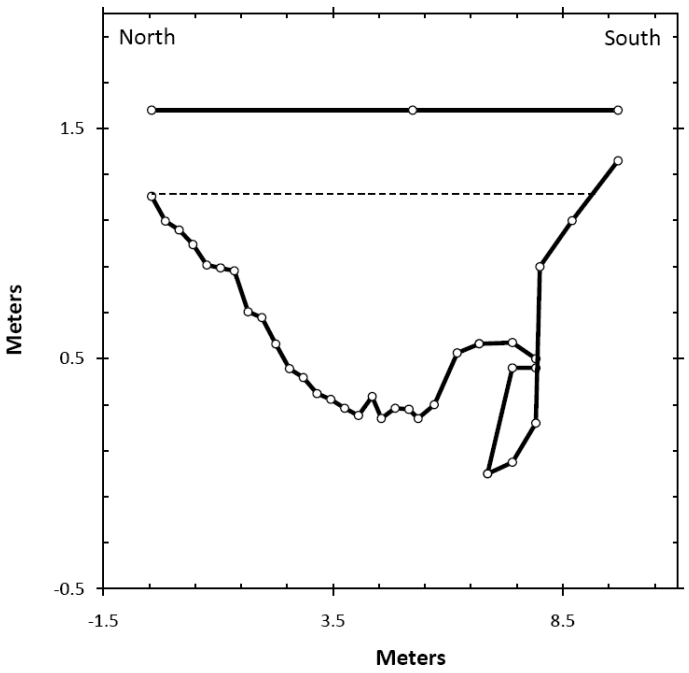

Station 11
Tumbling Creek (Cave Stream)
02/28/09

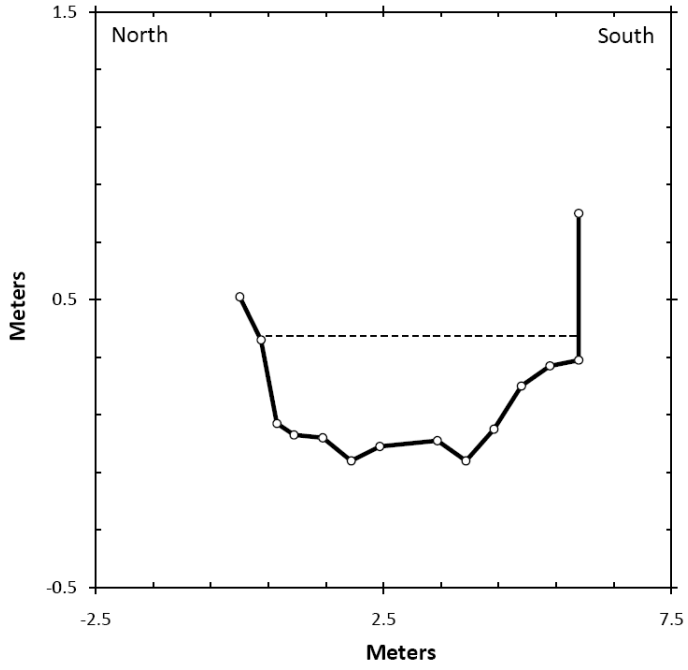

APPENDIX B

Symbols for variables used throughout the paper, including dimensions are presented in this section, with a short description of their meaning or definition.

Notation

Symbol	Dimensions	Description
a_1	-	y-intercept of log-log regression line (τ_{ci} as a function of D_i)
a_2	-	numerical coefficient
α_1	-	numerical coefficient
α_2	-	numerical coefficient
A	L^2	cross-sectional area
b	-	slope of log-log regression line (θ_{ci} as a function of θ_{c50} and D_i/D_{50})
c	-	slope of log-log regression line $((1/f)^{0.5}$ as a function of d/D)
d	L	mean water depth
d_{bf}	L	bankfull mean water depth
d_t	L	water depth in the thalweg
D_{16}	L	16th percentile grain size (sediment *b*-axis diameter)
D_{16s}	L	16th percentile grain size (sediment *b*-axis diameter) of the surface layer
D_{16ss}	L	16th percentile grain size (sediment *b*-axis diameter) of the subsurface layer
D_{50}	L	median grain size (sediment *b*-axis diameter)
D_{50s}	L	median grain size (sediment *b*-axis diameter) of the surface layer
D_{50ss}	L	median grain size (sediment *b*-axis diameter) of the subsurface layer
D_{84}	L	84th percentile grain size (sediment *b*-axis diameter)
D_{84s}	L	84th percentile grain size (sediment *b*-axis diameter) of the surface layer
D_{84ss}	L	84th percentile grain size (sediment *b*-axis diameter) of the subsurface layer
D_{85}	L	85th percentile grain size (sediment *b*-axis diameter)
D_i	L	grain size of interest
D_r	L	reference grain size diameter (unaffected by relative size effects)
f	-	Darcy-Weisbach friction factor
F_i	-	proportion of surface grains of D_i grain size on the bed before entrainment
g	LT^{-2}	gravitational acceleration
θ_{c50}	-	critical dimensionless shear stress (Shields parameter) for D_{50} grain size
θ_{c50b}	-	base critical dimensionless shear stress for D_{50} grain size
θ_{ci}	-	critical dimensionless shear stress for D_i grain size
θ_{cr}	-	critical dimensionless shear stress for D_r grain size

κ	-	von Karman constant
k_s	L	roughness height (for Prandtl-von Karman logarithmic flow resistance law)
L_i	L	mean displacement length for D_i grain size
m_1	-	y-intercept of log-log regression line ($(1/f)^{0.5}$ as a function of d/D)
m_2	-	numerical coefficient (for roughness height multiplied by
M_i	M	mass entrained per unit bed area for D_i grain size
m_i	M	mass of sediment (fraction represented by D_i grain size)
N_i	-	number of times D_i grain size is entrained
ρ	ML^{-3}	water density
ρ_s	ML^{-3}	sediment density
q	L^2T^{-1}	discharge per unit flow width (of water)
q_{aw}	L^2T^{-1}	discharge per unit active width (of water)
q_{bf}	L^2T^{-1}	bankfull discharge per unit flow width (of water)
q_c	L^2T^{-1}	critical discharge per unit width (of water)
q_{ci}	L^2T^{-1}	critical unit discharge (of water) for a grain size of interest D_i
q_{c16}	L^2T^{-1}	critical unit discharge (of water) for D_{16} grain size
q_{c50}	L^2T^{-1}	critical unit discharge (of water) for D_{50} grain size
q_{c84}	L^2T^{-1}	critical unit discharge (of water) for D_{84} grain size
q_c*	L^2T^{-1}	critical dimensionless discharge per unit width (of water)
q_i	$ML^{-1}T^{-1}$	transport rate for D_i grain size
Q	L^3T^{-1}	mean cross-sectional discharge (of water)
R	L	hydraulic radius (cross-sectional area divided by wetted perimeter)
R_d	L	daily rainfall
R_{e*}	-	grain Reynolds number = $(\tau/\rho)^{0.5}D_{50}/\nu$
R_s	-	submerged specific gravity for sediment = $(\rho_s-\rho)/\rho$
S	-	friction (energy) slope (approximated as channel bed or water surface slope)
S_b	-	bed slope
S_w	-	water slope
T	T	time duration of competent flow event
τ_0	$ML^{-1}T^{-2}$	bed shear stress (tractive force)
$\tau_{0,bf}$	$ML^{-1}T^{-2}$	bankfull bed shear stress
τ_{ci}	$ML^{-1}T^{-2}$	critical shear stress (tractive force) for a grain size of interest D_i
τ_{c16}	$ML^{-1}T^{-2}$	critical shear stress (tractive force) for D_{16} grain size
τ_{c50}	$ML^{-1}T^{-2}$	critical shear stress (tractive force) for D_{50} grain size
τ_{c84}	$ML^{-1}T^{-2}$	critical shear stress (tractive force) for D_{84} grain size
V	LT^{-1}	mean cross-sectional velocity
ν	L^2T^{-1}	kinematic viscosity of water
w	L	water (flow) top width
w_{bf}	L	bankfull water (flow) top width
x	-	slope of log-log regression line (τ_{ci} as a function of D_i)
Y_i	-	proportion of surface grains of D_i grain size entrained over time T
ω	MT^{-3}	stream power per unit area
ω_{bf}	MT^{-3}	bankfull stream power per unit area
ω_{ci}	MT^{-3}	critical stream power per unit bed area for a grain size of interest D_i
ω_{c16}	MT^{-3}	critical stream power per unit bed area for D_{16} grain size
ω_{c50}	MT^{-3}	critical stream power per unit bed area for D_{50} grain size
ω_{c84}	MT^{-3}	critical stream power per unit bed area for D_{84} grain size

APPENDIX C

Measurements of tracer particle displacements lengths, carried out by the methods described in Chapter 3, made in Bear Cave Hollow and Tumbling Creek Cave are plotted in this section. Maximum, mean, and minimum displacements of tracers having been transported past the starting line are plotted by their half-phi grain size class. Plots are presented in chronological order by the dates of survey for each of the four tracer line cross-sections. The number of tracers measured (*n*) is provided on each plot. Note that the vertical and horizontal scales vary from plot to plot

Bear Cave Hollow

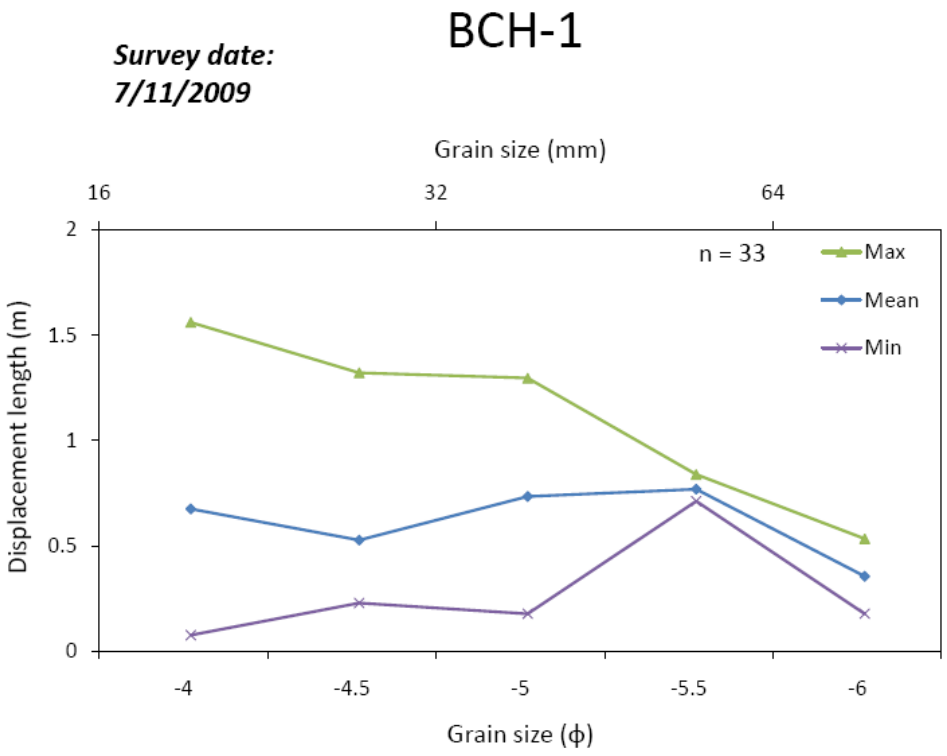

Survey date:
10/3/2009

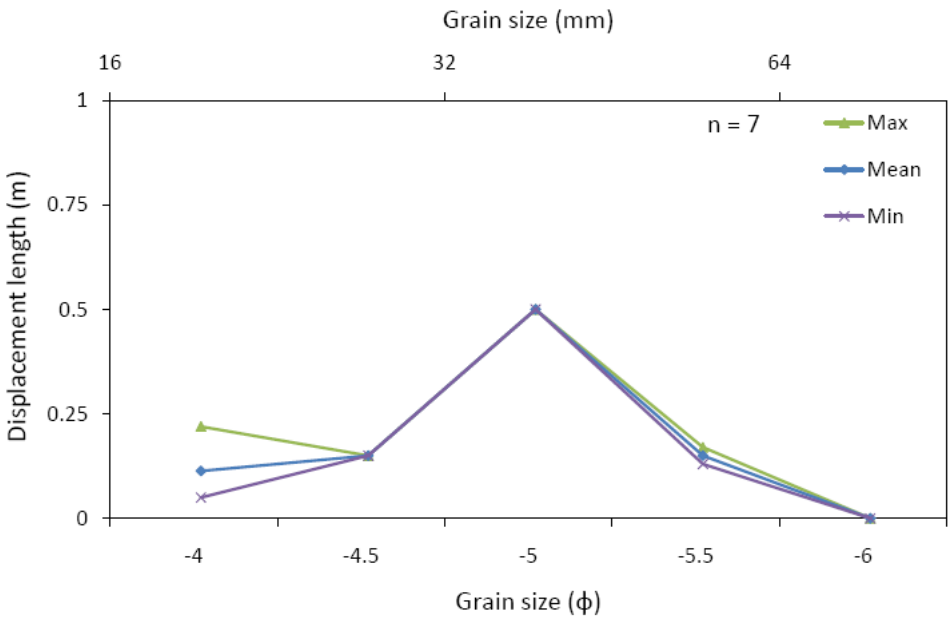

Survey date:
10/25/2009

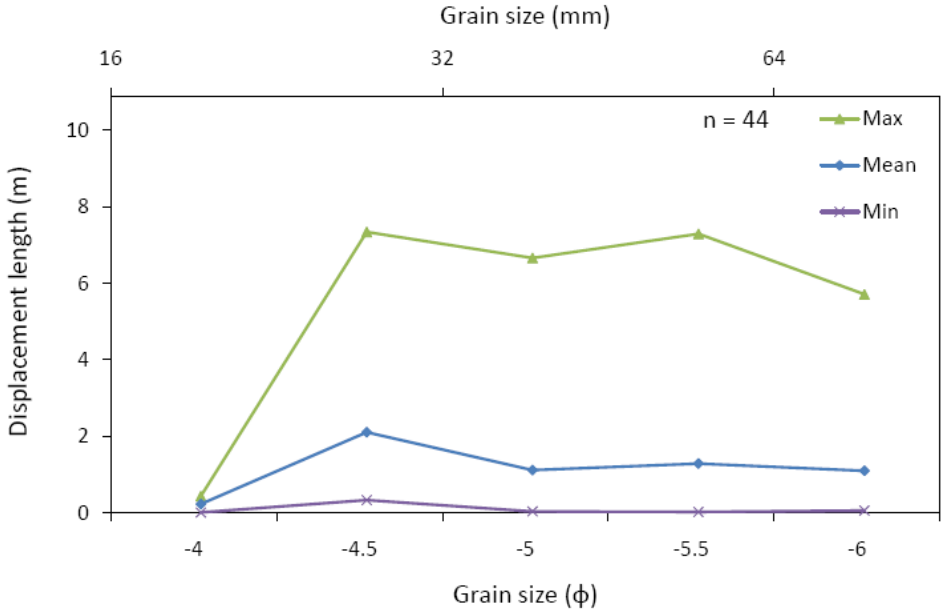

Survey date:
11/7/2009

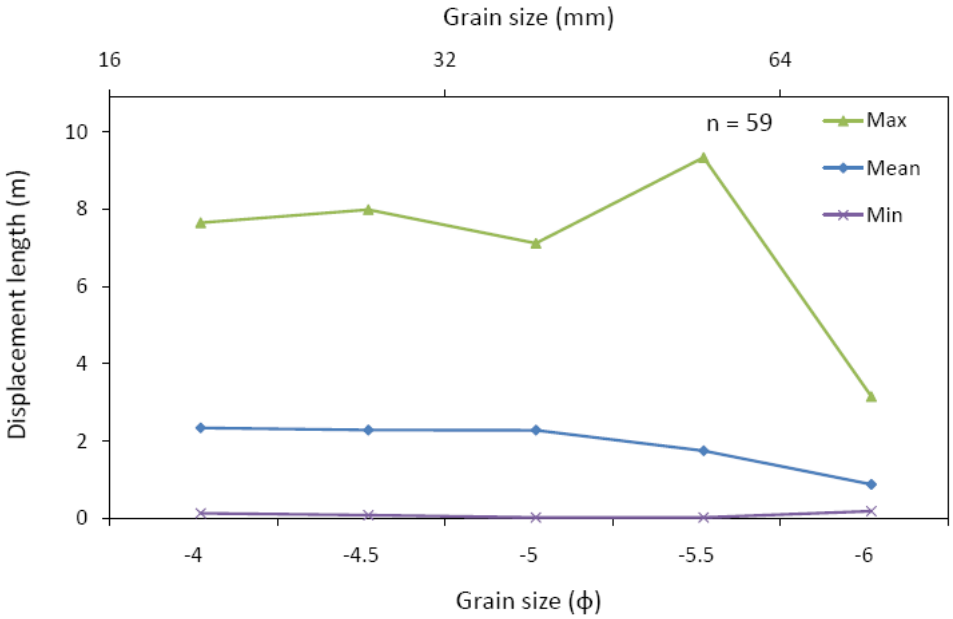

Survey date:
2/6/2010

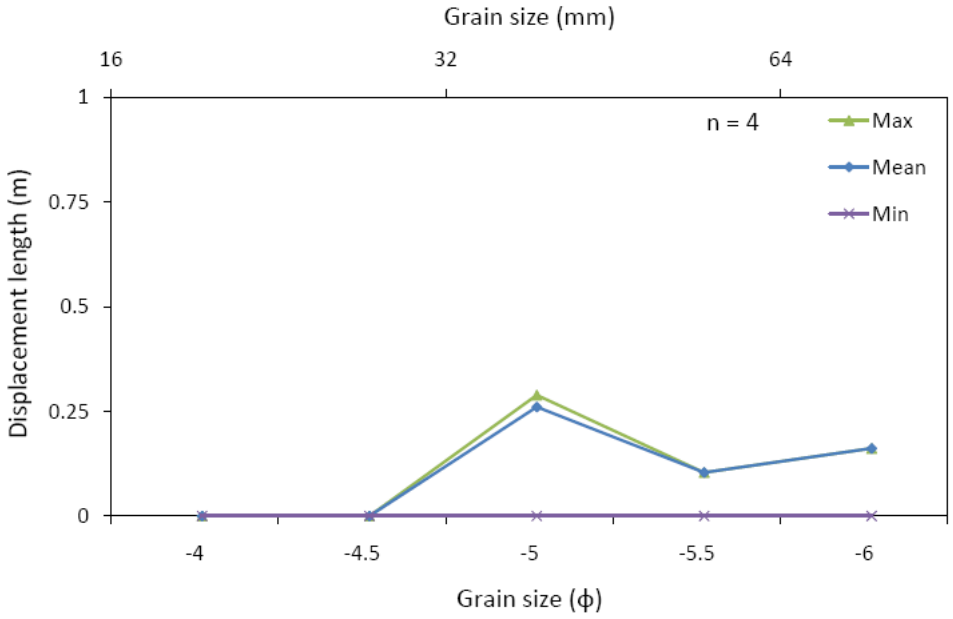

Survey date:
3/27/2010

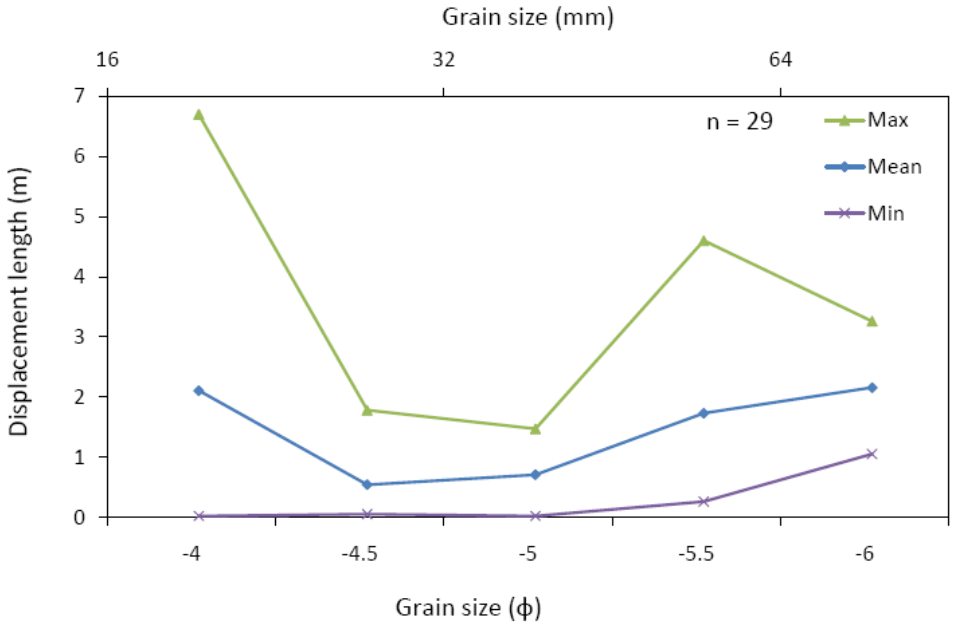

BCH-3

Survey date:
3/27/2010

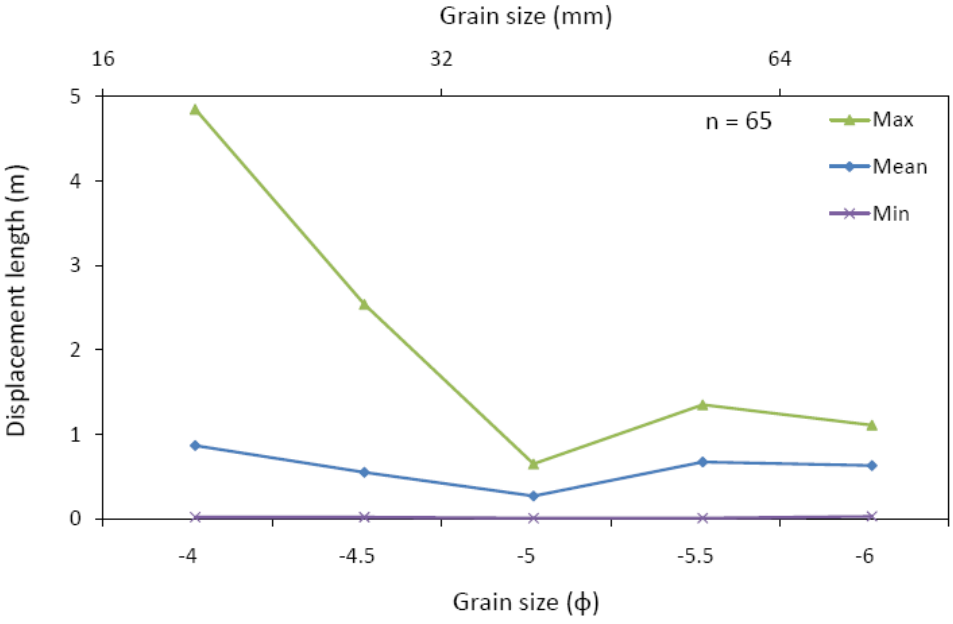

Tumbling Creek Cave

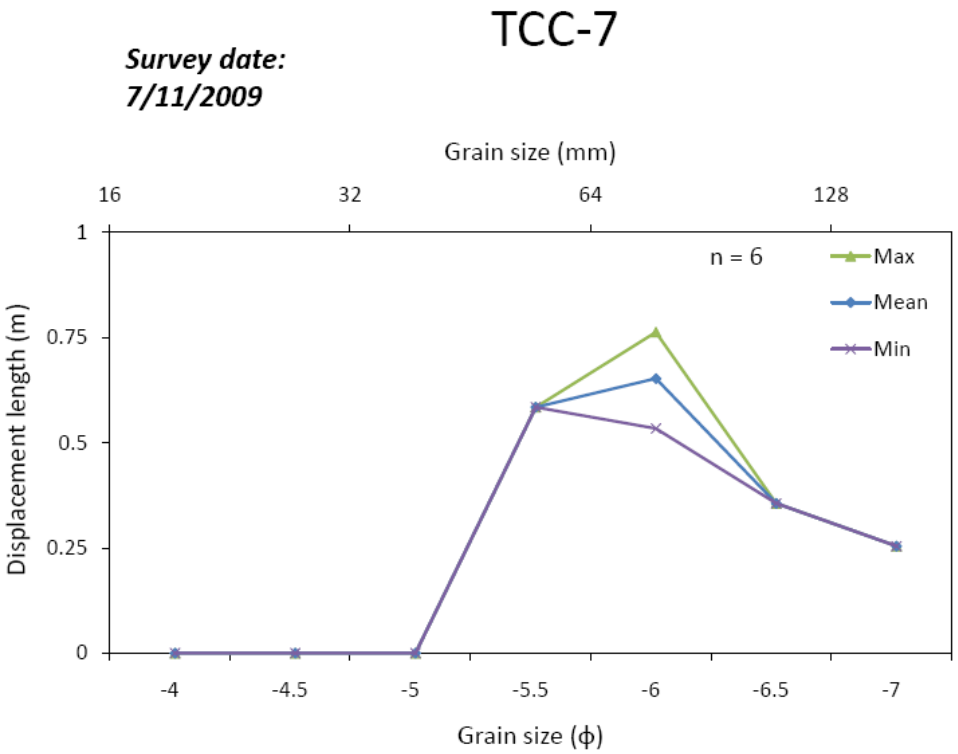

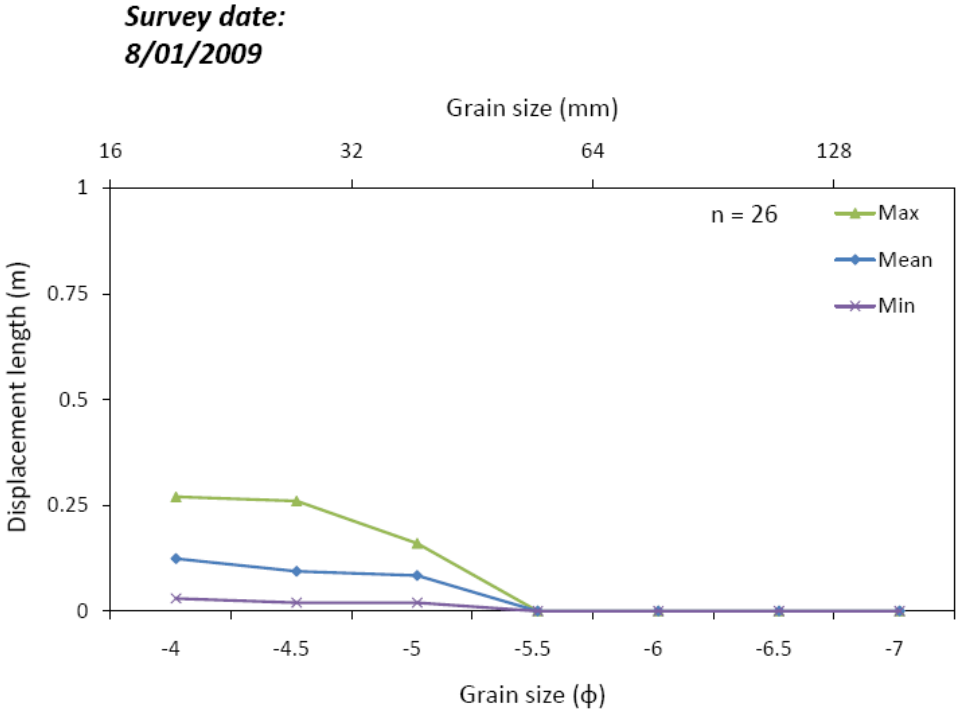

Survey date:
10/03/2009

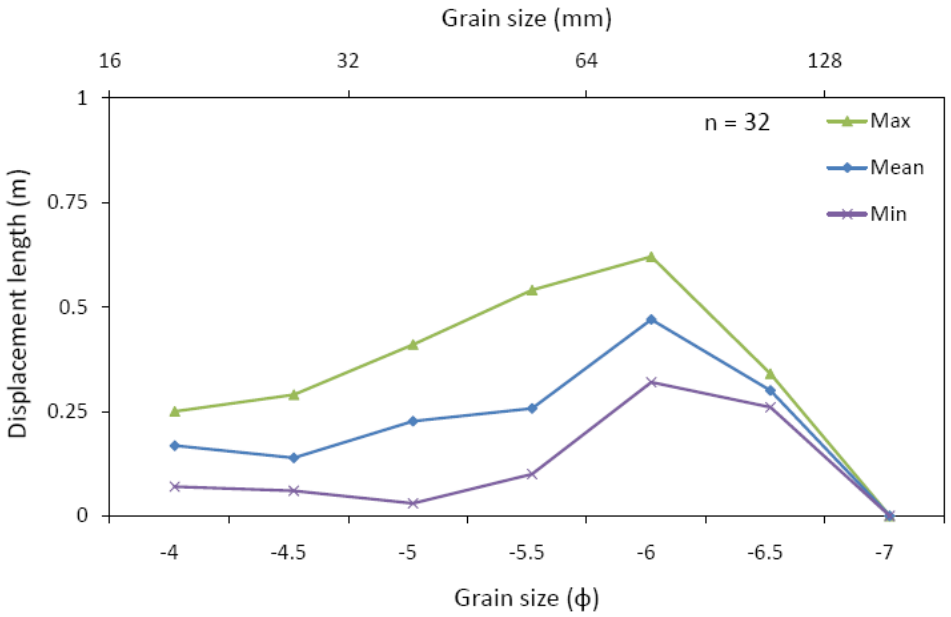

Survey date:
10/25/2009

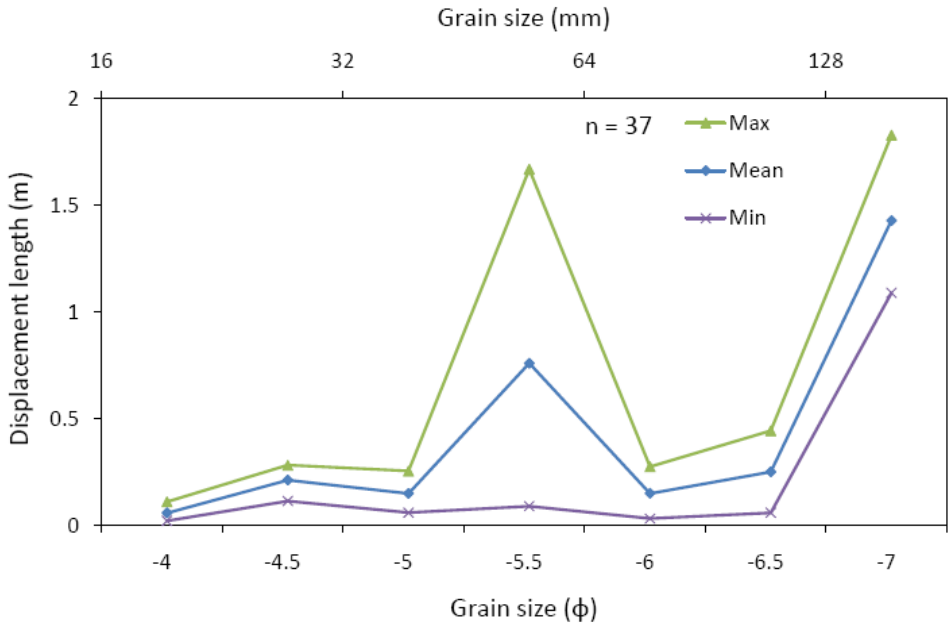

Survey date:
11/7/2009

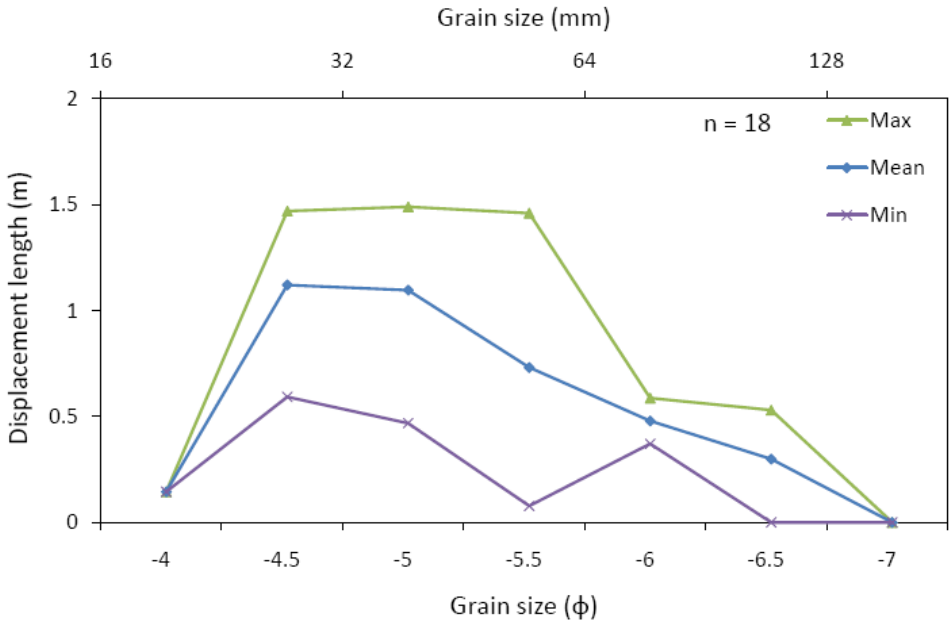

Survey date:
12/18/2009

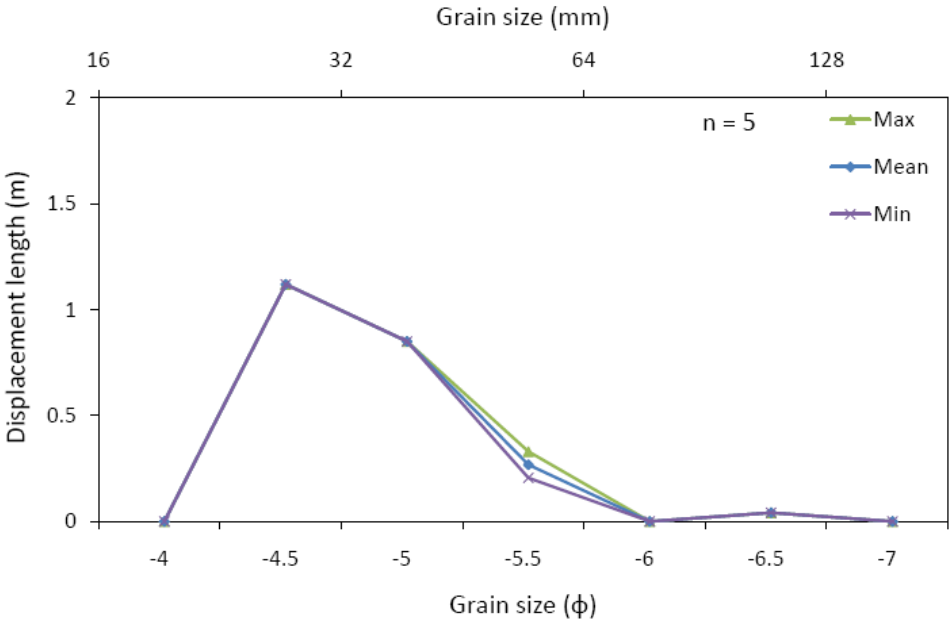

Survey date:
2/6/2010

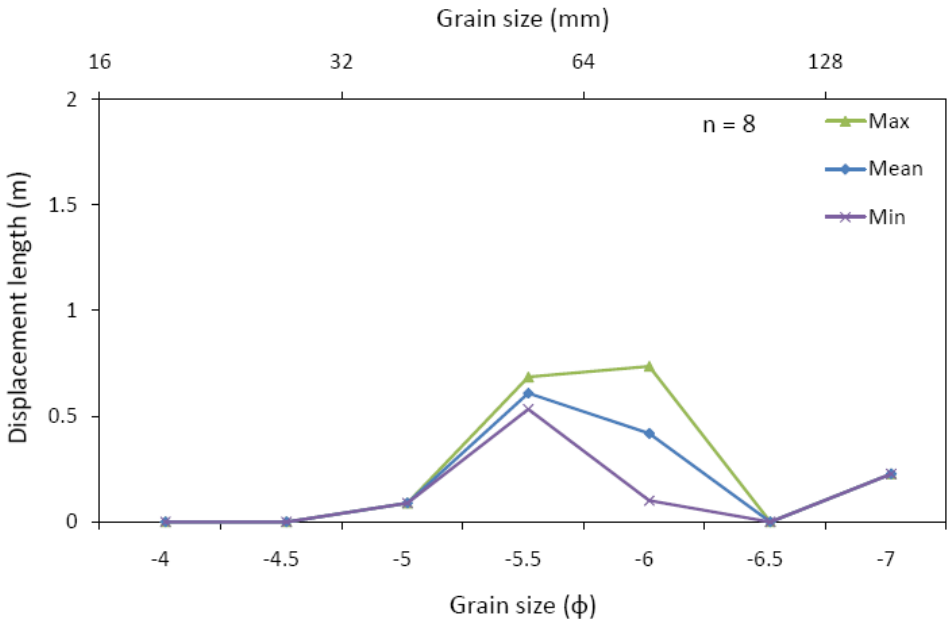

Survey date:
3/27/2010

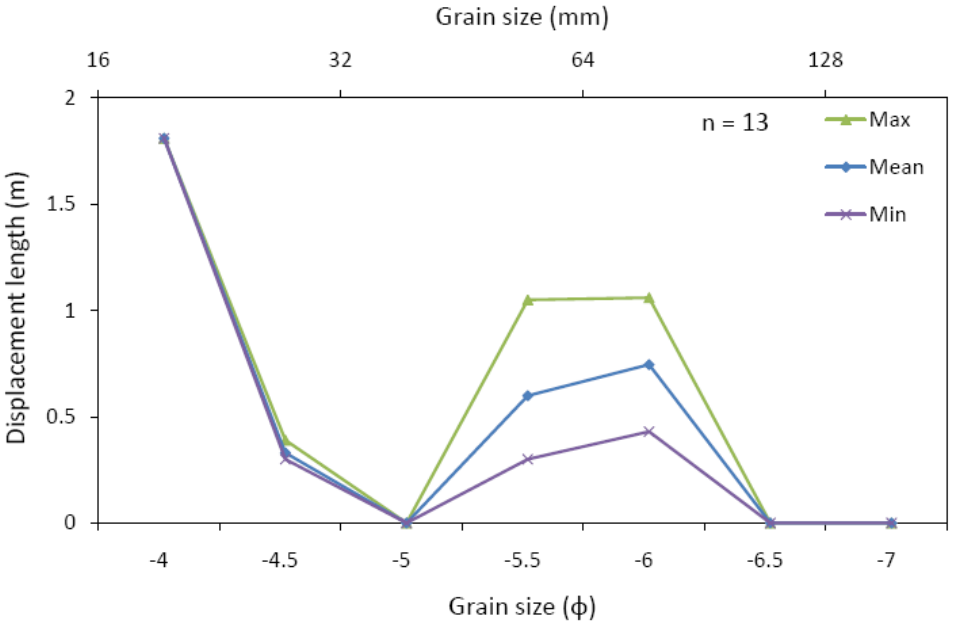

TCC-10

Survey date:
10/3/2009

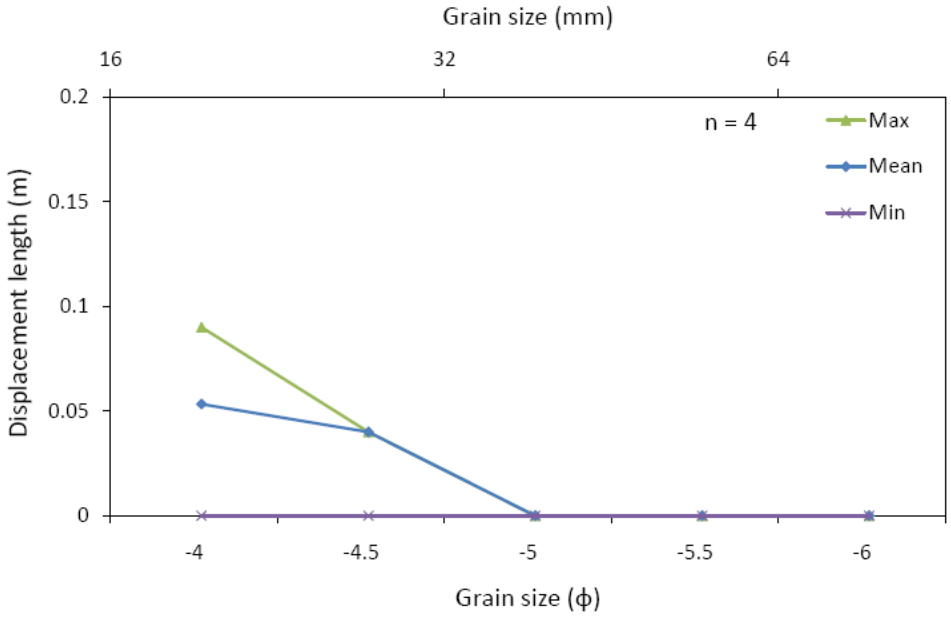

Survey date:
10/25/2009

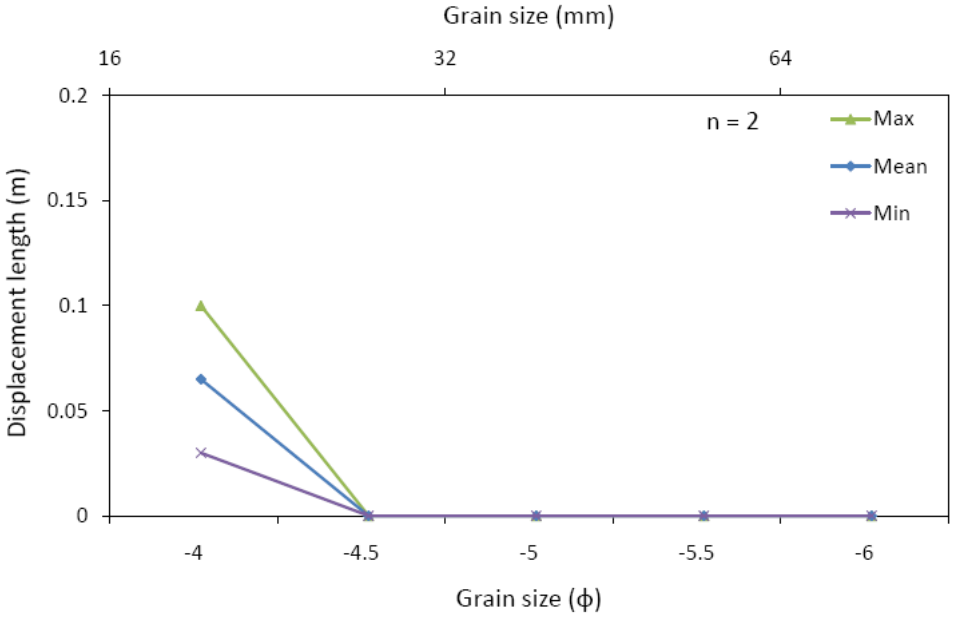

Survey date:
11/7/2009

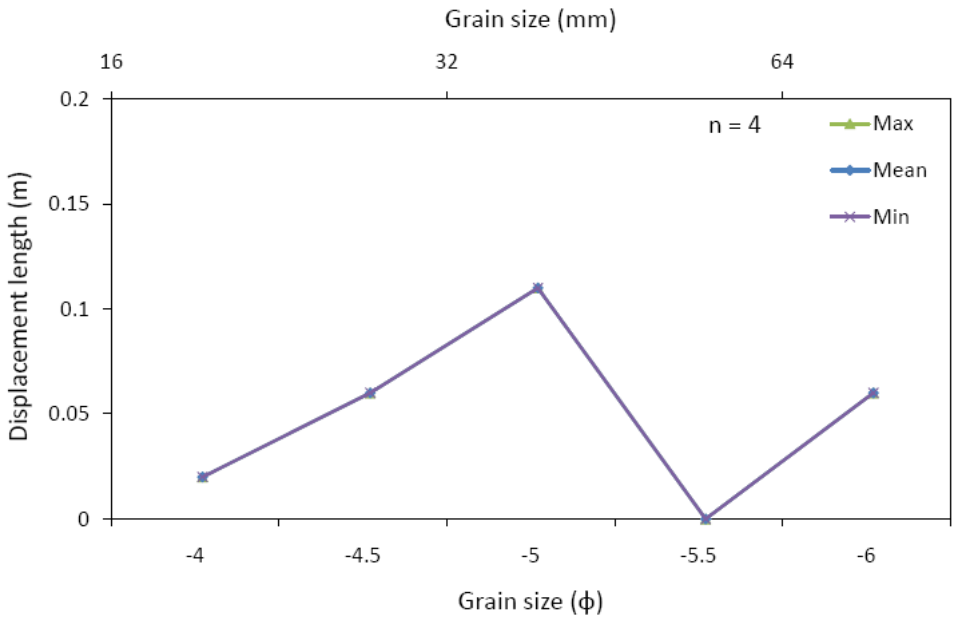

Survey date:
2/6/2010

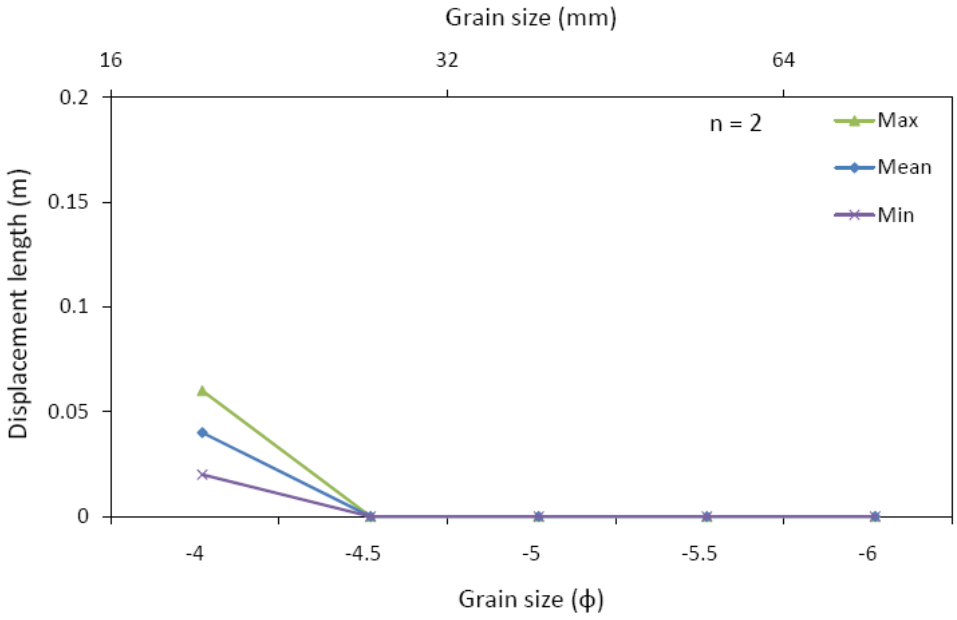

Survey date:
3/27/2010